BACTERIAL TRANSPORT AND HORIZONTAL GENE TRANSFER IN SUBSURFACE: MULTIPLE-SCALE EXPERIMENTAL STUDIES

BY

NANXI LV

DISSERTATION

Submitted in partial fulfillment of the requirements
for the degree of Doctor of Philosophy in Environmental Engineering in Civil Engineering
in the Graduate College of the
University of Illinois at Urbana-Champaign, 2014

Urbana, Illinois

Doctoral Committee:

Associate Professor Thanh H. Nguyen, Chair, Director of Research
Research Assistant Professor Julie L. Zilles, Co-Director of Research
Professor Charles J. Werth
Professor Albert J. Valocchi
Professor Tim R. Ginn, University of California, Davis

ABSTRACT

Horizontal gene transfer rapidly changes bacterial genetic repertoire and contributes to bacterial evolution. Natural transformation, one mechanism of horizontal gene transfer, is defined as the process by which bacterial cells successfully take up and incorporate extracellular DNA. The extracellular DNA and the bacterial cells are both exposed to various environmental conditions that may alter natural transformation. Bacterial fate and transport in the subsurface may influence bacterial transformation with adsorbed DNA on surfaces.

The objectives of this thesis were to investigate the physicochemical and biological factors affecting the extracellular DNA-bacterial cell interaction and the natural transformation, with a long-term goal of modelling and assessing natural transformation in the environment. This thesis developed experimental approaches to systematically study natural transformation with the model strain *Azotobacter vinelandii*. The systematic experimental approaches consisted of quartz crystal microbalance with dissipation (QCM-D) and Fourier transform infrared spectroscopy (FTIR) for measuring extracellular DNA adsorption and the conformation of the attached NOM on top of adsorbed DNA layer on model soil surfaces, a multi-scale approach for understanding bacterial fate and transport including the use of radial stagnation point flow (RSPF) cells, two-dimensional micromodels, and column experiments, and transformation assays for quantifying the natural transformation. The most important findings of this research are the following: 1) adsorbed DNA transforms bacterial cells in the presence of natural organic matter; 2) flagella affect the dynamics of bacterial deposition and swimming motility reduces bacterial deposition; 3) natural transformation kinetics depend on availability of transforming DNA; 4) extracellular DNA transforms both swimming and swimming-impaired *A. vinelandii* cells similarly. This work provided supporting evidences in addressing the environmental significance of natural transformation and quantified the transformation rates with the model organism *A.vinelandii*.

To my parents, Jinchun Lv and Wenting Ouyang

ACKNOWLEDGEMENTS

I would like to express my sincere gratitude to my advisor, Dr. Thanh H. (Helen) Nguyen and co-advisor Dr. Julie L. Zilles, for their dedicated mentoring, valuable advices, constant support, and immense patience during my Ph.D. study. I thank them for helpful advice on being a professional researcher and all that they have done for me during the past years. I especially want to thank Dr. Nguyen for her sound guidance and unflinching encouragement over the years and the opportunities and resources she provided me to explore the new technologies and unknown territories. I appreciate Dr. Zilles for providing me perspectives and knowledge of microbiology to enrich my study. She continually stimulated my critical thinking skills and provided skillful comments and helpful advices. I would like to thank the committee members, Dr. Charles J. Werth and Dr. Albert J. Valocchi, and Dr. Tim R. Ginn, for their insights and inputs in the field of transport. It is my great pleasure and privilege to communicate with them in both research and classes. I am very grateful for their dedication to serving on my committee, for their insightful comments and suggestions, and for their scientific and critical thinking that helped me improve this dissertation.

Never enough thank you for Nugyen and Zilles group members. I will forever cherish the time that we spend together in the lab as well as celebrating each achievements. I greatly thank my collaborators, Dr. Arash Massoudieh, Xiaomeng Liang, Dr. Tamir Kamai, Dr. Changyong Zhang, Dr. Dehong Hu, Dr. Rong Kang, Dr. Rohit Bhargava, and Dr. Steven E. Mylon for many helpful discussions in the research. I want to express my deep gratitude to Dr. Vernon L. and Jeannie M. Snoeyink, who have always been there to share with me great wisdom and pleasure. I appreciate Dr. Shaoying Qi, our lab manager, for his dutifully maintenance of the lab. I thank all the fellows in the Department of Civil and Environmental Engineering who made my study here a wonderful experience. I thank all my friends who shared my life and encouraging me moving forward.

I give my deepest gratitude to my parents, Jinchuan Lv and Wenting Ouyang, my fiancé, Dr. Yihong Wu, and my family for their unconditional love, understanding and supports.

Finally, I acknowledge National Science Foundation (NSF), the Center of Advanced Materials for the Purification of Water with Systems under the National Science Foundation (Water CAMPWS), and Environmental Molecular Sciences Laboratory (EMSL) sponsored by the DOE, Office of Biological and Environmental Research and located at PNNL.

TABLE OF CONTENTS

CHAPTER 1

INTRODUCTION

1.1 Background

1.1.1 Horizontal gene transfer

Horizontal gene transfer (HGT) enables a genetic communication between bacterial cells from heredity.[1] HGT affects our perceptions on evolutionary biology in the various levels, especially within its major component, the microbes. At the cellular level, microbes obtain new genetic traits from the surrounding environment and express the new genetic functions as conditions permit. Genetic studies provided ample evidence that some transferrable genetic traits rendered the transformed microbes more adaptable to the environment.[2-4] Environmental stressors are considered as one of the major factors affecting HGT.[3] The environmental stressors, including UV,[5] heavy metal,[5, 6] and antibiotics,[5, 7, 8] apply pressures to the microbes and potentially increase the rates of HGT. HGT contributed to antibiotic resistance dissemination in different bacterial strains.[9, 10] Resistances to several classes of antibiotics were identified in various human habituated non-pathogenic and pathogenic bacteria due to HGT (**Table 1**).[11] The rise of multi-drug resistant pathogenic bacteria, "superbugs", was declared as a serious worldwide threat by WHO and is causing great harm to public health. At the population level, bacterial cells response to environmental changes and change the functional and composition dynamics within and between populations.[12, 13] At the taxonomic level, gene sequencing studies strongly implied genetic communications among the three domains of life.[2, 4, 14] The discussion has also been initiated on that is it HGT evolves three domains of life gradually or with the growing knowledge on HGT processes and others, should we reconsider or reconstruct the domains of life and the taxonomy?[14]

The three major HGT mechanisms are conjugation (gene exchange through plasmids), transformation (gene exchange through extracellular DNA) and transduction (virus or phages transferring the gene). Until now, there was no solid evidence on the relative significance of the

three mechanisms in HGT. The transformation mechanism encourages special interests from environmental engineers because of two specific reasons. First, both extracellular DNA and living cells involved in this mechanism are subjected to variable environmental factors that may or may not have a substantial impact on transformation. Second, extracellular DNA was found to be persistent as adsorbed form on surfaces and remain transformable to re-enter the biota in the subsurface environment.[15] Extracellular DNA with potential risks needs to be understood, monitored and handled with care.

Table 1 HGT contributed to the occurance of following antibiotic resistance in the strains.

Antibiotics	Strains	Pathogenicity	Ref.
β-lactams	*Staphylococcus aureus, Staphylococcus epidermidi, Staphylococcus haemolyticus*	Yes	[16, 17]
Aminoglycosides	*Staphylococcus aureus, Enterococcus* species	Yes and No	[17, 18]
Fluoroquinolones	*Eschicheria coli, Klebsiella* spp (*K. pneumoniae* and *K. oxytoca*), *Enterobacter* spp (*E. cloacae, E. amnigenus,* and *E. sakazakii*), *Citrobacter freundii,* and *Providencia stuartii*	Yes and No	[19]
Glycopeptides	*Enterococcus faecium, Enterococcus faecalis*	Yes	[20]
Macrolides	*Streptococcus pneumoniae*	Yes	[21]
Tetracyclines	*Streptococcus intermediu, Campylobacter sp., Enterococcus sp., Streptococcus sp. (S. pyogenes* and *S. pneumoniae, Enterococcus faecali*	Yes	[22]

1.1.2 Adsorbed DNA in the subsurface

DNA adsorption to surfaces protects it from enzymatic degradation and results in its persistence in the soil.[15, 23, 24] Extracellular DNA makes up to 9-13% and 53% of extracted P in the tundra and natural wetland soil, respectively and ranges from 20 to 207 μg/g soil in various

samples.[24] The persistence of DNA various according to the surrounding environment and goes up to years.[24] DNA has affinity to various soil constituents, including hydrophobic clay and sand minerals and hydrophilic humic acids and is consequently protected from enzymatic degradation.[23] Physicochemical factors, especially the size and conformation of DNA molecules, mineralogy, hydrophobicility or/and hydrophilicity of soil components, and pH and ionic composition of the surrounding fluids, control DNA-soil surfaces interactions.[23] The main mechanism for adsorbed DNA protection was proposed to be the adsorption of nucleases by the surface materials and thus physically separation of adsorbed DNA and nucleases.[25]

1.1.3 Adsorbed DNA transformation

The fact that soil surface associated DNA maintains the ability to pass the genetic information to other species after its survival from enzymatic degradation for a prolonged period of time has encouraged numerous work on adsorbed DNA transformation.[26] This transformibility of surface associated DNA was tested in a range of naturally competent bacterial species in the soil.[26-41] Considerable evidence confirmed the adsorbed DNA transformation with *Acinetobacter calcoaceticus*[27-29], *Azotobacter vinelandii*[30-32], *Bacillus subtilis*[26, 33-38, 42], and *Pseudomonas stutzeri*[39-41]. The efforts were to replicate the natural environmental conditions where natural DNA exists, adsorbs to surfaces and transforms different bacterial species, including soil grains[28, 41], clay minerals[26, 43, 44], sediments[28, 33, 37, 42] and humic acids[45, 46], and study transformation under environmental influences, and provide assessment on the significance of adsorbed DNA transformation in the environment.

However, the focus was the transformation outcome instead the interaction between the environmental factors and the adsorbed DNA and more importantly, there was no documented work on the kinetic rate model of natural transformation, especially with adsorbed DNA transformation.

1.1.4 Bacterial fate and transport in the subsurface

Understanding and predicting bacterial transport in subsurface is important for protecting water resources from bacterial pathogens, improving *in-situ* bioremediation performances, and

conducting risk assessments of natural transformation related to antibiotic resistance and pathogenicity in the subsurface.

On one hand, classical colloidal filtration theory (CFT) has been providing an arguably appropriate framework for evaluating and modeling laboratory and field-scale microbial fate and transport in the porous media. The microbial transport and the related processes were carefully reviewed in several work.[47-49] The framework of modeling used to describe physicochemical processes in bacterial fate and transport in the subsurface was summarized by Murphy and Ginn.[47] The framework considered both the bacterial transport with flow and bacterial mass exchange between aqueous and solid phases as well as several different mechanisms during the two processes.[49]

On the other hand, profound deviations of bacterial transport from the existing models have promoted insightful research into the roles of specific bacterial characteristics in the fate and transport. The deviations can be classified into two groups, 1) the inaccuracy of the model parameters in the reproducing experimental observation of the processes and 2) the inadequacy of the model structures in capturing and predicting the processes. The attachment (α) and collision (η) coefficients and the blocking effect (simplified as $\frac{(C_{im}^{max}-C_{im})}{C_{im}^{max}}$, C_{im}^{max} stands for maximal surface attaching ability, C_{im} accounts for the amount/concentrations of cells attached) were apparently more complex to determine in the microbial fate and transport systems.[49-51] The simplification of the existing models from biological processes and biological properties guaranteed a convenient and easy application from abiotic colloids to microbes but was also proved ineffective in capturing the real microbial fate and transport. The effects of microbial growth and death, heterogeneous and dynamic microbial characteristics, random motility and chemotaxis were often discussed.[51-54] We followed with detailed discussion on the role of motility and flagella in the fate and transport in next section.

1.1.5 Flagella and swimming motility in bacterial transport

Physical transport models, such as radial stagnation point flow cells (RSPF) [51, 55], parallel flow chambers [56, 57] and pack-bed columns with glass beads [55, 58, 59], subsurface sediments [60] or real soil [61] were employed to investigate the effect of motility on bacterial transport in subsurface. In general, attachment-detachment kinetics determined transport of motile and non-

motile bacteria. In most of the studied conditions, motile bacteria showed higher attachment to soil surfaces than non-motile bacteria, indicating longer transport distance for non-motile bacteria. Specifically, attachment rate coefficient was found to be a better predictor for bacteria transport for it considers the influences of bacterial characteristics and hydrodynamics.[58] Higher attachment rate coefficients for motile bacteria compared to non-motile strains were reported in a number of studies.[51, 55, 56, 58, 59] De Kerchove and Elimelech hypothesized the higher deposition was due to lower blocking effects and higher surface coverage from motile bacteria.[51] However, attachment-detachment kinetics changed with varying environmental conditions. For example, higher temperature led to higher motility and as a result, more detachment was observed.[60] In addition, swimming bacteria were observed to avoid attachment at low fluid velocity while enhanced attachment was observed at higher fluid velocity.[41, 45] While the importance of bacterial motility on attachment and detachment has been recognized, a comprehensive study using multiple-scale tools has not been conducted to relate bacteria motility to macroscopic bacteria transport.

Bacterial movement near solid surfaces has been well studied both in the absence and presence of advective flow field. Distinctive appendage-specific motility was found to control bacteria movement near or on surfaces.[62] Flagella dependent motility assisted attachment by flagellar rotation, and flagellated bacteria slowed down close to the surfaces and tended to move parallel along the surfaces.[63-66] The parallel movement along the surfaces was considered as the trapping of swimming bacteria by hydrodynamic forces[66] and was predicted by hydrodynamic models.[67] Upstream swimming of *E.coli* was also attributed to hydrodynamic surface interaction.[68] Gibiansky et al. developed an approach combining microscope and tracking methods by imaging every *P. aeruginosa* cell and extracting motility information from cell trajectories to build a searchable database. Using this database, they observed multiple motility behaviors including flagella mediated movements and type IV pili mediated crawling and walking upright on the surfaces. In addition, they identified cooperation between distinct motility appendages of bacteria during transition from planktonic to surface-associated states.[62, 69, 70] Despite the extensive studies of bacterial motility and movement near surfaces, there were few attempts linking this knowledge to bacterial transport. De Kechove et al. hypothesized that bacterial upstream swimming increased collector surface coverage.[51] Narayanaswamy et al.[71] and

Liu et al.[72] used motile bacteria surface association (i.e. idling time) to explain bacterial deposition and transport in packed bed columns and to develop mathematical models.

However, direct observation of attachment-detachment kinetics to explain the relationship between bacteria motility near surface and bacteria transport in porous media is missing. Moreover, bacteria, even though understood as one important role in the process of natural transformation, the bacterial fate and transport in the soil and subsurface, related to bacterial interaction with surface adsorbed DNA, has not been examined in relevance to natural transformation.

1.1.6 Soil bacterium *Azotobacter vinelandii*

A. vinelandii is an aerobic, soil indigenous, gram-negative bacterium. The bacterial cells can adapt to a variety of nutritional conditions. Depending on the availability of carbon source and other cultural conditions, *A. vinelandii* can go into Encystment.[73] Wild-type *A.vinelandii* is a diazotroph able to fix atmospheric nitrogen and manufacture from the inorganic nitrogen to organic nitrogen for life supplement. Three nitrogenases with different subunit and metal cofactor compositions, namely, the molybdenum nitrogenase, the vanadium nitrogenase, and the iron-only nitrogenase were identified and the related genetic systems were extensively studied.[74, 75] The development and regulation of the three nitrogenases depends on the metal configuration in the nutrients. [59]

A. vinelandii is naturally competent for DNA uptake. Unlike many model organisms used in studying competence, it does not require specific sequences for DNA uptake,[76] increasing the potential for gene transfer between different types of microorganisms. The growth conditions inducing competence have been extensively studied and were well documented for *A. vinelandii* (e.g. [77-79]). An extensive review by Lorenz and Wackernagel[15] listed transformation frequencies ranging from 10^{-9} to 10^{-2}. For example, the cell growth conditions (in particular limiting iron and molybdenum) were able to promote the development of competence.

Wild-type *A. vinelandii* is described as motile with peritrichious flagella. There was one study focusing on *A.vinelandii* motility to search for the flagella regulon in the *A.vinelandii* genome. Inactivation of *flhDC* and subsequent imaging for the loss of flagella and semi-quantitative agar plate testing (for the loss of motility indicated the *flhDC* regulated flagella

biogenesis.[80] To our knowledge, there is no other literature documenting *A.vinelandii* motility and its implication on *A.vinelandii* fate and transport in the subsurface.

1.2 Overview of the Objectives

The overall objective of this work is to investigate the physicochemical and biological factors affecting the bacterial cells and the extracellular DNA interaction and the resulting natural transformation. The results of this study will improve the understanding of bacteria transport and horizontal gene transfer and assist the modelling and assessing natural transformation in the subsurface. In this work, we initiated with a thorough study on adsorbed DNA transformation of *A.vinelandii* in the presence of NOM. The roles of bacterial flagella and motility on *A.vinelandii* transport in the subsurface environment were studied through multiple-scale physical models ranging from radial stagnation point flow cells, to two-dimensional micromodels to three-dimensional bench scale columns. The factors controlling horizontal gene transfer were tested in the natural transformation assays. Our knowledge gained on horizontal gene transfer in the subsurface will provide a basis for risk assessment of agricultural bacterial contamination. Specifically, the objectives of this project are:

Objective 1: to understand extracellular DNA interaction with model soil surfaces in the presence of NOM and to investigate the natural transformation with adsorbed DNA under environmentally relevant conditions;

Objective 2: to determine the role of bacterial flagella on *A.vinelandii* deposition dynamics and elucidate transport mechanisms in multiple-scale physical models;

Objective 3: to determine the role of swimming motility on bacterial fate and transport in multiple-scale physical models and elucidate transport mechanisms;

Objective 4: to link the frequency and rate of horizontal gene transfer with bacterial fate and transport and to establish a quantitative model to evaluate natural transformation rates in the subsurface.

1.3 Experimental Approach

The dissolved NOM interaction and attachment to adsorbed DNA layer on model soil surfaces were studied by the complimentary tools including quartz crystal microbalance with dissipation (QCM-D) and Fourier transformed infrared spectroscopy (FTIR). QCM-D was used to study the kinetics of dissolved NOM attachment to adsorbed DNA on the surfaces. The application of FTIR on dissolved and adsorbed DNA in the absence/presence of NOM was to reveal the specific binding mechanisms between DNA and the surfaces.

A multiple-scale study, including a pack-bed column with glass spheres for 3-dimensional transport processes, a 2-dimensional (2-D) pore structure micromodel and a radial stagnation point flow (RSPF) cell, was conducted to investigate physicochemical and biological factors on bacterial fate and transport mechanisms in the porous media (**Figure 1**). Pack-bed column studies replicate transport phenomena in the subsurface more realistically but lack of microscopic information. Both the RSPF cell and the micromodel provide real time microscopic observation of bacterial transport. The RSPF cell, as the most simplified flow cells for subsurface environment, pinpoints a specific surface region of interests and gives more flexibility in surface modification and hydrodynamic control.

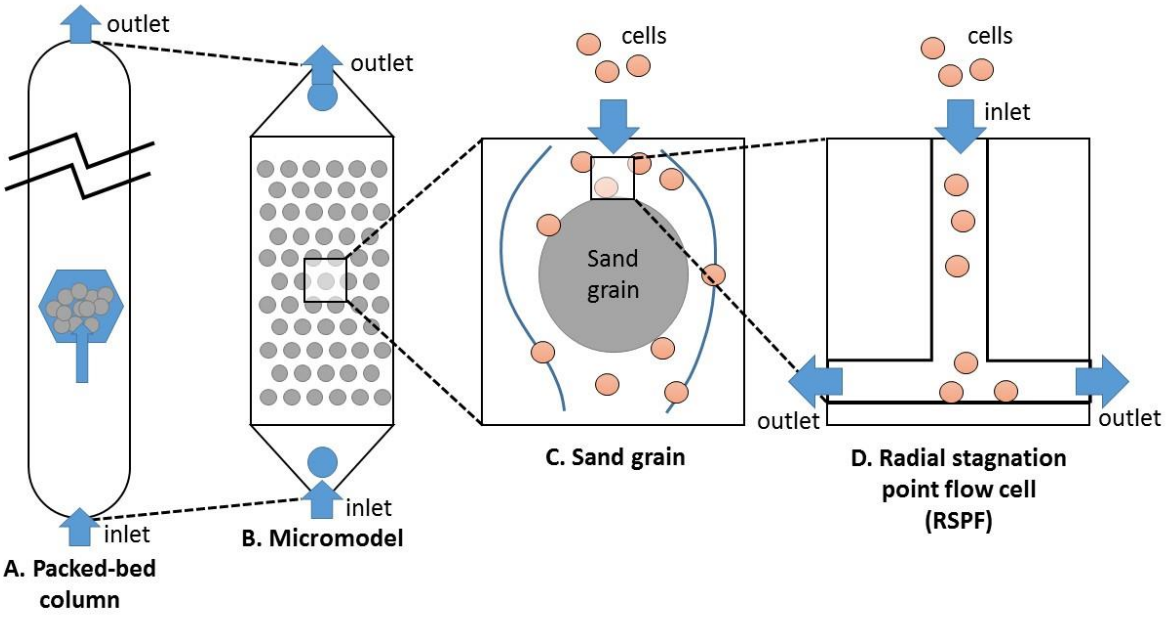

Figure 1 Outline of the multiple-scale physical model setups. A) Column setup mimics the 3D porous media composition; B) micromodel depicts 2D porous media; C) the scheme of a single sand grain encounters bacterial cells; D) radial stagnation point flow (RSPF) cell shows the deposition at forward stagnation point region.

Natural transformation assays with *A.vinelandii* were performed using the selective media approach. Either auxotrophic complementation (nitrogen fixing function) or antibiotic resistance (tetracycline resistance) was used as selection markers. Auxotrophic selection has relevance to the nutritional conditions in the natural environment and antibiotic resistance is attributed to the spreading of elevated levels of antibiotic resistance gene into the soil by manure application.

1.4 Dissertation Organization

In Chapter 2, the adsorbed chromosomal transformation of *A.vinelandii* cells was studied under environmentally relevant conditions. The adsorption kinetics of dissolved NOM onto adsorbed chromosomal DNA on the model soil surfaces was measured by QCM-D. QCM-D recorded information for modeling and computing the mass of the thin deposited NOM layer (nm level) under the environmentally relevant conditions. The transformability of adsorbed DNA

with *A.vinelandii* cells under different conditions was tested systematically using natural transformation assays.

The results indicated that adsorbed DNA under different conditions transformed *A.vinelandii* at similar frequencies as compared to dissolved DNA. The facts that the presence of NOM did not disrupt natural transformation led us to redirect our attention to the competent bacterial cells (able to take up extracellular DNA) in this thesis. The following Chapter 3 and 4 elaborate on our findings with bacterial fate and transport in the subsurface.

In Chapter 3, the role of flagella in the bacterial fate and transport was investigated using pack-bed column setups combined with step-wise modeling to identify the important mechanisms. The characteristic deposition with flagellated bacterial cells in the columns were also compared to those in the RSPF cells and micromodels.

In Chapter 4, we employed a combination of bacterial strains with strong swimming motility, impaired swimming motility and no swimming motility to investigate the effect of motility on bacterial transport with respect to surface attachment. Micromodel setup and the RSPF flow cells together provided real-time microscopic monitoring of fate and transport with different bacterial strains. Micromodels were used to evaluate bacterial transport in 2D porous media and to investigate the deposition locations. The RSPF flow cells with well-controlled hydrodynamics and monitoring measures were used to further investigate the mechanisms by which swimming motility affected bacterial fate and transport.

From the above work, we found that the fate and transport of *A.vinelandii* in the porous media was affected by both flagella and swimming motility. We therefore took a step further to connect horizontal gene transfer and bacterial swimming motility.

In Chapter 5, we linked transformation rate with swimming motility experimentally and aimed at building up the natural transformation rate model and investigating whether having swimming motility would result in a different rate model or only different model parameters. The modeling work conducted through collaboration is documented in the Appendix for reference.

The main findings and contribution of this research are summarized in the last chapter, Chapter 6. Future work is also suggested in the same chapter.

The work in Chapter 2 and 3 have been published. The work in Chapter 4 was recently submitted and the work in Chapter 5 will be submitted soon.

1.5 References

1. Thomas, C. M.; Nielsen, K. M., Mechanisms of, and Barriers to, Horizontal Gene Transfer between Bacteria. *Nature Reviews Microbiology* **2005,** *3*, (9), 711-721.
2. Chia, N.; Goldenfeld, N., Statistical Mechanics of Horizontal Gene Transfer in Evolutionary Ecology. *Journal of Statistical Physics* **2011,** *142*, (6), 1287-1301.
3. Aminov, R. I., Horizontal Gene Exchange in Environmental Microbiota. *Frontiers in Microbiology* **2011,** *2*.
4. Polz, M. F.; Alm, E. J.; Hanage, W. P., Horizontal Gene Transfer and the Evolution of Bacterial and Archaeal Population Structure. *Trends in Genetics* **2013,** *29*, (3), 170-175.
5. Beaber, J. W.; Hochhut, B.; Waldor, M. K., Sos Response Promotes Horizontal Dissemination of Antibiotic Resistance Genes. *Nature* **2004,** *427*, (6969), 72-74.
6. Martinez, R. J.; Wang, Y.; Raimondo, M. A.; Coombs, J. M.; Barkay, T.; Sobecky, P. A., Horizontal Gene Transfer of Pib-Type Atpases among Bacteria Isolated from Radionuclide- and Metal-Contaminated Subsurface Soils. *Applied and Environmental Microbiology* **2006,** *72*, (5), 3111-3118.
7. Úbeda, C.; Maiques, E.; Knecht, E.; Lasa, Í.; Novick, R. P.; Penadés, J. R., Antibiotic-Induced Sos Response Promotes Horizontal Dissemination of Pathogenicity Island-Encoded Virulence Factors in *Staphylococci*. *Molecular Microbiology* **2005,** *56*, (3), 836-844.
8. Maiques, E.; Úbeda, C.; Campoy, S.; Salvador, N.; Lasa, Í.; Novick, R. P.; Barbé, J.; Penadés, J. R., B-Lactam Antibiotics Induce the Sos Response and Horizontal Transfer of Virulence Factors in *Staphylococcus aureus*. *Journal of Bacteriology* **2006,** *188*, (7), 2726-2729.
9. Davies, J., Inactivation of Antibiotics and the Dissemination of Resistance Genes. *Science* **1994,** *264*, (5157), 375-382.
10. Martínez, J. L., Antibiotics and Antibiotic Resistance Genes in Natural Environments. *Science* **2008,** *321*, (5887), 365-367.
11. Barlow, M., What Antimicrobial Resistance Has Taught Us About Horizontal Gene Transfer. In *Horizontal Gene Transfer*, Springer: 2009; pp 397-411.
12. Gogarten, J. P.; Townsend, J. P., Horizontal Gene Transfer, Genome Innovation and Evolution. *Nature Reviews Microbiology* **2005,** *3*, (9), 679-687.

13. Andam, C. P.; Fournier, G. P.; Gogarten, J. P., Multilevel Populations and the Evolution of Antibiotic Resistance through Horizontal Gene Transfer. *FEMS Microbiology Reviews* **2011,** *35*, (5), 756-767.

14. Syvanen, M., Evolutionary Implications of Horizontal Gene Transfer. *Annual Review of Genetics* **2012,** *46*, (1), 341-358.

15. Lorenz, M. G.; Wackernagel, W., Bacterial Gene Transfer by Natural Genetic Transformation in the Environment. *Microbiological Reviews* **1994,** *58*, (3), 563-602.

16. Hanssen, A.-M.; Ericson Sollid, J. U., Sccmec in *Staphylococci*: Genes on the Move. *FEMS Immunology & Medical Microbiology* **2006,** *46*, (1), 8-20.

17. Pantosti, A.; Sanchini, A.; Monaco, M., Mechanisms of Antibiotic Resistance in *Staphylococcus aureus*. *Future Microbiology* **2007,** *2*, (3), 323-334.

18. Shakil, S.; Khan, R.; Zarrilli, R.; Khan, A., Aminoglycosides Versus Bacteria-a Description of the Action, Resistance Mechanism, and Nosocomial Battleground. *Journal of Biomedical Science* **2008,** *15*, (1), 5-14.

19. Robicsek, A.; Jacoby, G. A.; Hooper, D. C., The Worldwide Emergence of Plasmid-Mediated Quinolone Resistance. *The Lancet infectious diseases* **2006,** *6*, (10), 629-640.

20. Willems, R. J.; Bonten, M. J., Glycopeptide-Resistant *Enterococci*: Deciphering Virulence, Resistance and Epidemicity. *Current Opinion in Infectious Diseases* **2007,** *20*, (4), 384-390.

21. Roberts, M., Resistance to Macrolide, Lincosamide, Streptogramin, Ketolide, and Oxazolidinone Antibiotics. *Molecular Biotechnology* **2004,** *28*, (1), 47-62.

22. Roberts, M. C., Update on Acquired Tetracycline Resistance Genes. *FEMS Microbiology Letters* **2005,** *245*, (2), 195-203.

23. Pietramellara, G.; Ascher, J.; Borgogni, F.; Ceccherini, M. T.; Guerri, G.; Nannipieri, P., Extracellular DNA in Soil and Sediment: Fate and Ecological Relevance. *Biology and Fertility of Soils* **2009,** *45*, (3), 219-235.

24. Levy-Booth, D. J.; Campbell, R. G.; Gulden, R. H.; Hart, M. M.; Powell, J. R.; Klironomos, J. N.; Pauls, K. P.; Swanton, C. J.; Trevors, J. T.; Dunfield, K. E., Cycling of Extracellular DNA in the Soil Environment. *Soil Biology & Biochemistry* **2007,** *39*, (12), 2977-2991.

25. Cai, P.; Huang, Q. Y.; Zhang, X. W., Interactions of DNA with Clay Minerals and Soil Colloidal Particles and Protection against Degradation by DNase. *Environmental Science & Technology* **2006,** *40*, (9), 2971-2976.

26. Gallori, E.; Bazzicalupo, M.; Dalcanto, L.; Fani, R.; Nannipieri, P.; Vettori, C.; Stotzky, G., Transformation of *Bacillus subtilis* by DNA-Bound on Clay in Nonsterile Soil. *FEMS Microbiology Ecology* **1994,** *15*, (1-2), 119-126.

27. Nielsen, K. M.; vanWeerelt, M. D. M.; Berg, T. N.; Bones, A. M.; Hagler, A. N.; vanElsas, J. D., Natural Transformation and Availability of Transforming DNA to *Acinetobacter calcoaceticus* in Soil Microcosms. *Applied and Environmental Microbiology* **1997,** *63*, (5), 1945-1952.

28. Chamier, B.; Lorenz, M. G.; Wackernagel, W., Natural Transformation of *Acinetobacter calcoaceticus* by Plasmid DNA Adsrobed on Sand and Groundwater Aquifer Material. *Applied and Environmental Microbiology* **1993,** *59*, (5), 1662-1667.

29. Demaneche, S.; Jocteur-Monrozier, L.; Quiquampoix, H.; Simonet, P., Evaluation of Biological and Physical Protection against Nuclease Degradation of Clay-Bound Plasmid DNA. *Applied and Environmental Microbiology* **2001,** *67*, (1), 293-299.

30. Lu, N.; Zilles, J. L.; Nguyen, T. H., Adsorption of Extracellular Chromosomal DNA and Its Effects on Natural Transformation of *Azotobacter vinelandii*. *Applied and Environmental Microbiology* **2010,** *76*, (13), 4179-4184.

31. Goetsch, H. E.; Mylon, S. E.; Butler, S.; Zilles, J. L.; Nguyen, T. H., Oxytetracycline Interactions at the Soil–Water Interface: Effects of Environmental Surfaces on Natural Transformation and Growth Inhibition of *Azotobacter vinelandii*. *Environmental Toxicology and Chemistry* **2012,** *31*, (10), 2217-2224.

32. Lu, N.; Mylon, S. E.; Kong, R.; Bhargava, R.; Zilles, J. L.; Nguyen, T. H., Interactions between Dissolved Natural Organic Matter and Adsorbed DNA and Their Effect on Natural Transformation of *Azotobacter vinelandii*. *Science of the Total Environment* **2012,** *426*, 430-435.

33. Aardema, B. W.; Lorenz, M. G.; Krumbein, W. E., Protection of Sediment-Adsorbed Transforming DNA against Enzymitic Inactivation. *Applied and Environmental Microbiology* **1983,** *46*, (2), 417-420.

34. Lorenz, M. G.; Wackernagel, W., Adsorption of DNA to Sand and Variable Degradation Rates of Adsorbed DNA. *Applied and Environmental Microbiology* **1987,** *53*, (12), 2948-2952.

35. Lorenz, M. G.; Aardema, B. W.; Wackernagel, W., Highly Efficient Genetic Transformation of *Bacillus subtilis* Attached to Sand Grains. *Journal of General Microbiology* **1988,** *134*, 107-112.

36. Khanna, M.; Stotzky, G., Transformation of *Bacillus subtilis* by DNA Bound on Montmorillonite and Effect of Dnase on the Transforming Ability of Bound DNA. *Applied and Environmental Microbiology* **1992,** *58*, (6), 1930-1939.

37. Romanowski, G.; Lorenz, M. G.; Wackernagel, W., Plasmid DNA in a Groundwater Aquifer Microcosm - Adsorption, Dnase Resistance and Natural Genetic Transformaiton of *Bacillus Subtilis Molecular Ecology* **1993,** *2*, (3), 171-181.

38. Khanna, M.; Yoder, M.; Calamai, L.; Stotzky, G., X-Ray Diffractometry and Electron Microscopy of DNA from *Bacillus subtilis* Bound on Clay Minerals. *Sciences of Soils* **1998,** *3*, (1), 1-10.

39. Stewart, G. J.; Sinigalliano, C. D.; Garko, K. A., Binding of Exogenous DNA to Marine Sediments and the Effect of DNA/Sediment Binding on Natural Transformation of *Pseudomonas stutzeri* Strain Zobell in Sediment Columns. *FEMS Microbiology Ecology* **1991,** *85*, (1), 1-8.

40. Sikorski, J.; Graupner, S.; Lorenz, M. G.; Wackernagel, W., Natural Genetic Transformation of *Pseudomonas stutzeri* in a Non-Sterile Soil. *Microbiology-Sgm* **1998,** *144*, 569-576.

41. Lorenz, M. G.; Wackernagel, W., Natural Genetic Transformation of *Pseudomonas stutzeri* by Sand-Adsorbed DNA. *Archives of Microbiology* **1990,** *154*, (4), 380-385.

42. Lorenz, M. G.; Aardema, B. W.; Krumbein, W. E.; Wackernagel, W., Sediment-Adsorbed DNA-Stability of the Complex, Protection against Enzymatic Degradation and Transformation by *Bacillus subtilis*. *Systematic and Applied Microbiology* **1984,** *5*, (2), 279-279.

43. Paget, E.; Monrozier, L. J.; Simonet, P., Adsorption of DNA on Clay Minerals - Protection against DNase I and Influence on Gene Transfer *FEMS Microbiology Letters* **1992,** *97*, (1-2), 31-39.

44. Pietramellara, G.; Ascher, J.; Ceccherini, M. T.; Nannipieri, P.; Wenderoth, D., Adsorption of Pure and Dirty Bacterial DNA on Clay Minerals and Their Transformation Frequency. *Biology and Fertility of Soils* **2007,** *43*, (6), 731-739.

45. Crecchio, C.; Stotzky, G., Binding of DNA on Humic Acids: Effect on Transformation of *Bacillus subtilis* and Resistance to Dnase. *Soil Biology & Biochemistry* **1998,** *30*, (8-9), 1061-1067.

46. Crecchio, C.; Ruggiero, P.; Curci, M.; Colombo, C.; Palumbo, G.; Stotzky, G., Binding of DNA from *Bacillus subtilis* on Montmorillonite-Humic Acids-Aluminum or Iron Hydroxypolymers: Effects on Transformation and Protection against DNase. *Soil Science Society of America Journal* **2005,** *69*, (3), 834-841.

47. Murphy, E. M.; Ginn, T. R., Modeling Microbial Processes in Porous Media. *Hydrogeology Journal* **2000,** *8*, (1), 142-158.

48. Ginn, T. R.; Wood, B. D.; Nelson, K. E.; Scheibe, T. D.; Murphy, E. M.; Clement, T. P., Processes in Microbial Transport in the Natural Subsurface. *Advances in Water Resources* **2002,** *25*, (8–12), 1017-1042.

49. Tufenkji, N., Modeling Microbial Transport in Porous Media: Traditional Approaches and Recent Developments. *Advances in Water Resources* **2007,** *30*, (6-7), 1455-1469.

50. Tufenkji, N.; Elimelech, M., Correlation Equation for Predicting Single-Collector Efficiency in Physicochemical Filtration in Saturated Porous Media. *Environmental Science & Technology* **2003,** *38*, (2), 529-536.

51. de Kerchove, A. J.; Elimelech, M., Bacterial Swimming Motility Enhances Cell Deposition and Surface Coverage. *Environmental Science & Technology* **2008,** *42*, (12), 4371-4377.

52. Walker, S. L.; Redman, J. A.; Elimelech, M., Influence of Growth Phase on Bacterial Deposition: Interaction Mechanisms in Packed-Bed Column and Radial Stagnation Point Flow Systems†. *Environmental Science & Technology* **2005,** *39*, (17), 6405-6411.

53. Fontes, D. E.; Mills, A. L.; Hornberger, G. M.; Herman, J. S., Physical and Chemical Factors Influencing Transport of Microorganisms through Porous Media. *Applied and Environmental Microbiology* **1991,** *57*, (9), 2473-2481.

54. Ford, R. M.; Harvey, R. W., Role of Chemotaxis in the Transport of Bacteria through Saturated Porous Media. *Advances in Water Resources 30*, (6-7), 1608-1617.

55. Haznedaroglu, B. Z.; Zorlu, O.; Hill, J. E.; Walker, S. L., Identifying the Role of Flagella in the Transport of Motile and Nonmotile *Salmonella enterica* Serovars *Environmental Science & Technology* **2010,** *44*, (11), 4184-4190.

56. Mueller, R. F., Bacterial Transport and Colonization in Low Nutrient Environments. *Water Research* **1996,** *30*, (11), 2681-2690.

57. McClaine, J. W.; Ford, R. M., Characterizing the Adhesion of Motile and Nonmotile *Escherichia coli* to a Glass Surface Using a Parallel-Plate Flow Chamber. *Biotechnology and Bioengineering* **2002,** *78*, (2), 179-189.

58. Camper, A. K.; Hayes, J. T.; Sturman, P. J.; Jones, W. L.; Cunningham, A. B., Effects of Motility and Adsorption Rate Coefficient on Transport of Bacteria through Saturated Porous Media. *Applied and Environmental Microbiology* **1993,** *59*, (10), 3455.

59. Becker, M. W.; Collins, S. A.; Metge, D. W.; Harvey, R. W.; Shapiro, A. M., Effect of Cell Physicochemical Characteristics and Motility on Bacterial Transport in Groundwater. *Journal of Contaminant Hydrology* **2004,** *69*, (3-4), 195-213.

60. McCaulou, D. R.; Bales, R. C.; Arnold, R. G., Effect of Temperature-Controlled Motility on Transport of Bacteria and Microspheres through Saturated Sediment. *Water Resources Research* **1995,** *31*, (2), 271-280.

61. Camesano, T. A.; Logan, B. E., Influence of Fluid Velocity and Cell Concentration on the Transport of Motile and Nonmotile Bacteria in Porous Media. *Environmental Science & Technology* **1998,** *32*, (11), 1699-1708.

62. Conrad, J. C.; Gibiansky, M. L.; Jin, F.; Gordon, V. D.; Motto, D. A.; Mathewson, M. A.; Stopka, W. G.; Zelasko, D. C.; Shrout, J. D.; Wong, G. C. L., Flagella and Pili-Mediated near-Surface Single-Cell Motility Mechanisms. *Biophysical Journal* **2011,** *100*, 1608-1616.

63. Frymier, P. D.; Ford, R. M.; Berg, H. C.; Cummings, P. T., Three-Dimensional Tracking of Motile Bacteria near a Solid Planar Surface. *Proceedings of the National Academy of Sciences of the United States of America* **1995,** *92*, (13), 6195-6199.

64. Vigeant, M.; Ford, R., Interactions between Motile *Escherichia coli* and Glass in Media with Various Ionic Strengths, as Observed with a Three-Dimensional-Tracking Microscope. *Applied and Environmental Microbiology* **1997,** *63*, (9), 3474-3479.

65. McClaine, J. W.; Ford, R. M., Reversal of Flagellar Rotation Is Important in Initial Attachment of *Escherichia coli* to Glass in a Dynamic System with High- and Low-Ionic-Strength Buffers. *Applied and Environmental Microbiology* **2002,** *68*, (3), 1280-1289.

66. Vigeant, M. A.-S.; Ford, R. M.; Wagner, M.; Tamm, L. K., Reversible and Irreversible Adhesion of Motile *Escherichia coli* Cells Analyzed by Total Internal Reflection Aqueous Fluorescence Microscopy. *Applied and Environmental Microbiology* **2002,** *68*, (6), 2794-2801.
67. Lauga, E.; DiLuzio, W. R.; Whitesides, G. M.; Stone, H. A., Swimming in Circles: Motion of Bacteria near Solid Boundaries. *Biophysical Journal* **2006,** *90*, (2), 400-412.
68. Hill, J.; Kalkanci, O.; McMurry, J. L.; Koser, H., Hydrodynamic Surface Interactions Enable *Escherichia coli* to Seek Efficient Routes to Swim Upstream. *Physical Review Letters* **2007,** *98*, (6), 68101.
69. Jin, F.; Conrad, J. C.; Gibiansky, M. L.; Wong, G. C. L., Bacteria Use Type-Iv Pili to Slingshot on Surfaces. *Proceedings of the National Academy of Sciences* **2011**.
70. Gibiansky, M. L.; Conrad, J. C.; Jin, F.; Gordon, V. D.; Motto, D. A.; Mathewson, M. A.; Stopka, W. G.; Zelasko, D. C.; Shrout, J. D.; Wong, G. C. L., Bacteria Use Type Iv Pili to Walk Upright and Detach from Surfaces *Science* **2010,** *330*, (6001), 197-.
71. Narayanaswamy, K.; Ford, R. M.; Smith, J. A.; Fernandez, E. J., Surface Association of Motile Bacteria and Apparent Tortuosity Values in Packed Column Experiments. *Water Resources Research* **2009,** *45*, (7), W07411.
72. Liu, J.; Ford, R. M.; Smith, J. A., Idling Time of Motile Bacteria Contributes to Retardation and Dispersion in Sand Porous Medium. *Environmental Science & Technology* **2011**, in press.
73. Sadoff, H., Encystment and Germination in *Azotobacter vinelandii*. *Microbiology and Molecular Biology Reviews* **1975,** *39*, (4), 516.
74. Jacobson, M. R.; Brigle, K. E.; Bennett, L. T.; Setterquist, R. A.; Wilson, M. S.; Cash, V. L.; Beynon, J.; Newton, W. E.; Dean, D. R., Physical and Genetic Map Pf the Major Nif Gene Cluster from *Azotobacter vinelandii*. *Journal of Bacteriology* **1989,** *171*, (2), 1017-1027.
75. Setubal, J. C.; dos Santos, P.; Goldman, B. S.; Ertesvåg, H.; Espin, G.; Rubio, L. M.; Valla, S.; Almeida, N. F.; Balasubramanian, D.; Cromes, L.; Curatti, L.; Du, Z.; Godsy, E.; Goodner, B.; Hellner-Burris, K.; Hernandez, J. A.; Houmiel, K.; Imperial, J.; Kennedy, C.; Larson, T. J.; Latreille, P.; Ligon, L. S.; Lu, J.; Mærk, M.; Miller, N. M.; Norton, S.; O'Carroll, I. P.; Paulsen, I.; Raulfs, E. C.; Roemer, R.; Rosser, J.; Segura, D.; Slater, S.; Stricklin, S. L.; Studholme, D. J.; Sun, J.; Viana, C. J.; Wallin, E.; Wang, B.; Wheeler, C.; Zhu, H.; Dean, D. R.; Dixon, R.; Wood, D., Genome Sequence of *Azotobacter vinelandii*, an Obligate Aerobe

Specialized to Support Diverse Anaerobic Metabolic Processes. *Journal of Bacteriology* **2009,** *191*, (14), 4534-4545.

76. Renaud, C. S.; Pasternak, J.; Glick, B. R., Integration of Exogenous DNA into the Genome of *Azotobacter vinelandii*. *Archives of Microbiology* **1989,** *152*, (5), 437-440.

77. Page, W. J., Optimal Conditions for Induction of Competence in Nitrogen-Fixing *Azotobacter vinelandii*. *Canadian Journal of Microbiology* **1982,** *28*, (4), 389-397.

78. Page, W. J.; Grant, G. A., Effect of Mineral Iron on the Development of Transformation Competence in *Azotobacter vinelandii*. *FEMS Microbiology Letters* **1987,** *41*, (3), 257-261.

79. Page, W. J.; von Tigerstrom, M., Induction of Transformation Competence in *Azotobacter vinelandii* Limited Cultures. *Canadian Journal of Microbiology* **1978,** *24*, (12), 1590-1594.

80. León, R.; Espín, G., Flhdc, but Not Fleq, Regulates Flagella Biogenesis in *Azotobacter vinelandii*, and Is under Algu and Cydr Negative Control. *Microbiology* **2008,** *154*, (6), 1719.

CHAPTER 2

INTERACTIONS BETWEEN DISSOLVED NATURAL ORGANIC MATTER AND ADSORBED DNA AND THEIR EFFECTS ON NATURAL TRANSFORMATION OF *AZOTOBACTER VINELANDII*

Published:

Nanxi Lu, Steven E. Mylon, Rong Kong, Rohit Bhargava, Julie L. Zilles, Thanh H. Nguyen, Interactions between dissolved natural organic matter and adsorbed DNA and their effect on natural transformation of *Azotobacter vinelandii*, *Science of The Total Environment*, Volume 426, 1 June 2012, Pages 430-435, ISSN 0048-9697.

Contribution: I have conducted and analyzed all the experiments presented in this chapter except for the data collection of adsorbed DNA on beads from TEM and energy-dispersive X-ray spectroscopy and the data acquisition and analysis of FTIR experiments.

2.1 Abstract

To better understand gene transfer in the soil environment, the interactions between dissolved natural organic matter (NOM) and chromosomal or plasmid DNA adsorbed to silica surfaces were investigated. The rates of NOM adsorption onto silica surfaces coated with DNA were measured by quartz crystal microbalance (QCM) and showed a positive correlation with carboxylate group density for both soil and aquatic NOM in solutions containing either 1 mM Ca^{2+} or Mg^{2+}. Increasing total dissolved organic carbon (DOC) concentrations of the NOM solution also resulted in an increase in the adsorption rates, likely due to divalent cation complexation with NOM carboxylate groups and the phosphate backbone of the DNA. The results from Fourier transform infrared spectroscopy (FTIR) for dissolved DNA and DNA adsorbed on silica beads also suggest that adsorption may result from divalent cation complexation with the DNA's phosphate backbone. The interactions, between DNA and NOM, however, did not influence natural transformation of *Azotobacter vinelandii* by DNA. These results suggest that DNA adsorbed to NOM-coated silica or otherwise complexed with NOM remains available for natural transformation in the environment.

2.2 Introduction

Horizontal gene transfer can decrease or increase environmental contamination through its effects on microbial communities and their rates of adaptation to changes in their environments.[1, 2] For example, both the ability to degrade chemical pollutants and resistance to antimicrobials have been known to develop and disseminate through horizontal gene transfer.[3, 4] Recent studies have suggested to include ecological exposure to human and animal antimicrobial drugs in risk assessment framework.[5, 6] A more complete understanding of the physical, chemical, and biological factors that control horizontal gene transfer in the environment is likely to suggest new techniques for predicting and controlling contamination.

One mechanism of horizontal gene transfer, natural transformation, requires the uptake of extracellular DNA.[1, 7] This mechanism was not originally considered important within soil environments due to the presence of DNA-degrading enzymes.[8] However, there is now compelling evidence for the recalcitrance of DNA resulting from the adsorption to common soil components.[8] Furthermore, from the pioneering work of Lorenz, Aardema, and Wackernagel [9, 10]

and subsequent studies (e.g. [11-14]), it is apparent that DNA adsorbed to sand, clay minerals, humic acids, and soils remains available for transformation. To understand the role natural transformation plays in the evolution and adaptation of soil microbial communities, the factors that control DNA adsorption and the efficiency of natural transformation by adsorbed DNA need to be characterized. In the current work we focus on the impact of a common soil component, natural organic matter (NOM)[8] on adsorbed DNA and its effect on natural transformation.

The adsorption of DNA to soil particles, including clay minerals and silica substances, may be controlled by van der Waals interactions, electrostatic interactions, and/or cation bridging.[15-18] Atomic force microscope imaging and both Monte Carlo and molecular dynamics simulations revealed the roles of van der Waals and electrostatic interactions on deposition of linear plasmid DNA fragments on charged mica surfaces.[15] Low temperature scanning electron microscopy measurements showed a compact conformation of linear chromosomal DNA in 5 mM Ca^{2+} solution. Resulting from the suppression of the double layer interactions, there was increased contact area between DNA and clay minerals.[18] A model that included long-range van der Waals forces and double-layer interactions accurately described the adsorption of linear plasmid DNA fragments onto mica.[15]

Other studies specifically considered the mechanisms of adsorption of DNA to soil or NOM.[8, 11, 19-21] Electrostatic interactions were found to control plasmid DNA adsorption to humic substances[8] and NOM-coated silica surfaces.[16, 17] Spectral data obtained using Fourier transform infrared spectroscopy (FTIR) suggested that the DNA phosphate backbone involved in DNA adsorption onto clay minerals or humic acids.[11, 19] Specific binding of Ca^{2+} between DNA phosphate groups and surface charge groups of silica minerals was proposed to explain the strong and irreversible adsorption of plasmid DNA on silica or NOM-coated surfaces measured by quartz crystal microbalance (QCM).[16, 20] In other work, the adsorption of chromosomal or plasmid DNA was controlled by ionic strength and the presence of divalent cations, due to charge screening and cation bridging respectively.[16, 21]

Although the effects of interactions between adsorbed DNA and dissolved unfractionated NOM on natural transformation have not, to our knowledge, been studied, one component of NOM, humic acids, has been studied. DNA bound to humic substances or to mixtures of montmorillonite-humic acid enriched with either Al or Fe transformed competent *Bacillus subtilis*, although the frequency of transformation was 10 times lower than for free DNA.[12, 13]

The addition of 5% humic acid to chromosomal DNA led to an average of 32% reduction in transformation frequency for *Acinetobacter* sp. strain BD413, but again did not eliminate transformation.[22] The frequency of heat shock transformation for *Escherichia coli* DH5α also decreased from 10^{-2} to 10^{-6} as the concentration of humic acid increased from 0.01 mg/L to 100 mg/L.[14] This last study may not be directly comparable to natural transformation experiments, because the mechanism of DNA uptake in artificial heat shock transformation is not known and is likely to be different than that used in natural transformation.[23, 24] However, all of these studies indicate that NOM has the potential to attenuate the rate of natural transformation.

The objectives of this work were to study the interactions of dissolved NOM with adsorbed DNA and to probe how these interactions affect the ability of adsorbed DNA to transform bacteria. We investigated DNA adsorption to NOM using QCM for real-time determination of adsorption kinetics of the adsorbed layers and FTIR spectroscopy for identifying specific functional groups of DNA involved in adsorption. Pahokee Peat NOM and Suwannee River NOM were selected as model soil and aquatic NOM. *Azotobacter vinelandii* was chosen as a model soil bacteria because this bacterium is naturally transformable with both plasmid[25] and chromosomal DNA[21] Transformations were performed with both chromosomal and plasmid DNA in the presence of different concentrations and types of NOM.

2.3 Materials and Methods

Solution Chemistries. Dissolved NOM stocks were prepared from Pahokee Peat humic acid reference material (IHSS) and aquatic Suwannee River NOM (SRNOM, IHSS) as previously described.[21] Briefly, NOM was dissolved in DI water, stirred for 24 hours, and filtered through 0.22 μm-pore-size cellulose acetate filters. The solution for coating silica beads and QCM sensors with soil NOM was prepared by diluting the filtrate to 4.6 mg C/L with 10 mM NaCl and filtering through a cellulose acetate filter again. For most other experiments dissolved NOM solutions with different DOC concentrations were diluted from NOM stocks using 20 mM MOPS buffer containing 1mM Ca^{2+} or 1mM Mg^{2+}. For QCM experiments, 4-(2-hydroxyethyl)-1-piperazineethanesulfonic acid (HEPES) buffer and Poly-L-lysine hydrobromide (PLL, Sigma) were also filtered through 0.22 μm-pore-size cellulose acetate filters and stored at 4°C until use.

.

Carboxyl Group Density Determination for SRNOM and Soil NOM. Potentiometric titrations with NaOH were employed to determine the carboxyl group density for soil NOM and SRNOM.[26] A 400-mL solution of each NOM sample was diluted from the stock to a known final concentration of *ca.* 6 mg C/L with 0.1 M NaCl as the background electrolyte. A 100-mL aliquot of each sample was transferred to a 250 mL three-neck vessel for titration. The sample was adjusted to pH 3.0, purged with nitrogen gas for 20 min to remove CO_2, and then continually stirred under nitrogen atmosphc during the titration. A 25.0-mL microburette filled with carbonate-free 0.005 M NaOH was used to titrate the sample to an endpoint of pH 8. Each titration was completed in 10 to 15 min. At least three replicate titrations for each NOM preparation were conducted. The pH probe was calibrated before each use. Calculation of the carboxyl group concentration from the titration results was based on the electroneutrality equation as described previously. Carboxyl group densities are reported in units of milli-equivalent/g C (mequiv/g).

Preparation and Characterization of DNA. Chromosomal DNA was extracted from *A.vinelandii* wildtype (strain DJ, obtained from Dr. Dennis Dean) as described previously.[21] Plasmids pBR325 (purchased from DSMZ, Germany) and pDB17 ([27], obtained from Dr. Dennis Dean) were propagated in *E. coli* strain DH5α and purified using the QIAGEN Plasmid Maxi Kit (QIAGEN, Cat. no, 12163). DNA concentration and size were determined by Nanodrop® ND-1000 (Thermo Scientific) and gel electrophoresis, respectively. The DNA stock was divided into aliquots and stored at -20°C; it was warmed to room temperature immediately before use and diluted in MOPS buffer with 1mM Ca^{2+} (chromosomal DNA) or 1mM Mg^{2+} (plasmid DNA) to a final concentration of 20 mg/liter. For FTIR, extracted DNA was further concentrated to 6000 mg/L by ethanol precipitation.

Transmission Electron Microscopy (TEM). Micrographs of silica bead-adsorbed DNA complexes were obtained on a TEM (JEM-2100, JEOL, Tokyo, Japan) operating at 80 kV and energy-dispersive X-ray spectroscopy was processed by Philips CM12 TEM. After DNA adsorption, silica beads were collected by centrifugation at 16,900 g for 1 min and resuspended in a few drops of Karnovsky's fixative for 20 min. The suspensions were applied to holey-carbon-coated copper grids of 300 mesh and stained with 2% osmium tetroxide for 15 min.

Dissolved NOM Interaction with Adsorbed DNA Layers. Real-time monitoring of dissolved NOM deposition onto adsorbed DNA layers was performed with a QCM (D300, Q-sense AB, Gothenburg, Sweden). As described in previous publications,[20, 21, 28] this technique allows monitoring of adsorbed wet mass of the adsorbed layers. Before each experiment, the sensor was soaked in 2% Hellmanex II (Hellma GmbH & Co. KG, Müllheim, Germany) detergent for at least 2 hours, rinsed thoroughly with deionized water, dried with ultrahigh-purity N_2, and oxidized in a UV chamber (Bioforce Nanosciences, Inc., Ames, IA) for 30 min. The clean sensor was then mounted in a chamber configured as a radial stagnant point flow cell with the temperature controlled at 25 ^{o}C.

A syringe pump in suction mode was employed to inject solutions into the sensor chamber at a speed of 0.1 mL/min. For each experiment, DI water was first introduced into the chamber until a stable baseline was obtained (1 to 2 Hz change in frequency/h). The sensor was equilibrated with electrolyte solution and then DNA was adsorbed to the sensor surface as follows: first a PLL layer was deposited, followed by a soil NOM layer, and then a DNA layer as described before.[21] To investigate the interaction of dissolved NOM with the adsorbed DNA, we monitored the frequency change when solutions of either soil NOM or SRNOM were introduced into the flow cell. Dissolved NOM solution in the same buffer was injected for 20-30 minutes until the frequency change leveled off indicating a saturated surface. Dissolved SRNOM solutions had concentrations of 0, 10, or 100 mg C/L, while the soil NOM solution was 6 mg C/L. After each experiment, the system was washed by injecting 2% Hellmanex II for 30 minutes and then DI water for at least 2 hours. When studying the attachment of NOM to DNA layers, the attachment rate of NOM was calculated as the initial slope for the linear portion of the frequency vs. time curve as described.[20]

FTIR Spectroscopic Measurements of Adsorbed DNA. IR absorption spectra were acquired using a Perkin-Elmer Spotlight 400 imaging spectrometer in point mode using a single element HgCdTe detector cooled by liquid nitrogen. Dissolved chromosomal DNA (6000 mg/L), plain silica beads, and DNA-adsorbed silica beads were measured. Background spectra were first acquired using two CaF_2 substrate slides in the absence of sample. A 10 µl sample was then dropped onto one CaF_2 substrate slide and covered with another slide. The background and sample single beam spectra were collected using a 100 µm x100 µm aperture at 2 cm^{-1} resolution with 100 scans at the same sampling location. A mirror scan speed of 1 cm/s was employed to

record data over the free scanning spectral range of the instrument (7200-0 cm^{-1}) and Norton-Beer medium apodization was used during the Fourier transformation. Spectra were analyzed using SpecManager software from Advanced Chemistry Development (ACD Labs, Toronto Ontario). FTIR experiments with NOM-coated silica beads were attempted. However, the peaks from NOM overwhelmed the DNA signals.

Natural Transformation Assays. For natural transformations the recipient strain was *A. vinelandii* DJ77, which contains a deletion in the *nifH* gene that prevents nitrogen fixation ([27], obtained from Dr. Dennis Dean). Competent (transformable) cells of DJ77 were prepared by growth on modified (no molybdenum) Burke's medium plates with addition of 0.013 mol/L ammonium acetate at 30°C for 2 days and then in liquid media of the same composition, shaking at 170 rpm for 18 to 20 h.[27] The cells were centrifuged and washed twice with MOPS buffer before being resuspended in MOPS buffer with 1 mM Ca^{2+} or Mg^{2+} for transformation with chromosomal or plasmid DNA, respectively. Transformations were conducted by mixing 200 μL of competent cells, 200 μL of MOPS buffer with the specified salt, dissolved SRNOM or soil NOM, and dissolved or adsorbed chromosomal DNA or dissolved plasmid DNA (target mass of 2 μg DNA) sequentially. After incubating at room temperature for 20-30 min, the mixture was diluted and plated in duplicate on selective and non-selective media for transformed and viable cell counts respectively. Selective media were Burke's medium for chromosomal DNA transformations and Burke's medium with 20 μg/mL carbenicillin and 0.013 mol/L ammonium for plasmid DNA, while the non-selective medium was Burke's medium with 0.013 mol/L ammonium. Plates were grown at 30°C for 3-5 days. Transformation frequency was determined by dividing the number of transformed cells by that of viable cells. There were at least three replicates (parallel transformations) for each condition within a batch of competent cells. Independent biological replicates were reported separately. For transformation with plasmid DNA only dissolved plasmids pDB17 and pBR325 was conducted due to the difficulty in extracting and purifying enough plasmid DNA for adsorption experiments.

2.4 Results and Discussion

Adsorbed DNA Characterization. After the DNA-coating procedure, we were able to observe a layer around silica beads in TEM micrographs (**Figure 2**). Energy-dispersive X-ray

spectroscopy for multiple locations in this layer confirmed that it contained DNA, based on the presence of phosphorus, for which DNA was the only source in these samples.

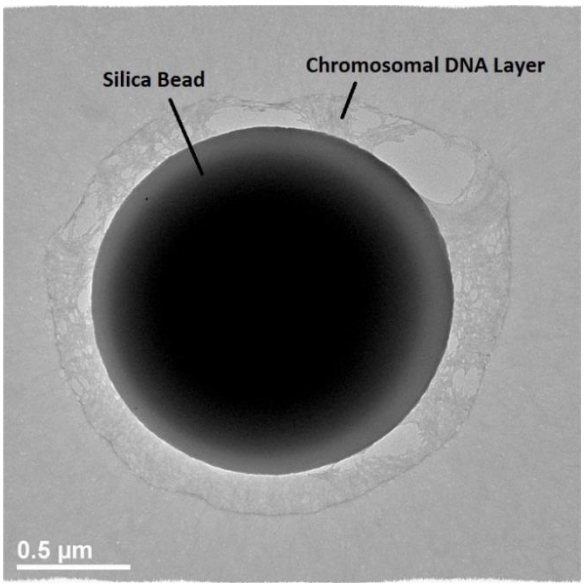

Figure 2 Characterization of DNA adsorbed on silica beads. Micrograph of a silica bead with adsorbed DNA, as observed by osmium staining and TEM. The diameter of the silica beads based on TEM was ca. 1.6 µm.

Dissolved NOM Interaction with Adsorbed DNA Layer. Figure 3a and b show how the adsorption rates (expressed in Hz/min) of dissolved NOM onto an adsorbed DNA layer were affected by NOM carboxyl group density and NOM concentration at pH 7.2. In the absence of NOM, changes due to interaction of buffer solution with the DNA layer were also plotted (i.e. zero carboxylate group density or zero DOC in **Figure 3**a and b, respectively).

An increase in the carboxylate group density for SRNOM and soil NOM from 180 ± 4 meq/g to 210 ± 1 meq/g more than doubled the rate of attachment of NOM on the DNA layer (**Figure 3**a). Divalent Ca^{2+} cations were present in our experiments at 1 mM and could form inner-sphere complexes with the NOM carboxylate groups and the phosphate backbone of the chromosomal DNA, as previously suggested.[29-31] These strong inner complexes facilitate the adsorption of NOM to the DNA layer. Dissolved NOM interactions with adsorbed plasmid DNA (both pBR325 and pDB17) were assessed in the presence of 1mM Mg^{2+} because Mg^{2+} instead of Ca^{2+} was required for the detection of natural transformation by plasmid DNA. For Mg^{2+} we suspect that an outer-sphere complexation mechanism would dominate resulting from the strongly bound water molecules within the inner-sphere of the hydration shell. The formation of

weak outer-sphere complexes by Mg^{2+} and carboxylate groups of NOM has been showed previously.[30, 32] In both Ca^{2+} and Mg^{2+} cases, however, metal cation interactions with carboxylate moieties from the NOM and the DNA phosphate backbone most likely control DNA adsorption to NOM or NOM adsorption to DNA. By the same reasoning the adsorption rates of dissolved NOM onto adsorbed chromosomal or plasmid DNA layer increased with DOC concentrations (**Figure 3**b).

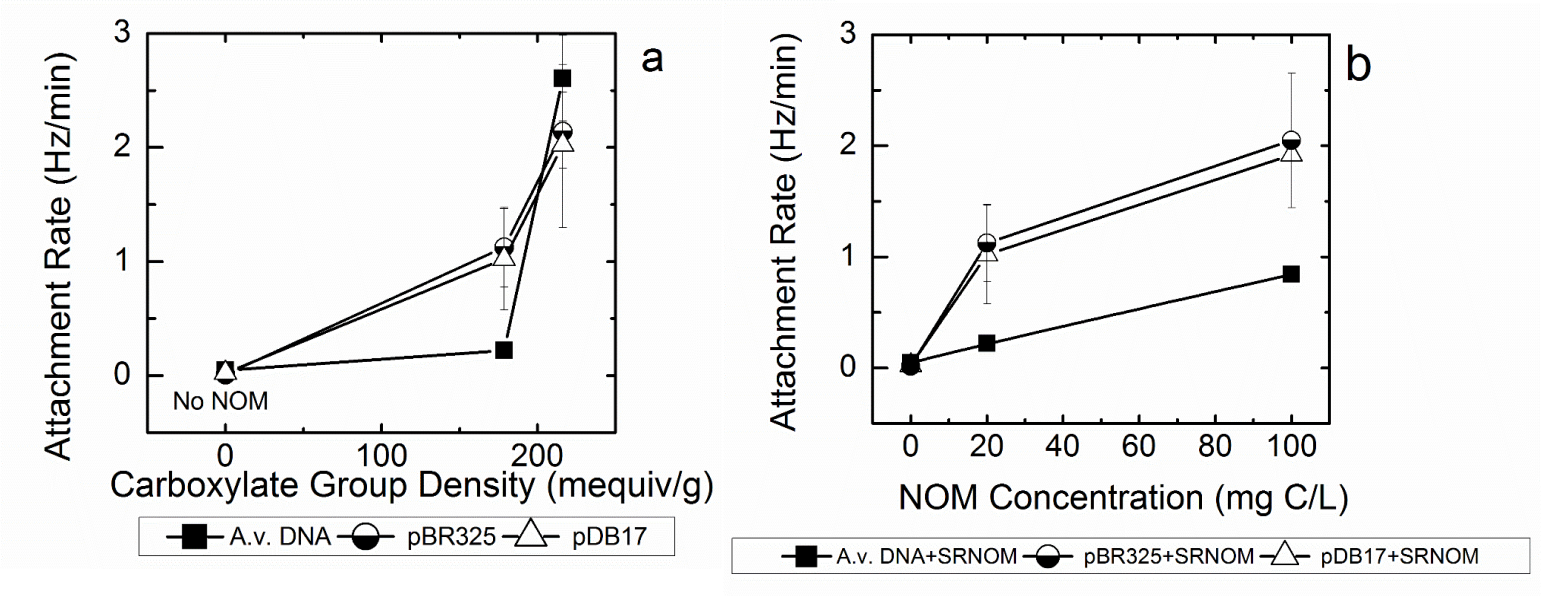

Figure 3 Adsorption of dissolved NOM to DNA-coated surfaces. a) Attachment rate vs. NOM carboxyl group density at pH 7.2. b) Adsorption rate vs. the concentration of dissolved NOM (mg C/L). The attachment rate was calculated as the initial slope for the linear portion of the frequency vs. time curve at around 2.89 min. The standard deviations were from the replicates of same conditions. 20 mM MOPS buffer containing 1mM Ca^{2+} was used in chromosomal DNA experiments (A.v. DNA), while plasmid DNA experiments used 20 mM MOPS buffer containing 1mM Mg^{2+}.

DNA has been shown to form surface complexes at the silica-water interface in previous research,[21] and our IR spectra confirmed the same based on differences between the IR spectrum for DNA and the spectrum of DNA adsorbed to silica (**Figure 4**). For example, the absorption peaks at 970, 1032 and 1086 cm^{-1} correspond to vibrational modes associated with the DNA backbone. Specifically, the 970 and 1032 cm^{-1} absorption peaks are assigned to the DNA backbone and the symmetrical PO_2^- stretch is assigned to the 1086 cm^{-1} peak.[33] Shifts in peak positions upon adsorption or otherwise significant changes in these peaks are indicative of

interactions of the DNA backbone or phosphate groups with the silica surface. Most significantly, we observed the disappearance of the peak at 1126 cm^{-1} (assigned as the asymmetric PO_2^- stretching mode) upon adsorption of DNA to silica.[33] The IR spectra for chromosomal DNA adsorption to silica spheres were similar to the results shown by Mao et al. for DNA adsorbed to crystalline silica.[33] Consistent with previous findings, we note the importance of the phosphate groups in adsorption onto silica beads in the presence of Ca^{2+}. These types of interactions have been observed for chromosomal DNA extracted from *B. subtilis* BD1512 on clay surfaces, where the importance of phosphate interaction with clay was observed to be through cationic bridges with the clay planar surface or with positive charges on the clay edges.[34] Dissolved Ca^{2+} was also found via IR spectroscopy to bind to both phosphate groups and base pairs of calf thymus DNA.[35] We also observed DNA interactions with silica beyond the phosphate backbone. The absorption peak at 1416 cm^{-1}, corresponding to base pairs, diminished after adsorption. In addition to indicating interaction at the base pairs, the loss of intensity of this peak may indicate structural changes in the adsorbed DNA. At a minimum, these results indicate that chromosomal DNA probably interacts with surfaces at multiple sites including its phosphate backbone in the presence of Ca^{2+}. Though the major peaks are identified, there is also some discordance between the spectra of DNA in solution and adsorbed DNA. Recently, it has become clear that the spectra recorded from microscopic samples (here, beads) can show sharp deviations from those recorded in bulk at specific frequencies due to anomalous dispersion and focusing optics.[36, 37] While a complete optical model and solution for the spherical case is under development, it is not possible to draw further quantitative conclusions at this point from the data.

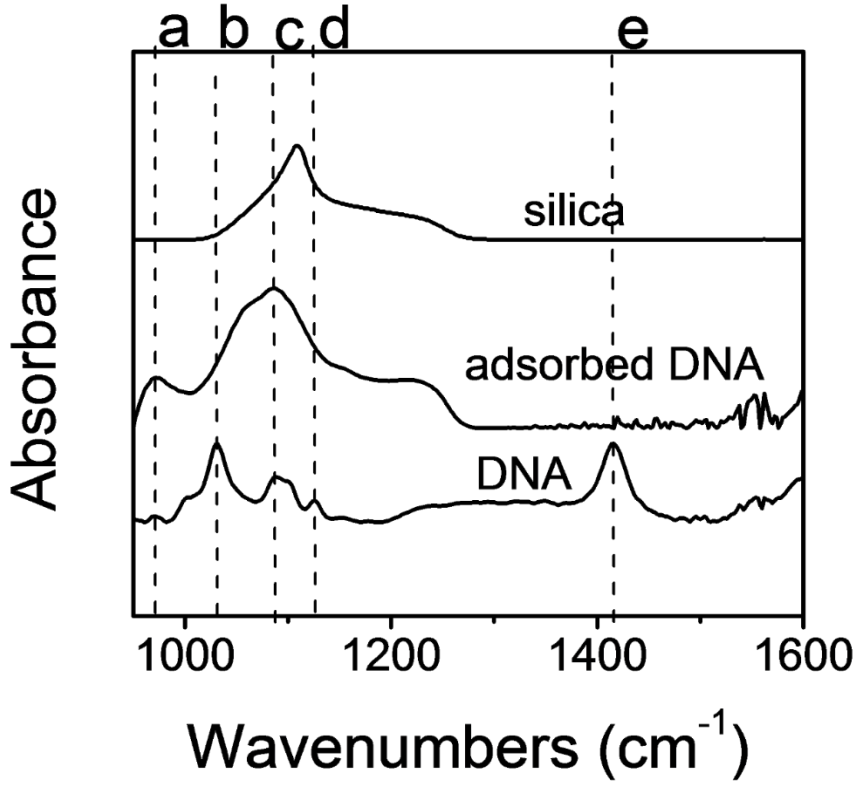

Figure 4 FTIR spectroscopy of silica (top), DNA adsorbed on silica (middle) and dissolved chromosomal DNA (bottom), all in the presence of 1mM Ca2+. The observed vibrational modes are 971 (a: DNA backbone absorption peak), 1030 (b: DNA backbone absorption peak), 1087 (c: symmetrical PO2– stretching mode), 1126 (d: asymmetric PO2– stretching mode), and 1416 (e: base pair absorption peak).

Natural transformation. We observed substantial variations in the transformation frequency for different batches of competent cells, up to 5.4×10^{-4} (see for example adsorbed chromosomal DNA transformation frequencies in the absence of NOM in **Figure 5**). The observation is similar as in our previous work.[21] Because of this we have presented the transformation results by batch of competent cells (i.e., competent cells prepared on the same day from the same plate) rather than averaging all values from the same condition. Each point represents triplicate transformations prepared from the same batch. The transformation frequencies observed ranged from 1.4×10^{-5} to 5.2×10^{-4} with chromosomal DNA (adsorbed and dissolved) and from 9.1×10^{-7} to 1.1×10^{-4} with dissolved pDB17. These results are comparable to previous reports in several *A. vinelandii* strains (**Table 2**).

Table 2 Comparison of transformation frequencies with different *Azotobacter vinelandii* strains.

Strains	Transformation frequencies[a]	Conditions	DNA	Reference
ATCC12837	3.0×10^{-4}-5.7×10^{-2}/μg DNA	transformation media	plasmid pRK2501, RSF1010, pGSS15	[38]
UW10	1.0×10^{-6}-2.0×10^{-3}		plasmid pKT210, pAvD-10	[39]
UW10	5.0×10^{-5}-7.0×10^{-2}		strain UW chromosomal DNA	[39]
Capsule-negative strain UW	5.0×10^{-8}-7.0×10^{-3}		crude strain 113 (Rif^r) DNA	[40]
DJ77	1.1×10^{-5}-1.1×10^{-3}	addition of none or Na^+ or Ca^{2+}	strain DJ chromosomal DNA	[21]
DJ77	1.4×10^{-5}-5.2×10^{-4}	addition of NOM and Ca^{2+}	strain DJ chromosomal DNA	this study
DJ77	9.1×10^{-7}-1.1×10^{-4}		plasmid pDB17	this study

[a] Transformation frequencies were calculated as numbers of successful transformants divided by numbers of viable cells.

Comparing transformation frequencies across NOM types (soil and aquatic, **Figure 5**a) and concentrations (**Figure 5**b) within a single batch, the differences are relatively small compared to the differences between batches; the largest difference observed for a given type of DNA is 3.6×10^{-4}, and the average difference is only 1.0×10^{-4}. Furthermore, there is no consistent trend in transformation frequencies with NOM type or concentration. Based on these data, although dissolved NOM interacted with adsorbed DNA, this interaction did not prevent or even strongly influence natural transformation of *A. vinelandii*.

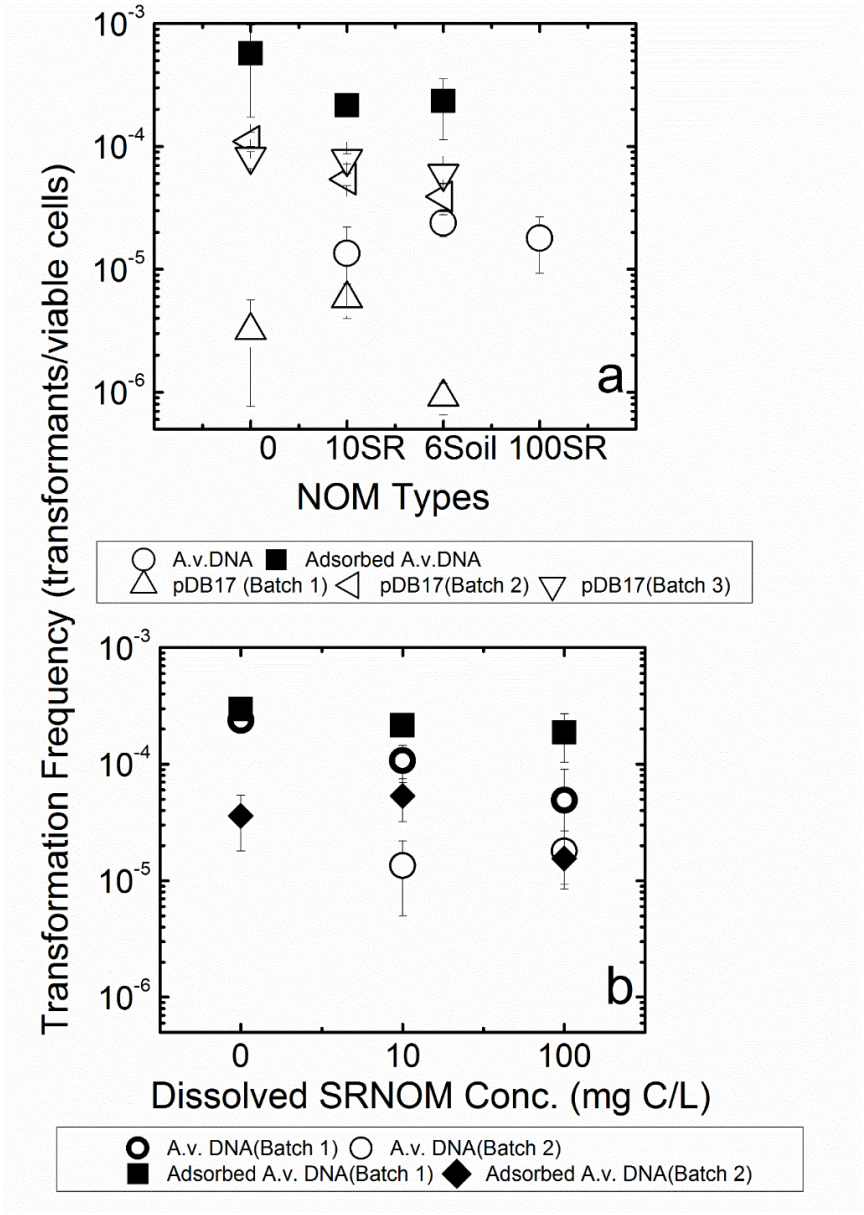

Figure 5 Effect of NOM on natural transformation of *A. vinelandii.* a) Effect of NOM type on natural transformation; b) Effect of NOM concentration on natural transformation. Transformation experiments were conducted with dissolved or adsorbed chromosomal DNA in MOPS buffer containing 1 mM Ca^{2+} at pH 7.2 and with plasmid pDB17 DNA in MOPS with 1 mM Mg^{2+}. The transformation frequency was calculated as the ratio of transformants to viable cells. Each data point was calculated from at least three replicates from the same batch of competent cells. Independent biological replicates, from separate batches of competent cells, are shown separately due to substantial variation amongst batches. The DNA concentration was approximately 5 µg/ml and DNA was dissolved in solution unless specified.

The finding that natural transformation was not prevented by the interactions between DNA and NOM is consistent with prior studies that demonstrated that transformation can occur in the presence of humic acids.[12, 13] However, in those studies a decrease in transformation frequency was observed in the presence of humic acids, while our research shows no difference in the frequency upon addition of NOM. Possible explanations for this discrepancy include at least two that are methodological. First, the microorganism employed to study transformation differed between the studies. Crecchio et al. used the Gram-positive *B. subtilis*, which has a different membrane structure from the Gram-negative *A. vinelandii* used in the current work. Differences in the membrane structure require differences in DNA uptake.[41] Second, Crecchio et al. used dissolved DNA as their control, whereas in the current work we compared DNA adsorbed to silica beads with and without NOM, thus removing any general influence of adsorption on transformation frequency. The literature is conflicted on whether adsorption to other surfaces will decrease natural transformation in *B. subtilis*.[9, 42]

The amount of chromosomal DNA in our natural transformation tests was based on saturating DNA concentrations for *A. vinelandii* strain UW10,[25] raising the concern that the DNA-NOM interactions could be reducing the DNA available for transformation without affecting the observed transformation frequency. Natural transformation experiments were repeated with 0.05 μg/ml DNA (a 100-fold reduction) in the presence of dissolved NOM. At this concentration the transformation frequency would be dependent on the amount of DNA.[25] We found that even at the lower concentration of DNA, *A. vinelandii* DJ77 was still transformed at similar frequencies with or without 100 mg C/L of dissolved SRNOM, on average 4.1×10^{-5} (with a standard deviation of 1.5×10^{-5}) and 4.1×10^{-5} (with a standard deviation of 4.4×10^{-5}), respectively.

The lack of impact on transformation frequency has at least two potential explanations. It may simply reflect incomplete NOM coverage of the DNA surface, despite a 20-fold excess of NOM. Alternatively, it is possible that different structural elements of the DNA interact with NOM than with the cell surface. Since the initial contact between DNA and a competent cell is not understood at a molecular level,[43] it is difficult to assess this possibility. Even for heavily studied model organisms, where some of the proteins interacting with DNA and affecting natural transformation have been identified, such as *Neisseria meningitidis* (PilQ[44] and PilG[45]) and *B. subtilis* (ComEA[46]), the specific mechanism of initial DNA binding is not yet known.

2.5 Environmental Implications

As a mechanism of gene transfer, natural transformation plays an important role in the evolution of soil microbial communities and thereby influences their ability to degrade contaminants and to resist antimicrobials. This study demonstrated interactions between extracellular DNA and dissolved NOM via the phosphate groups in the DNA backbone. However, these interactions did not reduce the availability of the DNA for transformation of *A. vinelandii*, supporting the idea that adsorbed DNA provides an environmental reservoir of genetic potential for soil microorganisms.

2.6 Acknowledgement

We gratefully acknowledge Ms. Lou Ann Miller and Dr. Changhui Lei from Material Research Laboratory at University of Illinois for their advice on TEM and Dr. Dennis Dean for supplying *A. vinelandii* strains and protocols. This research was supported by the USDA (grant 2008-35102-19143) and National Science Foundation agreement number EAR-1114385, CTS-0120978 and CHE-0957849.

2.7 References

1. Ochman, H.; Lawrence, J. G.; Groisman, E. A., Lateral Gene Transfer and the Nature of Bacterial Innovation. *Nature* **2000,** *405*, 299-304.

2. Gogarten, M. B.; Gogarten, J. P.; Olendzenski, L. C., *Horizontal Gene Transfer: Genomes in Flux*. Humana Pressq: New York, NY, 2009.

3. Springael, D.; Top, E. M., Horizontal Gene Transfer and Microbial Adaptation to Xenobiotics: New Types of Mobile Genetic Elements and Lessons from Ecological Studies. *Trends in Microbiology* **2004,** *12*, (2), 53-58.

4. Barlow, M., What Antimicrobial Resistance Has Taught Us About Horizontal Gene Transfer. In *Horizontal Gene Transfer: Genomes in Flux*, Gogarten, M. B.; Gogarten, J. P.; Olendzenski, L. C., Eds. Humana Press: New York, NY, 2009; Vol. 532, pp 397-411.

5. Crane, M.; Watts, C.; Boucard, T., Chronic Aquatic Environmental Risks from Exposure to Human Pharmaceuticals. *Science of the Total Environment* **2006,** *367*, (1), 23-41.

6. Rooklidge, S. J., Environmental Antimicrobial Contamination from Terraccumulation and Diffuse Pollution Pathways. *Science of the Total Environment* **2004,** *325*, (1-3), 1-13.

7. Chen, I.; Christie, P. J.; Dubnau, D., The Ins and Outs of DNA Transfer in Bacteria. *Science* **2005,** *310*, (5753), 1456.

8. Levy-Booth, D. J.; Campbell, R. G.; Gulden, R. H.; Hart, M. M.; Powell, J. R.; Klironomos, J. N.; Pauls, K. P.; Swanton, C. J.; Trevors, J. T.; Dunfield, K. E., Cycling of Extracellular DNA in the Soil Environment. *Soil Biology & Biochemistry* **2007,** *39*, (12), 2977-2991.

9. Lorenz, M. G.; Aardema, B. W.; Wackernagel, W., Highly Efficient Genetic Transformation of *Bacillus subtilis* Attached to Sand Grains. *Journal of General Microbiology* **1988,** *134*, 107-112.

10. Lorenz, M. G.; Wackernagel, W., Natural Genetic Transformation of *Pseudomonas stutzeri* by Sand-Adsorbed DNA. *Archives of Microbiology* **1990,** *154*, (4), 380-385.

11. Cai, P.; Huang, Q. Y.; Zhang, X. W., Interactions of DNA with Clay Minerals and Soil Colloidal Particles and Protection against Degradation by DNase. *Environmental Science & Technology* **2006,** *40*, (9), 2971-2976.

12. Crecchio, C.; Ruggiero, P.; Curci, M.; Colombo, C.; Palumbo, G.; Stotzky, G., Binding of DNA from *Bacillus subtilis* on Montmorillonite-Humic Acids-Aluminum or Iron Hydroxypolymers: Effects on Transformation and Protection against DNase. *Soil Science Society of America Journal* **2005,** *69*, (3), 834-841.

13. Crecchio, C.; Stotzky, G., Binding of DNA on Humic Acids: Effect on Transformation of *Bacillus subtilis* and Resistance to DNase. *Soil Biology & Biochemistry* **1998,** *30*, (8-9), 1061-1067.

14. Tebbe, C.; Vahjen, W., Interference of Humic Acids and DNA Extracted Directly from Soil in Detection and Transformation of Recombinant DNA from Bacteria and a Yeast. *Applied and Environmental Microbiology* **1993,** *59*, (8), 2657.

15. Sushko, M. L.; Shluger, A. L.; Rivetti, C., Simple Model for DNA Adsorption onto a Mica Surface in 1:1 and 2:1 Electrolyte Solutions. *Langmuir* **2006,** *22*, (18), 7678-7688.

16. Nguyen, T. H.; Chen, K. L., Role of Divalent Cations in Plasmid DNA Adsorption to Natural Organic Matter-Coated Silica Surface. *Environmental Science & Technology* **2007,** *41*, (15), 5370-5375.

17. Nguyen, T. H.; Elimelech, M., Adsorption of Plasmid DNA to a Natural Organic Matter-Coated Silica Surface: Kinetics, Conformation, and Reversibility. *Langmuir* **2007,** *23*, (6), 3273-3279.

18. Poly, F.; Chenu, C.; Simonet, P.; Rouiller, J.; Jocteur Monrozier, L., Differences between Linear Chromosomal and Supercoiled Plasmid DNA in Their Mechanisms and Extent of Adsorption on Clay Minerals. *Langmuir* **1999,** *16*, (3), 1233-1238.

19. Franchi, M.; Bramanti, E.; Bonzi, L. M.; Orioli, P. L.; Vettori, C.; Gallori, E., Clay-Nucleic Acid Complexes: Characteristics and Implications for the Preservation of Genetic Material in Primeval Habitats. *Origins of Life and Evolution of Biospheres* **1999,** *29*, (3), 297-315.

20. Nguyen, T. H.; Elimelech, M., Plasmid DNA Adsorption on Silica: Kinetics and Conformational Changes in Monovalent and Divalent Salts. *Biomacromolecules* **2007,** *8*, (1), 24-32.

21. Lu, N.; Zilles, J. L.; Nguyen, T. H., Adsorption of Extracellular Chromosomal DNA and Its Effects on Natural Transformation of *Azotobacter vinelandii*. *Applied and Environmental Microbiology* **2010,** *76*, (13), 4179-4184.

22. Nielsen, K. M.; Smalla, K.; van Elsas, J. D., Natural Transformation of *Acinetobacter* Sp. Strain Bd413 with Cell Lysates of *Acinetobacter* Sp., *Pseudomonas fluorescens*, and *Burkholderia cepacia* in Soil Microcosms. *Applied and Environmental Microbiology* **2000,** *66*, (1), 206-212.

23. Bukau, B.; Brass, J. M.; Boos, W., Ca^{2+}-Induced Permeabilization of the *Escherichia coli* Outer Membrane: Comparison of Transformation and Reconstitution of Binding-Protein-Dependent Transport. *Journal of Bacteriology* **1985,** *163*, (1), 61.

24. Sun, D.; Zhang, X.; Wang, L.; Prudhomme, M.; Xie, Z.; Martin, B.; Claverys, J. P., Transforming DNA Uptake Gene Orthologs Do Not Mediate Spontaneous Plasmid Transformation in *Escherichia coli*. *Journal of Bacteriology* **2009,** *191*, (3), 713.

25. Doran, J. L.; Bingle, W. H.; Roy, K. L.; Hiratsuka, K.; Page, W. J., Plasmid Transformation of *Azotobacter vinelandii* Op. *Journal of General Microbiology* **1987,** *133*, (8), 2059.

26. Collins, M.; Amy, G.; Steelink, C., Molecular Weight Distribution, Carboxylic Acidity, and Humic Substances Content of Aquatic Organic Matter: Implications for Removal During Water Treatment. *Environmental Science & Technology* **1986,** *20*, (10), 1028-1032.

27. Jacobson, M. R.; Brigle, K. E.; Bennett, L. T.; Setterquist, R. A.; Wilson, M. S.; Cash, V. L.; Beynon, J.; Newton, W. E.; Dean, D. R., Physical and Genetic Map of the Major *Nif* Gene Cluster from *Azotobacter vinelandii*. *Journal of Bacteriology* **1989,** *171*, (2), 1017-1027.

28. Voinova, M. V.; Rodahl, M.; Jonson, M.; Kasemo, B., Viscoelastic Acoustic Response of Layered Polymer Films at Fluid-Solid Interfaces: Continuum Mechanics Approach. *Physica Scripta* **1999,** *59*, (5), 391-396.

29. Gavryushov, S., Electrostatics of B-DNA in Nacl and Cacl2 Solutions: Ion Size, Interionic Correlation, and Solvent Dielectric Saturation Effects. *Journal of Physical Chemistry B* **2008,** *112*, (30), 8955-8965.

30. Iskrenova-Tchoukova, E.; Kalinichev, A. G.; Kirkpatrick, R. J., Metal Cation Complexation with Natural Organic Matter in Aqueous Solutions: Molecular Dynamics Simulations and Potentials of Mean Force. *Langmuir* **2010,** *26*, (20), 15909-15919.

31. Kankia, B. I., Interaction of Alkaline-Earth Metal Ions with Calf Thymus DNA. Volume and Compressibility Effects in Diluted Aqueous Solutions. *Biophysical Chemistry* **2000,** *84*, (3), 227-237.

32. Kalinichev, A.; Kirkpatrick, R., Molecular Dynamics Simulation of Cationic Complexation with Natural Organic Matter. *European Journal of Soil Science* **2007,** *58*, (4), 909-917.

33. Mao, Y.; Daniel, L. N.; Whittaker, N.; Saffiotti, U., DNA Binding to Crystalline Silica Characterized by Fourier-Transform Infrared Spectroscopy. *Environmental Health Perspectives* **1994,** *102*, (Suppl 10), 165.

34. Khanna, M.; Yoder, M.; Calamai, L.; Stotzky, G., X-Ray Diffractometry and Electron Microscopy of DNA from *Bacillus subtilis* Bound on Clay Minerals. *Sciences of Soils* **1998,** *3*, (1), 1-10.

35. Hackl, E. V.; Kornilova, S. V.; Blagoi, Y. P., DNA Structural Transitions Induced by Divalent Metal Ions in Aqueous Solutions. *International Journal of Biological Macromolecules* **2005,** *35*, (3-4), 175-191.

36. Davis, B. J.; Carney, P. S.; Bhargava, R., Theory of Midinfrared Absorption Microspectroscopy: I. Homogeneous Samples. *Analytical Chemistry* **2010,** *82*, (9), 3474-3486.

37. Davis, B. J.; Carney, P. S.; Bhargava, R., Theory of Infrared Microspectroscopy for Intact Fibers. *Analytical Chemistry* **2011,** *83*, (2), 525-532.

38. Glick, B. R.; Brooks, H. E.; Pasternak, J. J., Transformation of *Azotobacter vinelandii* with Plasmid DNA. *Journal of Bacteriology* **1985,** *162*, (1), 276-279.

39. Doran, J. L.; Bingle, W. H.; Roy, K. L.; Hiratsuka, K.; Page, W. J., Plasmid Transformation of *Azotobacter vinelandii* OP. *Journal of General Microbiology* **1987,** *133*, 2059-2072.

40. Page, W. J.; Grant, G. A., Effect of Mineral Iron on the Development of Transformation Competence in *Azotobacter vinelandii*. *FEMS Microbiology Letters* **1987,** *41*, (3), 257-261.

41. Chen, I.; Dubnau, D., DNA Uptake During Bacterial Transformation. *Nature Reviews Microbiology* **2004,** *2*, (3), 241-249.

42. Gallori, E.; Bazzicalupo, M.; Dalcanto, L.; Fani, R.; Nannipieri, P.; Vettori, C.; Stotzky, G., Transformation of *Bacillus subtilis* by DNA-Bound on Clay in Nonsterile Soil. *FEMS Microbiology Ecology* **1994,** *15*, (1-2), 119-126.

43. Krüger, N.-J.; Stingl, K., Two Steps Away from Novelty – Principles of Bacterial DNA Uptake. *Molecular Microbiology* **2011,** *80*, (4), 860-867.

44. Assalkhou, R.; Balasingham, S.; Collins, R. F.; Frye, S. A.; Davidsen, T.; Benam, A. V.; Bjørås, M.; Derrick, J. P.; Tønjum, T., The Outer Membrane Secretin Pilq from *Neisseria meningitidis* Binds DNA. *Microbiology* **2007,** *153*, (5), 1593.

45. Lång, E.; Haugen, K.; Fleckenstein, B.; Homberset, H.; Frye, S. A.; Ambur, O. H.; Tønjum, T., Identification of Neisserial DNA Binding Components. *Microbiology* **2009,** *155*, (3), 852.

46. Provvedi, R.; Dubnau, D., Comea Is a DNA Receptor for Transformation of Competent *Bacillus subtilis*. *Molecular Microbiology* **1999,** *31*, (1), 271-280.

CHAPTER 3 FLAGELLA-MEDIATED DIFFERENCES IN DEPOSITION DYNAMICS FOR *AZOTOBACTER VINELANDII* IN POROUS MEDIA

Published:

Lu, N.; Bevard, T.; Massoudieh, A.; Zhang, C.; Dohnalkova, A. C.; Zilles, J. L.; Nguyen, T. H., Flagella-Mediated Differences in Deposition Dynamics for *Azotobacter vinelandii* in Porous Media. *Environmental Science & Technology* **2013,** *47*, (10), 5162-5170.

Contribution: I have conducted all the experiments and analyzed the data presented in this chapter except for 1) image processing for motility characterization; 2) TEM imaging; 3) macro-scale modeling and parameter estimation; 4) relative biomass coverage comparison in micromodel.

3.1 Abstract

A multi-scale approach was designed to study the effects of flagella on deposition dynamics of *Azotobacter vinelandii* in porous media, independent of motility. In a radial stagnation point flow cell (RSPF), the deposition rate of a flagellated strain with limited motility, DJ77, was higher than that of a non-flagellated (Fla^-) strain on quartz. In contrast, Fla^- strain deposition exceeded that of DJ77 in two-dimensional silicon microfluidic models (micromodels) and in columns packed with glass beads. Both micromodel and column experiments showed decreasing deposition over time, suggesting that approaching cells were blocked from deposition by previously deposited cells. Modeling results showed that blocking became effective for DJ77 strain at lower ionic strengths (1mM and 10mM), while for Fla^- strain blocking was similar at all ionic strengths. In late stages of micromodel experiments, ripening effects were also observed, and these appeared earlier for the Fla^- strain. In RSPF and column experiments, deposition of the flagellated strain was influenced by ionic strength, while ionic strength dependence was not observed for the Fla^- strain. The observations in all three setups suggested flagella affect deposition dynamics, and in particular result in greater sensitivity to ionic strength.

3.2 Introduction

Understanding the fate and transport of bacteria in the soil environment is crucial for studying soil microbial communities, monitoring subsurface and groundwater quality and improving bioremediation performance.[1, 2] Processes controlling the transport of bacteria in porous media and associated modeling approaches have been extensively reviewed.[1, 3, 4] Macro-scale fate and transport of bacteria in porous media has often been described using advection, dispersion, attachment and detachment models,[2] similar to those developed for colloids.[2, 5] To incorporate the effect of DLVO forces between the colloids and collector surfaces, Colloid Filtration Theory (CFT), based on either analytical or trajectory analysis of colloid transport and deposition near spherical collectors,[6-12] has been used. However, in many cases the relationships provided by CFT to estimate the collision efficiency do not accurately represent colloid transport, particularly when conditions are unfavorable for deposition.[13-16] This has been attributed to the presence of repulsive electrostatic forces between colloids and the surface,[13, 15-17]

the heterogeneity of surface charges of colloids and collectors,[18-21] surface roughness,[22] hydrodynamic conditions[20, 23] and straining.[24]

Blocking occurs when interactions between deposited and incoming cells or colloids prevent attachment to the collector surfaces, causing a decrease in retention of the bacterial cells or colloids as the density of cells or colloids attached to the collector surfaces increases.[25-29] Previous studies have focused on how blocking is affected by ionic strength,[30, 31] cell concentration,[32] particle size,[30] hydrodynamics (flow velocity).[32] Increasing flow velocity and particle size and decreasing ionic strength result in stronger blocking effects.[30] To incorporate this effect into models, dynamic blocking functions based on Langmuirian[33] or Random Sequential Adsorption (RSA)[25, 26, 34, 35] are often used. Automatic parameter estimation approaches have also been widely used to estimate the transport and attachment parameters based on the breakthrough curves obtained from column studies (e.g. [36, 37]).

During the later stage of deposition, the deposition rates can also increase as multiple layers of bacterial cells form on the collectors, a phenomenon known as ripening.[29] Nascimento et al.[29] observed three phases of deposition of bacterial spores, characterized by steady, decreasing, and then increasing rates of deposition, and attributed these phases to simultaneous blocking and ripening effects. They also reported extensive ripening in the initial region of quartz sand columns.[29]

Despite studies on the dynamics of bacteria deposition, the mechanisms of blocking and ripening are not fully understood. Of particular importance for bacterial deposition or transport, as compared to other colloids, are the impacts of bacterial flagella, motility, and chemotaxis. This work focused on the effects of the physical flagella structure, which can extend up to 10-15 μm beyond the cell surface, several times the cell's length, as reviewed in Erhardt et al.[38] Few studies have separated the effects of flagella from those of flagellar-driven motility and chemotaxis. It is possible for cells to have flagella, but not be motile, either due to mutations that disrupt the flagellar motor[39] or transiently due to the environmental conditions.[40] The enhancement of transverse mixing due to the presence of motile bacteria, as studied in micromodels, requires motility, not just the presence of flagella.[41] For bacterial attachment and deposition, the conclusions of the few existing studies vary. McClaine and Ford[42] did not observe any impact of the flagellar structure on initial attachment rates of *E. coli* in flow cell experiments, while Haznedaroglu et al.[43] observed greater deposition of a flagellated, non-motile

Salmonella enterica serovar than that of a non-flagellated serovar in radial stagnation point flow cell (RSPF) and packed bed column experiments. Thus, the flagella of *Salmonella enterica*, although dysfunctional, facilitated cell-collector surface interactions. In addition, the role of flagella on the dynamics of deposition ranging from initial deposition on clean collectors to ripening has not been studied.

The objective of this work was to evaluate the effects of flagella on bacterial transport and deposition dynamics in porous media, using a multi-scale approach including the complementary techniques of radial stagnation point flow cell (RSPF), micromodel, and glass beads packed column setups. The RSPF system allows direct visualization of bacterial deposition on a clear quartz surface under well-defined hydrodynamic conditions, but is limited to analysis of bacteria to clean collector interactions. The micromodel is designed to resemble a thin slice of a packed column, allowing in-situ real-time observation and quantification of bacteria and collector interactions, bacteria and bacteria interactions, and bacteria deposition at different locations. The column setup is a 3-D porous media system most similar to the subsurface environment, but does not provide the high spatial resolution of the other two setups. An inverse modeling approach was used to identify important processes and to estimate parameters for transport of both flagellated and non-flagellated bacterial strains in the column experiments. This comprehensive approach was designed to reveal the role of flagella in the transport and deposition of the bacterium *Azotobacter vinelandii* and to facilitate the development of more accurate models for bacterial transport and deposition. *A. vinelandii* was selected based on its occurrence in the soil and ecologically important characteristics, including nitrogen fixation and competence for gene transfer.[44]

3.3 Materials and Methods

Strain Construction. Two *A. vinelandii* strains were used in this work. DJ77 contains a 128 bp deletion in *nifH*, resulting in a defect in nitrogen fixation.[45] To construct a non-flagellated strain, DJ77 was transformed with the plasmid pLRDC50, which contains a tetracycline resistance gene insertion mutation in the flagellar master regulatory gene *flhC*[46] and cannot replicate in *A. vinelandii*. Successful transformants with the tetracycline resistance gene insertion in *flhC* on the genome were identified by selection for tetracycline resistance, resulting in strain

JZ52 (referred to as Fla$^-$ based on its phenotype of lacking flagella). For characterization of motility, these two strains were compared to the wild type *A. vinelandii* strain DJ.

Bacterial Cell Preparation. *A. vinelandii* strains were grown on modified (no molybdenum) Burk's medium[47] plates with addition of 0.013 M ammonium acetate at 30°C for 2 days, and then in liquid media of modified (no molybdenum, no iron) Burk's medium[47] with addition of 0.013 M ammonium acetate shaking at 170 rpm for 18 to 20 h. This growth procedure is used to prepare cells for natural transformation assays,[48] and was used here to facilitate comparisons between deposition and natural transformation behavior in *A. vinelandii*. For the same reason, electrophoretic mobility measurement, deposition and transport experiments were conducted with MOPS buffer at pH 7.2. The cells were then centrifuged at 1000g for 10 min to remove the culture media. No further washing was performed to avoid breaking flagella. To allow replicate experiments from the same batch of cells, cell pellets were stored at 4^{o}C for up to 48 hours before experiments. Control experiments confirmed that cold storage for 24 or 48 hours did not affect viable cell counts or motility. A slight decrease, less than 10%, in transformation frequency was observed following 48 hours of cold storage.

Motility Characterization. Motility of Fla$^-$ and DJ77 in suspension was quantified using a particle tracking algorithm. A flagellated motile wild type strain DJ was also studied for motility comparison. Approximately 20 µL of bacterial cell suspension was prepared on a Hemocytometer slide and covered with a glass coverslip. A series of time-lapse images were taken with transmitted light microscope Leica DMI5000M at 400X magnification under static conditions. The images were processed using MATLAB image processing toolbox. Filtering was applied to remove the noise and a threshold based on the color intensity was utilized to identify the location and size of the cells. The thresholds were determined manually and varied among experiments. The MATLAB code produces a series of x,y coordinates at each time interval. A particle tracking algorithm developed using the C^{++} programming language was used to find the corresponding cells at sequential images and to extract the trajectories and quantify bacterial motility. The particle tracking algorithm calculated the most probable bacterial trajectories and the squared displacement for each cell between any two consecutive snapshots. About 500 images were processed for each sample of Fla$^-$ and DJ77, containing approximately about 40-60 and 80-100 individual cells per image, respectively. For the wild type strain (DJ), 1000 images

with about 125-150 cells per image were taken. The variance of cell displacement was obtained through trajectory analysis and was calculated using the following expression:

$$\sigma^2 = \frac{1}{n}\left\{\sum_{j=1}^{n}\left[(x_{j,t} - x_{j,0} - \overline{x}_t)^2 + (y_{j,t} - y_{j,0} - \overline{y}_t)^2\right]\right\} \qquad (1)$$

where n is the number of cells tracked, $x_{j,t}$ and $y_{j,t}$ are the coordinates of cell j in time step t, , $x_{j,0}$ and $y_{j,0}$ are the initial location of cell j, and $\overline{x_t}$ and $\overline{y_t}$ are the mean displacement of all cells in x and y directions at time-step t. In the analysis of mean squared displacement the cells that were detected to be non-moving were excluded. The variance of displacement as a function of time was fitted by a power law relationship. The relative frequency values are the number of instantaneous velocities that lie within the range of bins on the x axis normalized by the total number of instantaneous velocities.

Electrophoretic mobility and hydrophobicity. The electrophoretic mobility of the bacterial strains and all the porous media materials was measured with Zetasizer Nano ZS90 (Malvern Instruments, Southborough, MA). The electrophoretic mobility of the bacterial strains and all the porous media materials was measured with Zetasizer Nano ZS90 (Malvern Instruments, Southborough, MA). Bacterial suspensions were prepared by resuspending cell pellets grown as described above in MOPS buffer solutions with 1-100 mM KCl at pH 7.2. Glass beads were sonicated in buffered electrolyte solutions containing from 1 to 100 mM KCl at pH7.2 for 30 min to get the small glass particles suspended in these solutions. The RSPF quartz collector and the micromodel collectors were ground finely and the powders were resuspended in the same buffered electrolyte solutions for electrophoretic mobility measurements. Zeta potentials were calculated from the electrophoretic mobility measurements using the Smoluchowski equation. A paired t-test was used to compare the zeta potentials of the glass beads, RSPF quartz slide and micromodel silica dioxide surface with corresponding ionic strength. P value of 0.05 was considered significant.

Partitioning of bacteria in dodecane was used to characterize the cell hydrophobicity.The bacterial cells were diluted to 2-3×10^6 cells/mL using MOPS buffer at pH 7.2. 4 mL of each bacterial cell suspension was added into 1 mL dodecane and vigorously mixed for 2 min. The well-mixed solution was allowed to separate between dodecane and aqueous phase for 30 min. The cell concentrations of both the initial cell suspension and the separated aqueous phase were

quantified using a hemocytometer. The ratios of bacterial cells suspended in dodecane were calculated and compared between DJ77 and Fla^- strains.

Transmission Electron Microscopy (TEM). Five microliters of *A. vinelandii* cell suspensions was applied to 100 mesh Cu grids covered with formvar support film sputtered with carbon (Electron Microscopy Sciences, Hatfield, PA). The cells were allowed to adhere to the grids for 1 min before being blotted with filter paper and negatively stained with 5 uL Nano-W (Nanoprobes, Yaphank, NY). After 30 s, the excess liquid was removed by wicking, and the sample was allowed to air dry. Samples were examined with a Tecnai T-12 TEM (FEI Co., Hillsboro, OR) operating at 120 kV with a LaB6 filament. Images were collected digitally with a 2x2K Ultrascan 1000 charge-coupled device with a "U" scintillator (Gatan) calibrated to the TEM camera length to enable direct measurements correlated with the magnification of the acquired images. Digital Micrograph (Gatan) software was used for imaging and image analyses of cellular features. Representative images of at least 60 cells per sample were collected at 10,000 magnification and analyzed for the presence or absence of flagella.

Fluorescence Microscope. Ten milliliters of *A. vinelandii* cell suspensions were washed three times using buffer solution at pH 7.0 containing 0.01 M K_3PO_4, 0.067 M NaCl, 10^{-4} M EDTA. The washed cells were resuspended in 0.5 mL of same buffers and 100 µL buffer dissolved with 0.4 mg of Alexa Fluor 594 carboxylic acid succinimidyl ester. The Alexa Fluor stain was used to stain both the cell body and the flagella as recommended in Turner et al..[49] The solution pH was adjusted to pH 7.8 using 1M $NaHCO_3$ and each solution was mixed by rotating for at least an hour before washing out unused dye and spotting on glass sides for imaging. Stained cells were visualized using Zeiss fluorescence microscope.

Deposition in RSPF Setup. Bacterial attachment to a forward stagnation point on a quartz surface (Quartz coverslip, Cat. No. #26016, Ted Pella Inc.) was studied in a RSPF flow cell as described previously.[50] The RSPF setup has an injection capillary radius (R) of 1 mm and a distance from the injection point to the quartz surface (h) of 0.7 mm. Before every deposition experiment, the quartz surface was rigorously cleaned as follows: soaked in ethanol overnight, rinsed with DI water and then with 2% Hellmanex® III solution (Cat. No. 320.003, Hellma, Germany), soaked in the Hellmanex solution overnight, rinsed with DI water, soaked in 98% sulfuric acid with Nochrmoix® (Cat. No. 19-010, Godax Laboratories, Inc.) for 24 hours, and rinsed with DI water to the initial pH of the DI water (~6.5). The bacterial deposition

experiments were performed at pH 7.2 using MOPS buffer over ionic strengths from 1-100 mM KCl. The initial concentrations of bacterial suspension for deposition experiments varied from 2.72×10^7 ~ 4.17×10^7 cells/mL, as determined by direct counting using a hemocytometer. This concentration was chosen so that a minimum of 10 deposited bacterial cells were observed on the quartz surface and no cell aggregation was observed. Electrolyte solution was pumped into the RSPF setup at a steady flow of 1mL/min by a syringe pump (KD Scientific) for 5-10 minutes, followed by the bacterial suspension in the same electrolyte solution at the same flow rate for at least 30 min. The 296×222 μm-rectangular area on the quartz surface in the middle of the forward stagnation point was imaged every minute using an inverted Leica microscope. The number of bacterial cells deposited in each image was counted manually. The deposition rates (k_{rspf}) were calculated as the slope of the deposited cells over time, normalized by the initial cell concentration and the recording area. Each deposition condition was repeated at least twice.

Column Transport Experiments. Soda-lime glass spheres (Precision Grade Class V, MO-SCI Corporation, Rolla, MO) were used as model collectors. The diameters of the glass spheres were 0.180-0.212 mm, as reported by the manufacturer. The glass beads used in column experiments had a specific gravity of 2.5g/cm^3 and their chemical composition (by weight) was predominately SiO_2 (65~75%), with 0~5% Al_2O_3, 6~15% CaO, 1~5% MgO, 10~20% Na_2O, and <0.8% Fe_2O_3. These glass beads were cleaned as described above for the quartz RSPF surface, but without the initial cleaning in ethanol. Clean glass beads were dried in a 60^{o}C oven and packed into glass columns (1 cm diameter × 20 cm long). Column packing porosities of 40% were determined by the weight difference between the empty columns and packed columns. For the tracer test, 80 mg/L rose bengal (Sigma-Aldrich Co) in electrolyte MOPS buffer solution was pumped through the packed columns until complete breakthrough was observed. The dye solution was stirred by a magnetic bar in the injecting syringe. Cell-free electrolyte buffer solution was then pumped into the column for 2.2 pore volumes. The tracer in the column effluent were measured online at 280 nm using a UV-visible spectrophotometer and a flow through quartz cell. For transport experiments, the packed column was first equilibrated by pumping the electrolyte buffer solution through the column at a constant flow rate of 30 mL/hr for one hour, followed by overnight incubation without flow. Three pore volumes of newly sonicated electrolyte buffer solution were then followed by 2.2 pore volumes of bacterial cell suspension, with concentrations between 2.72×10^7 - 4.17×10^7 cells/mL and in the same

electrolyte buffer solution. This was the same cell concentration used for the RSPF experiments. The bacterial cells in the injecting syringe were kept monodispersed by magnetic stirring during the experiments, to avoid cell clumping prior to entering the micromodels. Then cell-free buffer solution with KCl followed by no KCl buffer was pumped through columns each for 2.2 pore volume to initiate the release of reversibly deposited bacterial cells. However, any detachment was below the detection limit of the UV-visible spectrophotometer. All conditions were repeated at least twice. The approaching velocity of 0.00011 m/s was used for all column experiments. For column experiments with 100 mM KCl, we sacrificed the column and recovered the packed beads after experiments. The packed beads were rinsed rigorously with DI water and the cells in the washing solutions were quantified by a hemocytometer and flow cytometer. Both methods of cell quantification gave similar results. The mass balances of the experiments were calculated based on initial cell concentration, effluent cell concentration and the amount of cells in the washing solutions. The mass balances of DJ77 and Fla$^-$ strains were 92.82% and 96.38%, respectively.

Macro-Scale Modeling of Bacteria Transport in Columns. The general form of the mechanistic bacterial transport model used in this study is based on the work by Massoudieh and Ginn.[51] It is assumed that cells can undergo both reversible and irreversible attachment to the surfaces. The advection-dispersion equation is considered to model colloid transport in the porous media:

$$\frac{\partial \theta G_m}{\partial t} + f\frac{\partial \left(G_{si}+G_{sr}\right)}{\partial t} + \frac{\partial \theta v_c G_m}{\partial z} = \frac{\partial}{\partial z}\left(D_c\theta\frac{\partial G_m}{\partial z}\right) \qquad (1)$$

where θ is the porosity of the medium, G_m [M/L^3] is the mass concentration of mobile (or planktonic) cells, G_{si} [M/L^2] is the surface concentration for cells that are irreversibly attached and G_{sr} [M/L^2] is the surface concentration of cells that are reversibly attached, f [L^2/L^3] is the specific surface area of the medium, v_c [L/T] is the advective velocity for cells, and D_c [L^2/T] is the dispersion coefficient. The basic assumption of the Colloid Filtration Theory (CFT) is that the rate of deposition of colloidal particles onto porous media is proportional to the frequency that the mobile colloids come into contact to the collector surface, known as the collision efficiency (η) and the fraction of collisions that leads to attachment, known as attachment efficiency (α)[6]

$$f\frac{\partial G_{si}}{\partial t} = \beta k_{att}\theta G_m \qquad (2)$$

and

$$f\frac{\partial G_{sr}}{\partial t} = (1-\beta)k_{att}\theta G_m - fk_{\det}G_{sr} \qquad (3)$$

where β is the fraction of cells undergoing irreversible attachment, k_{att} (1/T) is the attachment rate constant and $k_{\det}$ [1/T] is the detachment rate constant. Considering the effect of blocking then

$$k_{att} = \frac{1}{4} f\alpha\eta v_c B(G_s) \qquad (4)$$

where *B* represents the blocking function. Here the blocking function proposed by De Kerchove and Elimelech[35] is adopted and a step-wise method was used to determine the orders of the relationship to be retained in the final model:

$$B(G_s) = \left(1-\frac{G_{si}+G_{sr}}{G_{s,\max}}\right)\left[1+a_1\frac{G_{si}+G_{sr}}{G_{s,\max}}+a_2\left(\frac{G_{si}+G_{sr}}{G_{s,\max}}\right)^2+\cdots\right] \qquad (5)$$

where $G_{s,\max}$ is the maximum surface concentration of attached cells and $a_1, a_2 \cdots$ are empirical coefficients for the non-linear blocking functions. Detachment was assumed as a diffusion-limited process. Since the flow velocity did not change substantially during the column experiments, neither temporally or spatially in single experiments nor across different experiments, the shear stress can be assumed to be constant. Thus $k_{\det}$ is assumed constant. The advection-dispersion equations (1-3) were solved using a Crank-Nicholson finite element technique.[51]

Parameter Estimation. A hybrid genetic algorithm (HGA)[36] consisting of a conventional binary genetic algorithm, random numerical shaking and Simplex method[52] was used to estimate the optimal values of the parameters by minimizing the squared difference between the measured and modeled breakthrough curves. The method uses conventional GA to find the proximities of the global optima and then uses the Simplex method to find the exact

location of the optimal parameters in the parameter space. The code allows user designation of the parameters to be considered fixed and the range of parameters to be estimated using the HGA algorithm.

Two-dimensional Micromodel Experiments. To visualize deposition in porous media directly, silicon micromodels were fabricated through a standard photolithography procedure as described previously.[20] Within each micromodel, a total of 1440 cylindrical collectors (180 μm diameter, 114 μm in pore-body size, 28 μm in pore throat size) were etched to 22 μm depth in a Si wafer, resulting in a porosity of 0.4, similar to that of the packed-bed columns. For all micromodel experiments, electrolyte solutions containing bacterial cells were injected into the micromodel continuously at approaching velocity of 0.0002 m/s. Images were collected using a Leica microscope connected to a charge-coupled device (CCD) camera (Qimaging Retiga 2000R Fast 1394) and Image Pro 7.0 plus software.

The first set of micromodel experiments was conducted to determine the clean collector removal efficiency (η) as a function of time. After the bacteria started flowing into the collector field, gray-scale images of the entire micromodel collector field were collected every 5 min at 2 μm resolution. The deposition of bacterial cells on collectors was quantified manually. The average collector removal efficiency in our work is defined as the ratio of the average rate of attached cells determined for a single collector divided by the rate of cells approaching one collector.[12] The average rate of attached cells for a single collector was determined as the ratio of total attached cells in the micromodel divided by the product of the number of collectors and the experimental time. The rate of cell approaching a collector is calculated as the product of the projected area, Darcy velocity, and the influent cell concentration.

The second set of micromodel experiments was conducted to study ripening. From the first set of micromodel experiments, we observed ripening starting at minute 15 (Figure 4S). Therefore in the second set, after 15 min of cell injection, 1X SYBR® Green I nucleic acid stain (Lonza Rockland, Inc.) was injected into the micromodel overnight, washing away non-attached cells and staining the attached cells. Images of 5 collectors at each location, including the inlet, the middle and the outlet in the micromodel were obtained. For ease of visualization, gray-scale images of cells attached to collectors were rendered in pseudo-color in Matlab. Relative biomass coverage was determined using image thresholding and clustering methods.[53, 54] Specifically, an intensity threshold was set for each image to distinguish biomass, collector, and clean pore

space. The relative biomass was the area of biomass (i.e. pixels of biomass) over the total pixels of each image.

3.4 Results and Discussion

Electrophoretic mobility of study materials. DJ77 has peritrichous flagella stretching out around the cell surface, as visualized by TEM (**Figure 6**) and previously reported for *A. vinelandii*.[44] No flagella were observed in TEM visualization/images of approximately 60 Fla^- cells. However, both strains have similar electrophoretic mobility (**Figure 7**a), indicating that the presence of flagella did not influence electrophoretic mobilities values of these strains. The electrophoretic mobilities of both strains increased from -3.1 to around -1.1 (μm/s)/(V/cm) as the ionic strength rose from 1 to 200 mM KCl. These results suggest that, at least for these strains, flagella do not affect the surface charge.

The electrophoretic mobilities of cleaned glass beads, RSPF quartz slide and micromodel silica surface were slightly more negative than that of the bacterial cells and increased from -4.0 to -1.1 (μm/s)/(V/cm) as the ionic strength increased from 1 to 200 mM KCl. The electrophoretic mobilities of all three collector surfaces were statistically similar based on paired t-test with p value of 0.05.

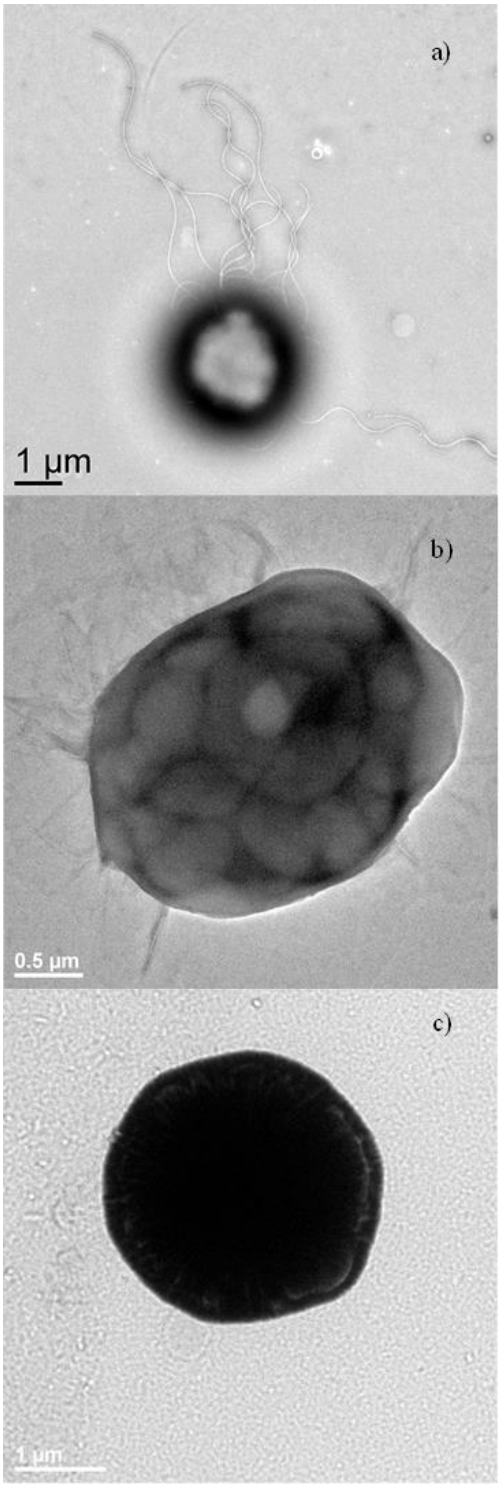

Figure 6 TEM images of flagellated (DJ77, a and b) and non-flagellated (JZ52, c) cells. Figure a was captured with the flagella in focus, while figure b was captured with the cell in focus. The light color filaments stretching out from DJ77 in panels a and b are the flagella. The dark halo around the cell in panel a is due to projecting shadows caused by the cell.

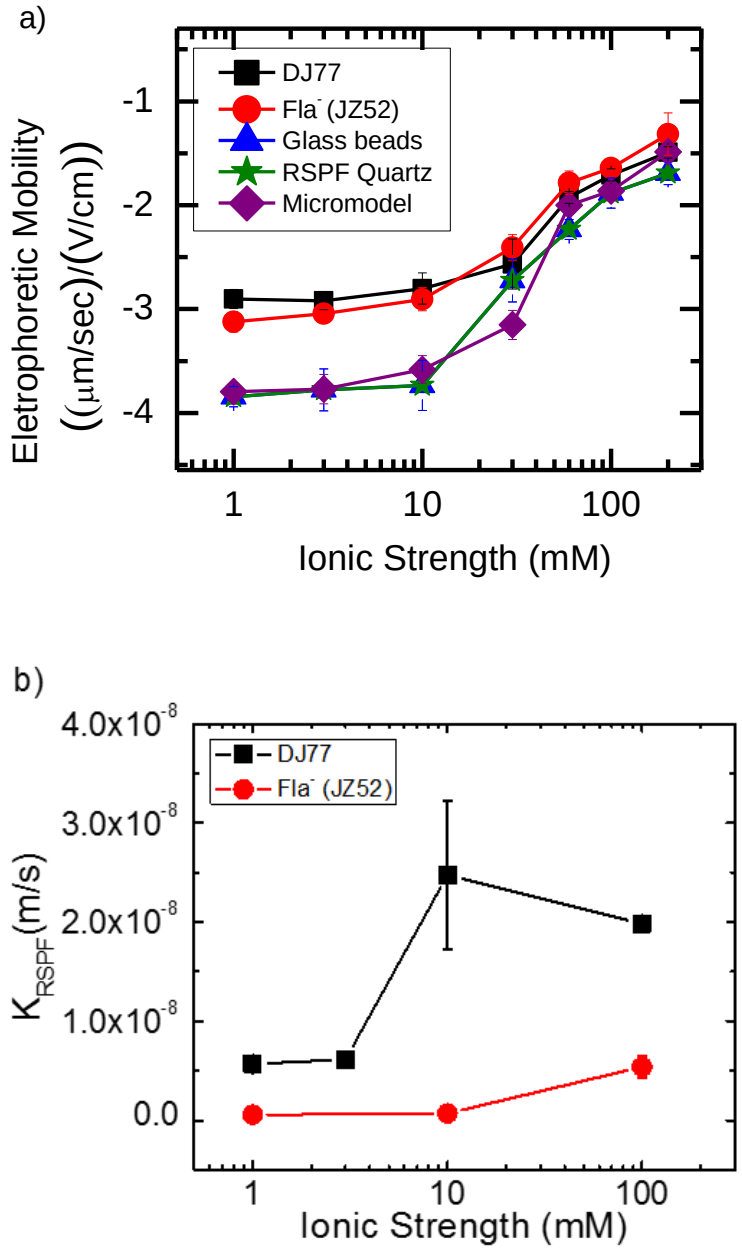

Figure 7 a) Electrophoretic mobilities of flagellated DJ77 and Fla- cells, glass beads used in column experiments, RSPF collectors and micromodel collectors as a function of ionic strength; b) RSPF deposition rates of flagellated DJ77 (solid squares) and Fla- (solid circles) as a function of ionic strength. MOPS buffer was used to maintain pH 7.2.

Bacterial Size and Motility Characterization. Three imaging methods were used to determine the sizes of the studied bacterial strains. From TEM images, we determined the diameters of the non-flagellated (Fla⁻) and flagellated (DJ77) cell body as 2.5±0.4 μm (N=5) and

2.3±0.5 μm (N=5), respectively. Because of the TEM sample preparation, this size corresponds to dehydrated cells. Using regular microscopy for unstained cells, we determined the diameter of the non-flagellated cells to be 3.5±0 μm (N=5). Using fluorescence staining (amine-reactive dyes Alexa Fluor 546 and 594), we determined the diameter of the Fla$^-$ and DJ77 cells as 2.5±0 μm (N=5) and 2.9±0.5 μm (N=5), respectively. When flagella are included in the calculations, the diameter of the flagellated DJ77 cells increased to 4.5±0.8 μm (N=5). Thus, the cell to collector ratio is 0.025, which is smaller than the ratio of 0.05 at which straining occurs.[55, 56]

Motility was quantified by applying a particle-tracking algorithm to time series microscope images from three strains, DJ77, Fla- and wild type DJ. The trajectories of individual cells (**Figure 8**a-c) were analyzed to assess i) whether these strains were actively motile or were simply subject to Brownian diffusion, ii) whether their movement was random or directed, and iii) what average velocity they exhibited. The data were plotted as the mean squared displacements with respect to cells' initial location as a function of time, fitted using a power function (Fig. 2d). For purely Brownian diffusion motion, the exponent of time in the power relationships should be equal to unity, while other mechanisms of motility will result in an exponent above one.[57] Both DJ77 and wild type DJ had exponents greater than one (1.51 for DJ77 and 1.23 for DJ), indicating motility mechanisms other than Brownian motion were occurring. This conclusion is also supported by these strains showing more consistency of their direction of movement, resulting in a correlated random walk and super-diffusion (**Figure 8**a-c). In contrast, for the Fla- cells the exponent was near one (0.91), indicating near Brownian motion of uncorrelated random jumps, with little change in the location of the cells.

A striking difference was observed in the movement velocity of the three strains, with DJ77 showed around an order of magnitude smaller overall displacement compared to wild type DJ (**Figure 8**d). This quantitative and statistical analysis showed that DJ77 exhibits much less motility than the wild type strain; it does not exhibit the characteristic swimming motility that would be expected for a strain with peritrichous flagella. To better understand the genetic basis for DJ77's unexpectedly poor motility, we tested whether correcting the known defect in nitrogen fixation would also repair the motility defect. When the *nifH* deletion was repaired and nitrogen fixation was restored, through transformation with chromosomal DNA, increased motility was also always observed (78 transformants tested). The motility defect in DJ77 therefore appears to be related to its *nifH* mutation. Although the molecular basis for the

connection between nitrogen fixation and motility is not understood, this phenomenon was fortuitous, because it provided a strain with flagella but with limited motility (DJ77), allowing us to specifically investigate the effects of the physical flagella structure on bacterial deposition.

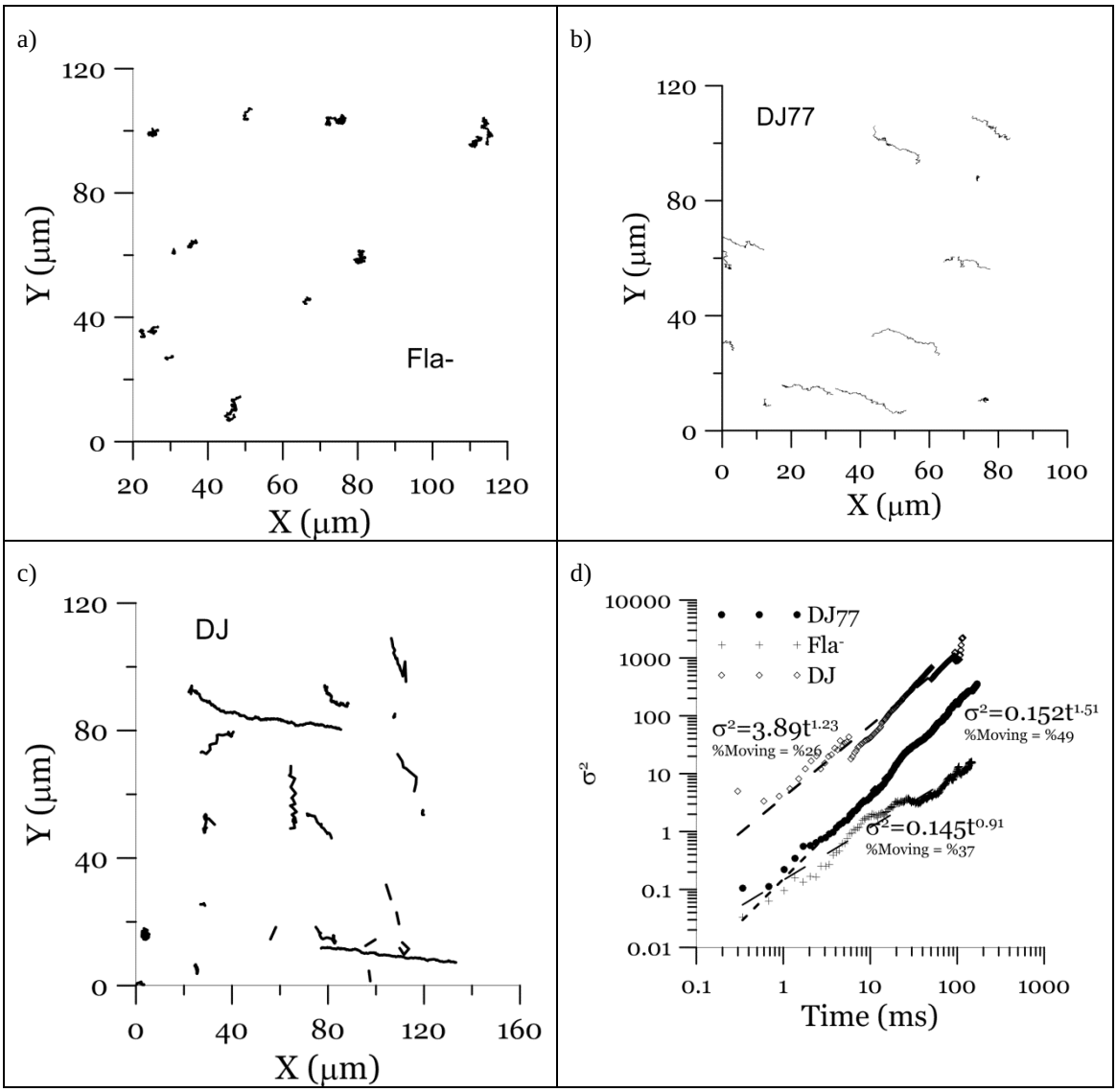

Figure 8 Sample trajectories of moving a) Fla-, b) DJ77 and c) DJ (wild type). Trajectories shown are from a single microscope field for each strain imaged over time. Note that the x-axes scales differ. d) Mean squared displacements with respect to cells' initial location as a function of time, fitted using a power function for DJ77, Fla- and DJ (wild type) for moving fraction of cells obtained from analyzing the trajectories in Figure a-c. The motion of Fla- cells seems to be an uncorrelated random walk resulting in sub-diffusion spread, while DJ77 and DJ exhibit correlated random walks resulting in super-diffusion.

Deposition in RSPF setup. Bacterial deposition on the forward stagnation point was dependent on ionic strength for the flagellated DJ77, but not for the Fla$^-$ strain (**Figure 7**b). In addition, flagellated DJ77 deposited more than Fla$^-$ under all ionic strengths tested. Based on similar electrophoretic mobilities for these two strains, these differences in deposition were not expected if only van der Waals and electrostatic interactions influenced the deposition. This observation suggests that electrophoretic mobilities alone are not a good indicator for deposition; deposition may also be controlled by other factors besides electrostatics. Hydrophobicity was suggested as a controlling factor for deposition of a highly hydrophobic and motile strain of *Sphingomonas wittichii* RW1.[58] In this study, however, the ratios of DJ77 and Fla$^-$ strains suspended in dodecane were 45.6%±4.6% and 33.6%±7.6%, respectively. This small difference in hydrophobicity is not likely to explain the observed difference in deposition with respect to ionic strength. Instead, changes in conformation of the flagella of DJ77 in different ionic strength solutions could result in ionic strength dependent deposition, while the lack of flagella in the Fla$^-$ strain allows deposition independent of ionic strength.

Blocking: column breakthrough curves and micromodel observations. The tracer curve showed no tailing and complete breakthrough at around 30 min (**Figure 9**). After a 30 min initial stage of bacteria deposition, the breakthrough curves obtained for all three ionic strengths (1, 10, and 100 mM KCl) and in all replicates of both strains did not reach a stable value, instead showing a decrease in the deposition rate (**Figure 10**a). This shape of breakthrough curves has been observed in earlier studies on a variety of colloids, including latex particles[16, 31] and bacteria,[23, 43, 59] and has been attributed to particles attached to the collector surfaces blocking the attachment of incoming particles. In contrast to RSPF results, in the column experiments the Fla$^-$ strain deposited more. We attribute this to cell-to-cell interactions, which cannot be observed in the RSPF experiments due to the camera position used to monitor the cells deposited on the collector surface. In addition, compared to the column setup the RSPF provides much less surface area for deposition and a simpler flow field. Differences were again observed in the response to ionic strength, with DJ77 showing changes in deposition rates with ionic strength, while the Fla$^-$ strain showed similar slopes of the breakthrough curves for all ionic strengths.

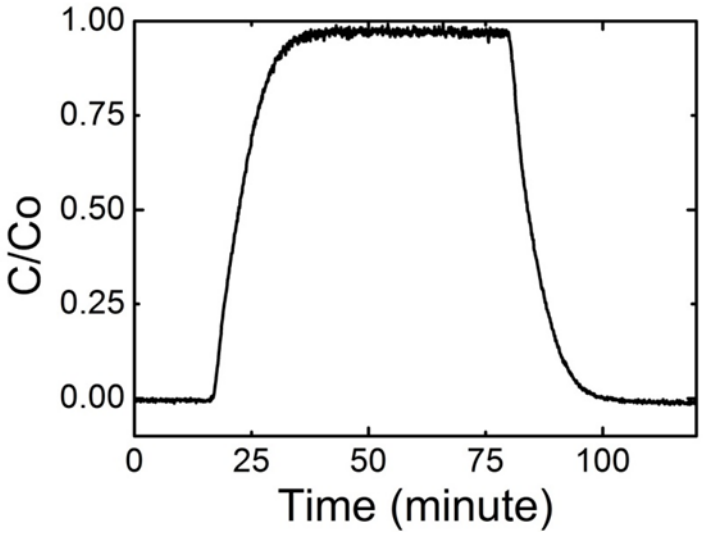

Figure 9 Tracer test for the packed-bed column setup. The conservative tracer solution was 80 mg/L rose bengal in MOPS buffer with 100 mM KCl.

To identify important processes for the transport of bacteria in the column, the breakthrough curves were initially modeled using the simplest model structure, including only advection and deposition, and then complexity was added through the step-wise addition of blocking, dispersion, and detachment. The HGA parameter estimation approach was used to estimate the parameters for each strain. The values of mean squared error (MSE) were calculated for each case and were used to identify the processes to be included in the final model structure. Modeled and measured breakthrough curves for DJ77 in 100 mM are shown in **Figure 10** for some of the model structures examined: 1) only attachment, 2) attachment and blocking, 3) attachment, Langmuirian (first-order) (i.e. a_1=0) blocking, and dispersion, 4) attachment, dispersion, Langmuirian blocking, and detachment, and 5) attachment, dispersion, 2nd order blocking, and detachment. The third model, that includes dispersion and first order blocking, reproduced the observed breakthrough curves well, although for DJ77 it was not able to capture the tail of the curve perfectly. Adding detachment (model 4) improved the fit in the tail region. We also examined higher order blocking functions where a_1 was among the parameters to be estimated (model 5), but no significant improvement in the match between the modeled and measured data was achieved (data not shown).

The model 4 structure was therefore applied to the breakthrough curves for both strains under various ionic strengths (**Figure 10**, **Table 3**). Since the dispersion coefficient is not deemed to be affected by the ionic strength, a single value of dispersivity was used for each strain under different ionic strengths. The deterministic parameter estimation method used in this work did not allow the assessment of the statistical significance of the difference between the dispersivity for flagellated and non-flagellated bacteria. To limit the degrees of freedom, the fraction of irreversibly attached cells and the detachment rate constant were also assumed to be independent of ionic strength. For DJ77 strain, the effective single collector removal efficiency ($\alpha\eta_0$) and the maximum surface coverage parameter ($G_{s,max}$) both increased with ionic strength between 1-100mM. The sensitivity of $G_{s,max}$ was higher with respect to ionic strength; i.e. the values of maximum surface coverage were severely limited at lower ionic strengths. For the Fla^- strain, the effective attachment rate also increased with ionic strength, although the sensitivity of the effective single collector removal efficiency ($\alpha\eta_0$) to the ionic strength was smaller compared to DJ77. On the other hand, for the Fla^- strain there was no consistent correlation between ionic strength and $G_{s,max}$. The values of $G_{s,max}$ at lower ionic strengths were also higher for the non-flagellated strain compared to the flagellated one. The dependence of $G_{s,max}$ values on ionic strength for the flagellated strain could be due to conformational changes of the micrometer-size flagella in different ionic strength solutions. The lack of this dependence for the non-flagellated strain may be due to steric interactions of the macromolecules on the cell surface with the collectors.

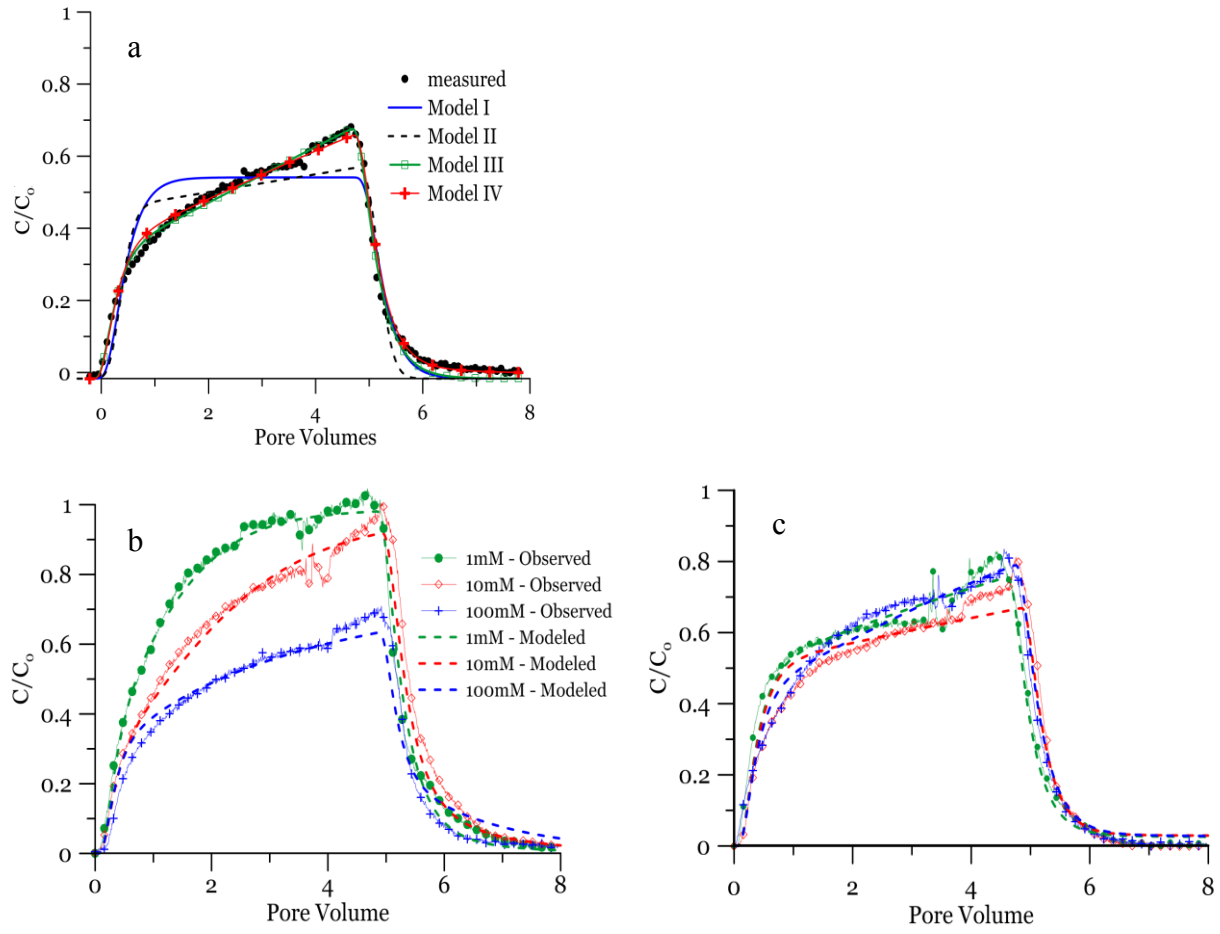

Figure 10 a) Stepwise evaluation of the controlling processes using best model fits for the DJ77 breakthrough curve under 100mM IS using various bacterial transport model structures.: Model I: No dispersion, no detachment and no blocking, Model II: Langmuirian blocking and no dispersion or detachment, Model III: Dispersion and Langmuirian blocking but no detachment, Model IV: Dispersion, Langmuirian blocking and detachment. The results with 2nd order blocking are not shown because they were almost identical with the Langmuirian blocking function. Modeled and observed breakthrough curves under various ionic strengths for b) DJ77 and c) Fla- strains using the model including blocking, dispersion, attachment and detachment (Model IV).

For both DJ77 and Fla$^-$ strains, the modeling results showed that about half the cells attached irreversibly (~56.5% and ~55.6% respectively). However, the rate of detachment under our experimental conditions was slow relative to the time-scale of the experiment, resulting in only a small fraction of the attached cells undergoing detachment during an experiment. The detachment rate of DJ77 is predicted to be almost four times larger than the Fla$^-$ strain. Since there seems to be a correlation between the detachment rate constant k_{det} and the fraction of cells

undergoing irreversible attachment (β), a more rigorous statistical inverse modeling is necessary to determine the uniqueness of this outcome.

Table 3 Parameter values and estimated parameters for column experiments.

Strain	DJ77 (flagellated)			JZ52 (non-flagellated, Fla$^-$)		
Ionic Strength	100mM	10mM	1mM	100mM	10mM	1mM
Injected concentration C_0 (cells/mL)	2.46×10^7	3.04×10^7	3.79×10^7	2.71×10^7	3.29×10^7	3.97×10^7
Porosity	0.407	0.404	0.391	0.404	0.386	0.391
Pulse Duration (min)	60	61	60	61	60	57
Flow rate (mL/hr)	30	30	30	30	30	30
Dispersivity (cm)		0.0692			0.076	
Effective single collector contact efficiency $(\alpha\eta_0)$[12]	7.74×10^{-7}	6.11×10^{-7}	3.92×10^{-7}	4.50×10^{-7}	5.29×10^{-7}	3.97×10^{-7}
Normalized maximum surface coverage ($G_{s,max}/C_0$, m)	1.41	0.515	0.204	0.830	0.980	0.861
Fraction of collector surfaces covered (%)	2.45	1.11	0.55	1.59	2.28	2.42
Detachment rate constant (k_{det}) (1/s)		9.77×10^{-5}			2.55×10^{-5}	
Fraction of irreversible attachment (β)		0.565			0.556	

Calculated values of average surface coverage G_s support a role for blocking during the early stages of deposition (**Figure 11**). For DJ77, the surfaces became saturated after 25-33 minutes and 50-60 minutes for 1mM and 10mM IS, respectively. For experiments with 100mM, the surfaces did not reach saturation: the saturation surface coverage normalized by the injection concentration (C_0), $G_{s,max}/C_0$ is estimated to be 1.41, while the maximum surface coverage attained during the experiment is about 0.8. For the Fla$^-$ strains, the surface coverage was not substantially affected by IS and surfaces were not saturated, although they got close to the

maximum surface coverage. This can be also seen by comparing the highest values of surface coverage and the maximum surface coverage parameters obtained through parameter estimation (**Table 3**). The column breakthrough curve results and the inverse modeling results suggest that in the early stage of deposition approaching cells are effectively blocked by already deposited cells.

A blocking mechanism was further supported through direct quantification of bacterial cell deposition in micromodel experiments. The micromodel clean collector removal efficiency (η) was calculated as the ratio of attached cells to the total number of the approaching cells. At 5 min, the average micromodel η were 4.48×10^{-4} for flagellated DJ77 and 8.05×10^{-4} for Fla^{-}. At 15 minutes, the values of η decreased to 2.31×10^{-4} and 4.69×10^{-4}, respectively. The decrease in η suggested blocking taking place between 5 and 15 min in the micromodel. η was not determined after 15 min, because multiple-layer deposition or ripening occurred as described below.

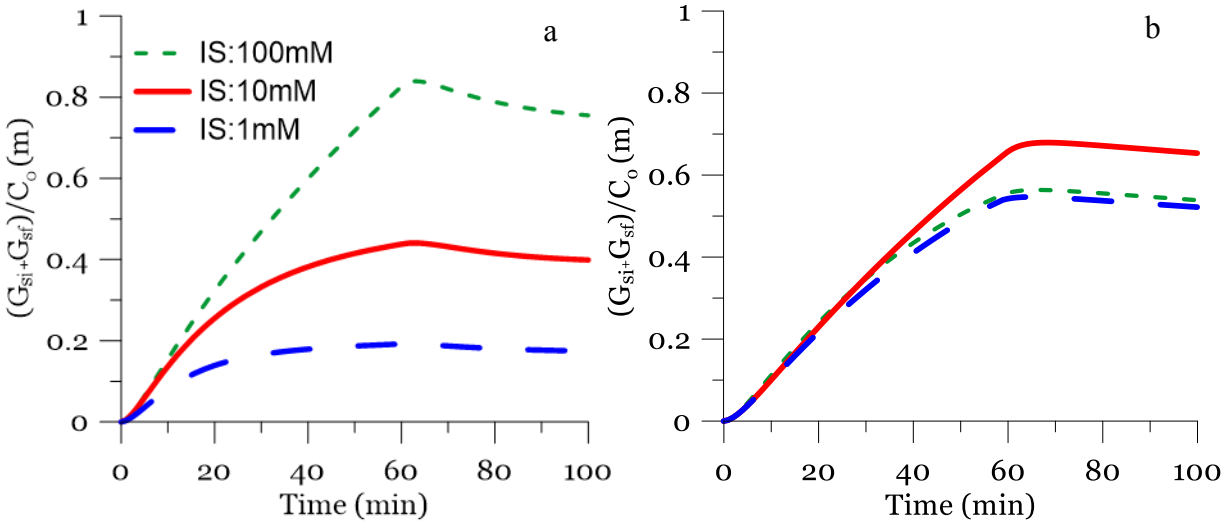

Figure 11 Modeled surface coverage of a) DJ77 and b) Fla- strains as a function of time under various ionic strengths. The surface coverage was calculated from the breakthrough curve to visualize bacterial deposition on the glass beads in the column.

Ripening: direct observation in the micromodel setup. As the micromodel experiments conducted with 100 mM KCl were continued, between 15-30 min of operation, ripening was also observed in both replicates of the Fla^{-} strain (representative images in **Figure 12** and **Figure 13**). For example, during the first 15 min of the experiment, the bacterial cells deposited on two locations on the forward part of the collector surface (**Figure 13**a-c). Between

15-30 min of the experiment, incoming bacterial cells deposited on top of the already attached cells and formed multiple-layer deposition (**Figure 13**d-f). Images shown in **Figure 12** were quantified to obtain relative biomass coverages (**Figure 14**). The relative biomass coverage of Fla^- cells on the collectors within the imaging area near the inlet was 0.107, compared to 0.006 in the middle and near the outlet. In contrast, for DJ77 the corresponding values were 0.010, 0.005, and 0.005, respectively (**Figure 14**). Rather than being blocked from attaching by previously attached cells, near the inlet the approaching Fla^- cells started to attach to them. In the middle and near the outlet the attachment of the two strains were similar. In a control experiment using 50% growth media, no cell growth was observed during 30 min incubation. Thus, cell growth was not expected in the micromodel due to the short 30 min duration and the use of buffered electrolyte rather than growth media. These micromodel results support our interpretation that cell-to-cell interactions lead to more deposition of the Fla^- strain, in contrast to RSPF experiments where only cell-to-surface interactions are considered and the deposition was greater with flagella.

The timescales for blocking and ripening were different depending on the experimental setup. In column experiments, deposition rates decreased during 60 min experiments due to blocking. However, in micromodel experiments ripening was observed after only 15 min. This is because a much lower number of collectors were available in the micromodels compared to the columns. In the 15 min micromodel experiment, the ratio of injected bacterial cells to collector surfaces was approximately 148 times higher than the 60 min column experiment.

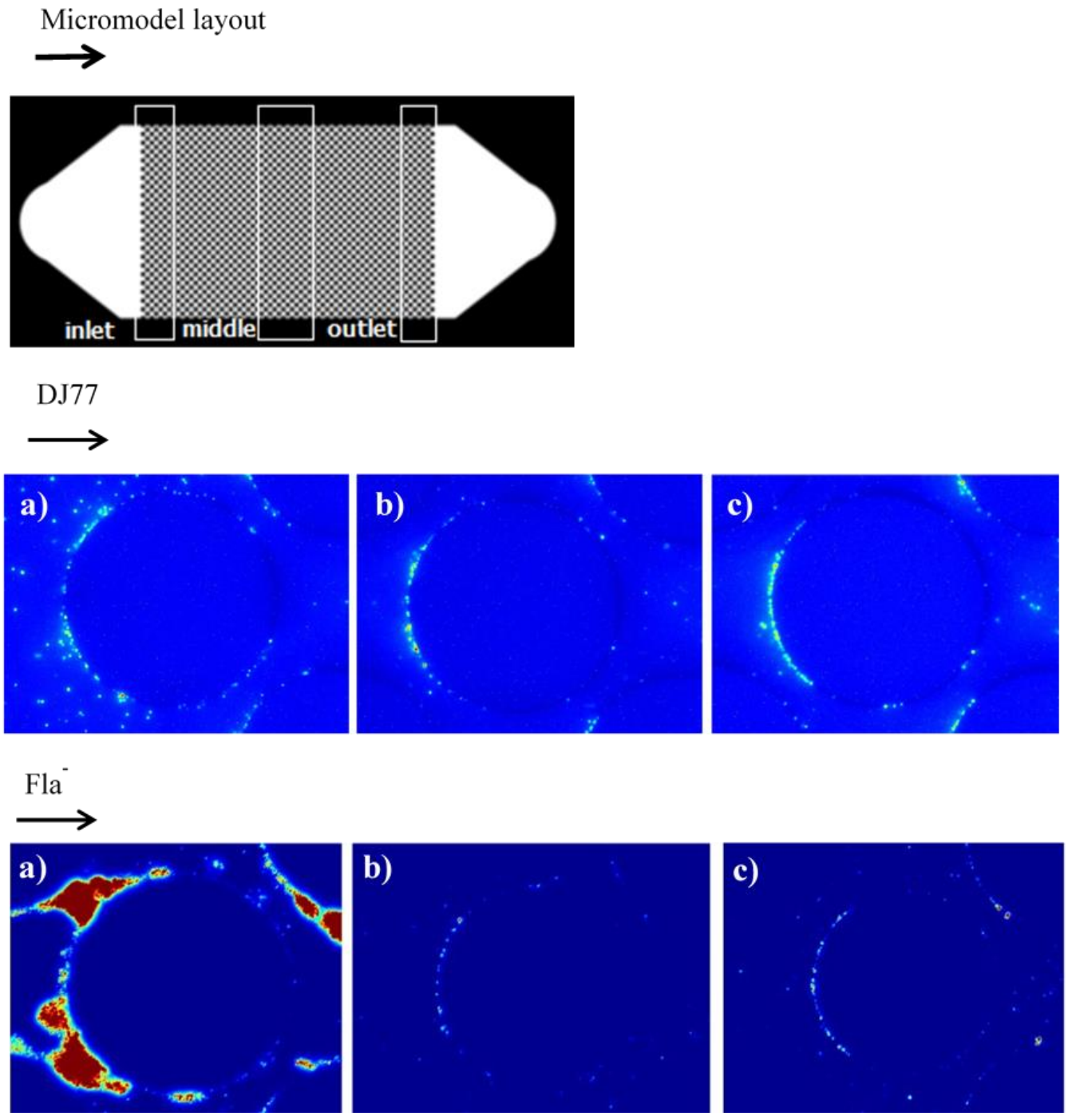

Figure 12 Direct observation of ripening phenomena in micromodels. The fluorescent images of DJ77 and Fla- were taken from different locations of micromodels. a) inlet; b) middle; c) outlet. The flow direction is from left to right. The dark circles in the center of the images are individual collectors in the micromodels. The black arrows in both the whole micromodel scheme and the first fluorescent image represent flow direction in the micromodel. Experiments were conducted with 100 mM KCl.

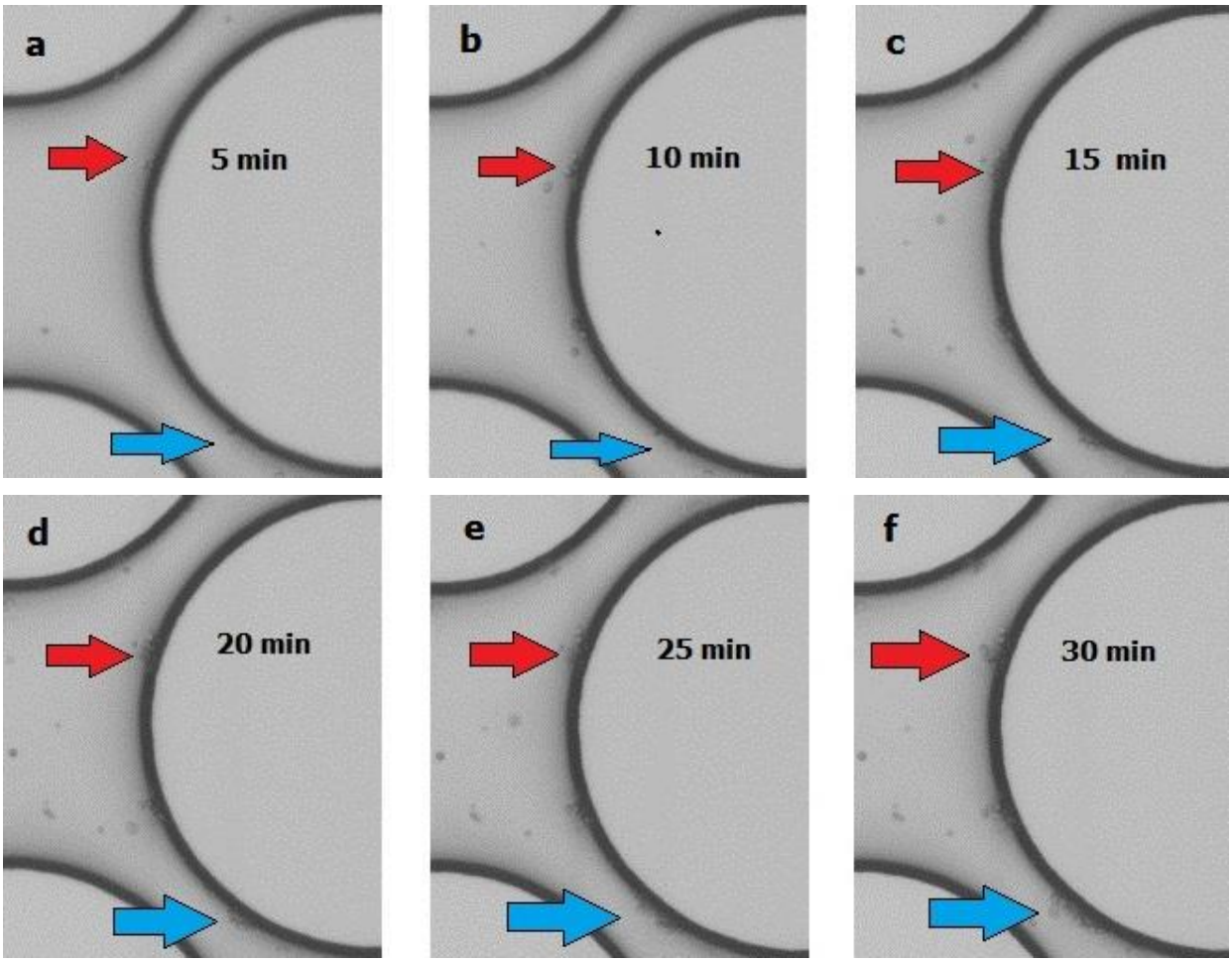

Figure 13 Time series images of non-flagellated JZ52 deposition dynamics on a single collector over a time period of 30 min (a-5 min, b-10 min, c-15 min, d-20 min, e-25 min, f-30 min of the experiment). The flow direction is from left to right in the porous media. The red and blue arrows indicate the spots where ripening was observed during the 30 min of the experiment.

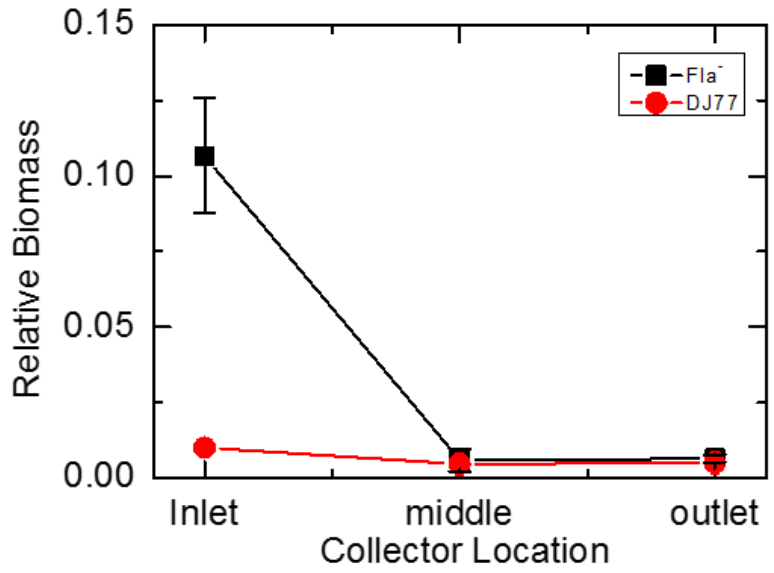

Figure 14 Relative biomass coverage of non-flagellated JZ52 (black cubes) and flagellated DJ77 (red circles) on single collectors in different locations of the micromodels. Relative biomass coverage was quantified as the number of pixels of fluorescent bacterial deposition over the total pixel number of an image. The standard deviation was obtained from 5 replicate collectors in each location.

3.5 Environmental Implications

Results from this comprehensive multi-scale study showed that the presence of flagella, independent of bacterial motility, could substantially influence the dynamics of bacterial transport through porous media. Bacterial motility is dependent on the cell's proton motive force, which supplies energy for flagellar rotation and is itself related to nutrient availability, and on the local hydration state.[40, 60] Because of this dependence on the local environment, cells that have flagella, but are not actively moving, may be common in the soil environment and are thus directly relevant to our understanding of bacterial transport and deposition. For porous media with clean sand grains, at environmentally relevant ionic strengths of 1 mM to 10 mM, the flagellated strain of *A. vinelandii* was more mobile than the non-flagellated strain. For the later stage of transport, ripening mechanism occurred earlier for the non-flagellated strain. The dynamics observed at different stages of bacteria transport in this study suggest that it is

important to conduct experiments at multiple scales ranging from microscopic to macroscopic and that modeling efforts should be based on observations across scales.

3.6 Acknowledgements

This work was supported by NSF Grant No. 1066152 and part of the research was conducted in the William R. Wiley Environmental Molecular Sciences Laboratory, a scientific user facility of the United States Department of Energy's Office of Biological and Environmental Research and operated by the Pacific Northwest National Laboratory.

3.7 References

1. Ginn, T. R.; Wood, B. D.; Nelson, K. E.; Scheibe, T. D.; Murphy, E. M.; Clement, T. P., Processes in Microbial Transport in the Natural Subsurface. *Advances in Water Resources* **2002,** *25*, (8-12), 1017-1042.

2. Harvey, R. W.; Garabedian, S. P., Use of Colloid Filtration Theory in Modeing Movement of Bacteria through a Contaminated Sandy Aquifer. *Environmental Science & Technology* **1991,** *25*, (1), 178-185.

3. Tufenkji, N., Modeling Microbial Transport in Porous Media: Traditional Approaches and Recent Developments. *Advances in Water Resources* **2007,** *30*, (6-7), 1455-1469.

4. Stevik, T. K.; Aa, K.; Ausland, G.; Hanssen, J. F., Retention and Removal of Pathogenic Bacteria in Wastewater Percolating through Porous Media: A Review. *Water Research* **2004,** *38*, (6), 1355-1367.

5. Kretzschmar, R.; Borkovec, M.; Grolimund, D.; Elimelech, M., Mobile Subsurface Colloids and Their Role in Contaminant Transport. *Advances in Agronomy, Vol 66* **1999,** *66*, 121-193.

6. Rajagopalan, R.; Tien, C., Trajectory Analysis of Deep Bed Filtration with Sphere in Cell Porous Media Model. *Aiche Journal* **1976,** *22*, (3), 523-533.

7. Nelson, K. E.; Ginn, T. R., Colloid Filtration Theory and the Happel Sphere-in-Cell Model Revisited with Direct Numerical Simulation of Colloids. *Langmuir* **2005,** *21*, (6), 2173-2184.

8. Nelson, K. E.; Ginn, T. R., New Collector Efficiency Equation for Colloid Filtration in Both Natural and Engineered Flow Conditions. *Water Resources Research* **2011,** *47*.

9. Yao, K. M.; Habibian, M. M.; Omelia, C. R., Water and Wastewater Filtration - Concepts and Applications. *Environmental Science & Technology* **1971,** *5*, (11), 1105-&.

10. Logan, B. E.; Jewett, D. G.; Arnold, R. G.; Bouwer, E. J.; Omelia, C. R., Clarification of Clean Bed Filtration Models. *Journal of Environmental Engineering-Asce* **1995,** *121*, (12), 869-873.

11. Long, W.; Hilpert, M., A Correlation for the Collector Efficiency of Brownian Particles in Clean-Bed Filtration in Sphere Packings by a Lattice-Boltzmann Method. *Environmental Science & Technology* **2009,** *43*, (12), 4419-4424.

12. Tufenkji, N.; Elimelech, M., Correlation Equation for Predicting Single-Collector Efficiency in Physicochemical Filtration in Saturated Porous Media. *Environmental Science & Technology* **2004,** *38*, (2), 529-536.

13. Tufenkji, N.; Elimelech, M., Breakdown of Colloid Filtration Theory: Role of the Secondary Energy Minimum and Surface Charge Heterogeneities. *Langmuir* **2005,** *21*, (3), 841-852.

14. Bradford, S. A.; Yates, S. R.; Bettahar, M.; Simunek, J., Physical Factors Affecting the Transport and Fate of Colloids in Saturated Porous Media. *Water Resources Research* **2002,** *38*, (12).

15. Elimelech, M.; Omelia, C. R., Effect of Particle Size on Collision Efficiency in the Deposition of Brownian Particles with Electrostatic Energy Barriers. *Langmuir* **1990,** *6*, (6), 1153-1163.

16. Tufenkji, N.; Elimelech, M., Deviation from the Classical Colloid Filtration Theory in the Presence of Repulsive DLVO Interactions. *Langmuir* **2004,** *20*, (25), 10818-10828.

17. Bradford, S. A.; Torkzaban, S.; Simunek, J., Modeling Colloid Transport and Retention in Saturated Porous Media under Unfavorable Attachment Conditions. *Water Resources Research* **2011,** *47*.

18. Bradford, S. A.; Torkzaban, S., Colloid Adhesive Parameters for Chemically Heterogeneous Porous Media. *Langmuir* **2012,** *28*, (38), 13643-13651.

19. Rizwan, T.; Bhattacharjee, S., Particle Deposition onto Charge-Heterogeneous Substrates. *Langmuir* **2009,** *25*, (9), 4907-4918.

20. Liu, Y.; Zhang, C.; Hilpert, M.; Kuhlenschmidt, M. S.; Kuhlenschmidt, T. B.; Nguyen, T. H., Transport of *Cryptosporidium Parvum* Oocysts in a Silicon Micromodel. *Environmental Science & Technology* **2012,** *46*, (3), 1471-1479.

21. Liu, Y.; Zhang, C.; Hu, D.; Kuhlenschmidt, M. S.; Kuhlenschmidt, T. B.; Mylon, S. E.; Kong, R.; Bhargava, R.; Nguyen, T. H., Role of Collector Alternating Charged Patches on Transport of *Cryptosporidium Parvum* Oocysts in a Patchwise Charged Heterogeneous Micromodel. *Environmental Science & Technology* **2013**.

22. Hoek, E. M. V.; Bhattacharjee, S.; Elimelech, M., Effect of Membrane Surface Roughness on Colloid-Membrane DLVO Interactions. *Langmuir* **2003,** *19*, (11), 4836-4847.

23. Torkzaban, S.; Tazehkand, S. S.; Walker, S. L.; Bradford, S. A., Transport and Fate of Bacteria in Porous Media: Coupled Effects of Chemical Conditions and Pore Space Geometry. *Water Resources Research* **2008,** *44*, (4), W04403.

24. Bradford, S. A.; Simunek, J.; Bettahar, M.; van Genuchten, M. T.; Yates, S. R., Significance of Straining in Colloid Deposition: Evidence and Implications. *Water Resources Research* **2006,** *42*, (12).

25. Ko, C. H.; Bhattacharjee, S.; Elimelech, M., Coupled Influence of Colloidal and Hydrodynamic Interactions on the Rsa Dynamic Blocking Function for Particle Deposition onto Packed Spherical Collectors. *Journal of Colloid and Interface Science* **2000,** *229*, (2), 554-567.

26. Song, L.; Elimelech, M., Dynamics of Colloid Deposition in Porous Media - Modeling the Role of Retained Particles. *Colloids and Surfaces a-Physicochemical and Engineering Aspects* **1993,** *73*, 49-63.

27. Chen, G.; Strevett, K. A., Microbial Deposition in Porous Media: A Surface Thermodynamic Investigation. *Environmental Engineering Science* **2003,** *20*, (3), 237-248.

28. Brown, D. G.; Abramson, A., Collision Efficiency Distribution of a Bacterial Suspension Flowing through Porous Media and Implications for Field-Scale Transport. *Water Research* **2006,** *40*, (8), 1591-1598.

29. Nascimento, A.; Totola, M.; Souza, C.; Borges, M.; Borges, A., Temporal and Spatial Dynamics of Blocking and Ripening Effects on Bacterial Transport through a Porous System: A Possible Explanation for Cft Deviation. *Colloids and Surfaces B: Biointerfaces* **2006,** *53*, (2), 241-244.

30. Ko, C.-H.; Elimelech, M., The "Shadow Effect" in Colloid Transport and Deposition Dynamics in Granular Porous Media: Measurements and Mechanisms. *Environmental Science & Technology* **2000,** *34*, (17), 3681-3689.

31. Johnson, P. R.; Elimelech, M., Dynamics of Colloid Deposition in Porous Media - Blocking Based on Randon Sequential Adsorption. *Langmuir* **1995,** *11*, (3), 801-812.

32. Camesano, T. A.; Logan, B. E., Influence of Fluid Velocity and Cell Concentration on the Transport of Motile and Nonmotile Bacteria in Porous Media. *Environmental Science & Technology* **1998,** *32*, (11), 1699-1708.

33. Camesano, T. A.; Unice, K. M.; Logan, B. E., Blocking and Ripening of Colloids in Porous Media and Their Implications for Bacterial Transport. *Colloids and Surfaces A-Physicochemical and Engineering Aspects* **1999,** *160*, (3), 291-308.

34. Schaaf, P.; Talbot, J., Surface Exclusion Effects in Adsorption Processes. *Journal of Chemical Physics* **1989,** *91*, (7), 4401-4409.

35. de Kerchove, A. J.; Elimelech, M., Bacterial Swimming Motility Enhances Cell Deposition and Surface Coverage. *Environmental Science & Technology* **2008,** *42*, (12), 4371-4377.

36. Massoudieh, A.; Mathew, A.; Ginn, T. R., Column and Batch Reactive Transport Experiment Parameter Estimation Using a Genetic Algorithm. *Computers & Geosciences* **2008,** *34*, (1), 24-34.

37. Levy, J.; Sun, K.; Findlay, R. H.; Farruggia, F. T.; Porter, J.; Mumy, K. L.; Tomaras, J.; Tomaras, A., Transport of *Escherichia coli* Bacteria through Laboratory Columns of Glacial-Outwash Sediments: Estimating Model Parameter Values Based on Sediment Characteristics. *Journal of Contaminant Hydrology* **2007,** *89*, (1-2), 71-106.

38. Erhardt, M.; Namba, K.; Hughes, K. T., Bacterial Nanomachines: The Flagellum and Type Iii Injectisome. *Cold Spring Harbor Perspectives in Biology* **2010**.

39. Khan, I. H.; Reese, T. S.; Khan, S., The Cytoplasmic Component of the Bacterial Flagellar Motor. *Proceedings of the National Academy of Sciences* **1992,** *89*, (13), 5956-5960.

40. Dechesne, A.; Wang, G.; Gulez, G.; Or, D.; Smets, B. F., Hydration-Controlled Bacterial Motility and Dispersal on Surfaces. *Proceedings of the National Academy of Sciences of the United States of America* **2010,** *107*, (32), 14369-14372.

41. Singh, R.; Olson, M. S., Transverse Mixing Enhancement Due to Bacterial Random Motility in Porous Microfluidic Devices. *Environmental Science & Technology* **2011,** *45*, (20), 8780-8787.

42. McClaine, J. W.; Ford, R. M., Characterizing the Adhesion of Motile and Nonmotile *Escherichia coli* to a Glass Surface Using a Parallel-Plate Flow Chamber. *Biotechnology and Bioengineering* **2002,** *78*, (2), 179-189.

43. Haznedaroglu, B.; Zorlu, O.; Hill, J.; Walker, S., Identifying the Role of Flagella in the Transport of Motile and Nonmotile *Salmonella enterica* Serovars. *Environmental Science & Technology* **2010,** *44*, (11), 4184-4190.

44. Kennedy, C.; Rudnick, P.; MacDonald, M. L.; Melton, T., *Genus Iii. Azotobacter*. Springer, New York, NY, USA.: 2005.

45. Jacobson, M. R.; Brigle, K. E.; Bennett, L. T.; Setterquist, R. A.; Wilson, M. S.; Cash, V. L.; Beynon, J.; Newton, W. E.; Dean, D. R., Physical and Genetic Map Pf the Major Nif Gene Cluster from *Azotobacter vinelandii*. *Journal of Bacteriology* **1989,** *171*, (2), 1017-1027.

46. León, R.; Espín, G., flhDC, but Not fleQ, Regulates Flagella Biogenesis in *Azotobacter vinelandii*, and Is under AlgU and CydR Negative Control. *Microbiology* **2008,** *154*, (6), 1719.

47. Strandberg, G. W.; Wilson, P. W., Formation of the Nitrogen-Fixing Enzyme System in *Azotobacter vinelandii*. *Canadian Journal of Microbiology* **1968,** *14*, (1), 25-31.

48. Lu, N.; Zilles, J. L.; Nguyen, T. H., Adsorption of Extracellular Chromosomal DNA and Its Effects on Natural Transformation of *Azotobacter vinelandii*. *Applied and Environmental Microbiology* **2010,** *76*, (13), 4179-4184.

49. Turner, L.; Ryu, W. S.; Berg, H. C., Real-Time Imaging of Fluorescent Flagellar Filaments. *Journal of Bacteriology* **2000,** *182*, (10), 2793-2801.

50. Liu, Y. Y.; Janjaroen, D.; Kuhlenschmidt, M. S.; Kuhlenschmidt, T. B.; Nguyen, T. H., Deposition of *Cryptosporidium parvum* Oocysts on Natural Organic Matter Surfaces: Microscopic Evidence for Secondary Minimum Deposition in a Radial Stagnation Point Flow Cell. *Langmuir* **2009,** *25*, (3), 1594-1605.

51. Massoudieh, A.; Ginn, T. R., Modeling Colloid-Enhanced Contaminant Transport in Stormwater Infiltration Basin Best Management Practices. *Vadose Zone Journal* **2008,** *7*, (4), 1215-1222.

52. Nelder, J. A.; Mead, R., A Simplex Method for Function Minimization. *Computer Journal* **1965,** *7*, (4), 308-313.

53. Chomsurin, C.; Werth, C. J., Analysis of Pore-Scale Nonaqueous Phase Liquid Dissolution in Etched Silicon Pore Networks. *Water Resources Research* **2003,** *39*, (9).

54. Zhang, C. Y.; Werth, C. J.; Webb, A. G., A Magnetic Resonance Imaging Study of Dense Nonaqueous Phase Liquid Dissolution from Angular Porous Media. *Environmental Science & Technology* **2002,** *36*, (15), 3310-3317.

55. Herzig, J. P.; Leclerc, D. M.; Goff, P. L., Flow of Suspensions through Porous Media—Application to Deep Filtration. *Industrial & Engineering Chemistry* **1970,** *62*, (5), 8-35.

56. Tufenkji, N.; Miller, G. F.; Ryan, J. N.; Harvey, R. W.; Elimelech, M., Transport of *Cryptosporidium* Oocysts in Porous Media: Role of Straining and Physicochemical Filtration†. *Environmental Science & Technology* **2004,** *38*, (22), 5932-5938.

57. Conrad, J. C.; Gibiansky, M. L.; Jin, F.; Gordon, V. D.; Motto, D. A.; Mathewson, M. A.; Stopka, W. G.; Zelasko, D. C.; Shrout, J. D.; Wong, G. C. L., Flagella and Pili-Mediated near-Surface Single-Cell Motility Mechanisms. *Biophysical Journal* **2011,** *100*, 1608-1616.

58. Gutman, J.; Walker, S. L.; Freger, V.; Herzberg, M., Bacterial Attachment and Viscoelasticity: Physicochemical and Motility Effects Analyzed Using Quartz Crystal Microbalance with Dissipation (QCM-D). *Environmental Science & Technology* **2012,** *47*, (1), 398-404.

59. Schinner, T.; Letzner, A.; Liedtke, S.; Castro, F. D.; Eydelnant, I. A.; Tufenkji, N., Transport of Selected Bacterial Pathogens in Agricultural Soil and Quartz Sand. *Water Research* **2010,** *44*, (4), 1182-1192.

60. Wong, P. T. W.; Griffin, D. M., Bacterial Movement at High Matric Potentials—I. In Artificial and Natural Soils. *Soil Biology and Biochemistry* **1976,** *8*, (3), 215-218.

CHAPTER 4

SWIMMING MOTILITY REDUCES *AZOTOBACTER VINELANDII* DEPOSITION TO SILICA SURFACES

Submitted:

Lu, N.; Massoudieh, A.; Liang, X.; Hu, D.; Kamai, T.; Ginn, T. R.; Zilles, J. L.; Nguyen, T. H., Swimming Motility Reduces *Azotobacter vinelandii* Deposition to Silica Surfaces.

Contribution: I conducted and analyzed all the experiments presented in this chapter expect for particle tracking analysis and cluster analysis.

4.1 Abstract

The role of swimming motility on bacterial transport and fate in porous media was evaluated. We present microscopic evidence showing that strong swimming motility reduces attachment of *Azotobacter vinelandii* cells to silica surfaces. Applying global and cluster statistical analyses to microscopic videos taken under non-flow conditions, wild type, flagellated *A. vinelandii* strain DJ showed strong swimming ability with an average speed of 13.1 μm/s, DJ77 showed impaired swimming averaged at 8.7 μm/s, and both the non-flagellated JZ52 and chemically treated DJ cells were non-motile. Quantitative analyses of trajectories observed at different distances above the collector of a radial stagnation point flow cell (RSPF) revealed that both swimming and non-swimming cells moved with the flow when at a distance of at least 20 μm from the collector surface. Near the surface, DJ cells showed both horizontal and vertical movement diverging them from reaching surfaces, while chemically treated DJ cells moved with the flow to reach surfaces, suggesting that strong swimming reduced attachment. In agreement with the RSPF results, the deposition rates obtained for two-dimensional multiple-collector micromodels were also lowest for DJ, while DJ77 and JZ52 showed similar values. Strong swimming specifically reduced deposition on the upstream surfaces of the micromodel collectors.

4.2 Introduction

Bacterial transport and fate in the soil and subsurface impacts soil microbial metabolism,[1, 2] adaption and evolution[3] and thus affects nutrient cycling and contamination degradation.[1, 2, 4, 5] Bacterial cells in groundwater streams, subjected to physiochemical factors,[5, 6] travel through the soil and subsurface porous structures, colliding with soil surfaces that intersect the flow paths and then either changing paths or attaching to soil surfaces. After decades of studies on bacterial transport and deposition, it is evident that biological properties and activities need to be considered.[5, 7, 8]

With respect to the relationship between bacterial swimming motility and bacterial transport, previous research has provided divergent observations. Reports of higher deposition from motile strains are common in radial stagnation point flow (RSPF) cells and parallel flow

cells.[9-11] However, motility has also been reported to decrease deposition[12], even for the same bacterial strains and experimental setup[13]. Faster travel speeds for motile strains moving through columns also suggest the motile strains have less surface attachment than non-motile strains.[14, 15]

Attempts to explain these contradictory results started from studies on bulk solution conditions, including the effects of ionic strength, solution chemistry, and flow velocity, and progressed to the observation of individual bacterial movement. Different responses to ionic strength and divalent cation concentrations have been observed for motile and non-motile *Pseudomonas* strains[9, 12], suggesting differences in the mechanisms controlling their attachment. The presence of flagella resulted in greater sensitivity to ionic strength for *Azotobacter vinelandii* deposition.[16] At low fluid velocity (0.56 m/day), swimming *Pseudomonas* cells were able to avoid attachment in packed-bed columns.[17] For *Escherichia coli* in a parallel flow setup, flagellar rotation also increased detachment of cells at low fluid velocity (0.0044 cm/s), but under higher fluid velocity (0.44 cm/s), enhanced attachment was observed for motile cells.[11] When either smooth or tumbling flagellar movement was eliminated, the cells showed less attachment in parallel flow chambers.[18] Qualitative microscope observations suggested that for smooth swimming cells the decreased attachment was linked to a decrease in time on the surface, while for continually tumbling cells the ability to approach the surface seemed to be impaired.[18] These observations suggest the potential to resolve the contradictory reports about the impact of motility on bacterial transport through quantitative analyses of the behavior of individual motile and non-motile cells.

Quantification of bacterial movement has advanced both experimentally and mathematically. A three-dimensional tracking microscope revealed a tendency for individual *E. coli* cells to swim in circles parallel towards a glass surface.[19-21] Complementary approaches allow three-dimensional trajectories to be reconstructed for multiple cells from the same time series of images, for example by relying on image analysis to recognize cells that are outside the focal plane[22] or by combining information from multiple cameras.[28] With three-dimensional trajectory recording techniques, individual cell activities were identified and grouped to represent types of bacterial movement.[19-22] However, these techniques cannot study the whole bacterial population, and could miss some rare cell activities which may have important roles in transport. Recently, an innovative image analysis technique was developed that not only identifies bacterial trajectories, but also the orientation of the individual rod-shaped cells of *Pseudomonas* within a population.[23]

With this approach, flagella-mediated, surface-anchored spinning was identified, and vertically oriented cells were observed to have higher probability of detachment.[23] These trajectory-based approaches have not yet been applied in combination with transport and deposition studies to understand the role of bacterial motility in bacterial transport in porous media.

In this study, we developed image-based global and clustered trajectory analyses, resolved bacterial movement and distribution on and above simplified collector surfaces using RSPF flow cells, and used multiple-collector micromodels to investigate the impact of different levels of swimming motility on population-scale bacterial deposition in porous media. *A. vinelandii* was selected as the model organism because it is a native soil organism and motile and non-motile strains were both available. Furthermore, the role of flagella, the appendages responsible for swimming motility, in deposition has been characterized for *A. vinelandii*, [16] allowing the current work to discriminate between the physical effects of the appendage and the effects specifically associated with its rotation and swimming. *A. vinelandii* is also naturally competent, i.e., able to receive extracellular DNA in a common mechanism of horizontal gene transfer,[24, 25] so its use here provides a comprehensive methodology for examining the role of motility in horizontal gene transfer in the porous media environment.

4.3 Materials and Methods

Bacterial strains and growth conditions. Three *A. vinelandii* strains were used: DJ (wild type, flagellated and motile), DJ77 (*nifH*-, flagellated but with impaired motility),[16, 26] and JZ52 (*nifH- flhC*-, non-flagellated and nonmotile[16]). *A. vinelandii* strains were grown on modified (no molybdenum) Burk's medium plates[27] with addition of 0.013 M ammonium acetate at 30°C for 2 days before inoculation into liquid media of modified (no molybdenum, no iron) Burk's medium with addition of 0.013 M ammonium acetate shaking at 170 rpm and 30°C for 18 to 20 h. The cells were then centrifuged at 1000g for 10 min, decanted to remove the culture media, and resuspended in the same volume of MOPS buffer solution with 100 mM KCl at pH 7.2 for use in transport experiments. This growth procedure was designed to induce competence for natural transformation assays and followed here to allow comparisons between transport and natural transformation behavior in *A. vinelandii*.[16] No further washing was performed to minimize flagellar damage. Cells were diluted 5 times in MOPS buffer with 100 mM KCl for used in motility characterization,

micromodel and RSPF experiments, resulting in a typical range of cell concentrations of 2.7×10^7-4.2×10^7 cells/mL as measured by hemocytometer counting. In addition to comparing these strains, where specified the swimming motility in DJ was de-energized by addition of the uncoupler FCCP (Carbonyl cyanide-4-(trifluoromethoxy)phenylhydrazone) at a final concentration of 2.0×10^{-4} M (FCCP-treated DJ).[28]

Characterization of Cell Motility. For characterization of motility in no-flow conditions, 400 μL of the diluted cell suspension in MOPS buffer with 100 mM KCl was spread in a No.0 glass bottom culture dish (MatTeck Corporation, USA). A video comprised of 1000 images with duration of 30 s was recorded for each strain using an inverted Axio Observer microscope (Carl Zeiss, Oberkochen, Germany) and an iXon 897 camera (Andor Technology, Belfast, UK) controlled by Solis software (Andor Technology). The magnification was 400×. The spatial resolution was 400 nm and 1 pixel was equivalent to 0.4 μm in the images. The movement of individual cells was analyzed by Particle Tracking Analysis.

RSPF Setup and Experiments. RSPF experiments were conducted as previously described.[16] In brief, the surface was quartz (Quartz coverslip, Cat. No. #26016, Ted Pella Inc.) and the setup contained a 1 mm-radius injection capillary at 0.7 mm from the quartz surface. Injection was controlled at a steady flow of 1mL/min by a syringe pump (KD Scientific). Images and video were recorded using the same setup as described in the motility analysis section.

RSPF experiments were conducted with one of two types of data collection. The first type quantified deposition rates as follows. The microscope was focused on the quartz surface and images were recorded every 30 seconds to monitor the bacterial attachment to the forward stagnation point over 15 minutes time. The deposition rates (k_{rspf}) were calculated as the slope of the deposited cells over time divided by the initial cell concentration and the recording area. Deposition was measured twice from the same batch of cells for each strain. The slopes of the normalized deposition versus time plots (k_{rspf}) for different strains were compared to determine if they were significantly different ($p < 0.05$) from each other using a multiple linear regression analysis.[29] The second type of data collection was designed to monitor cells at different distances from the surface. To do this, videos were taken at different distances (at the quartz surface and 20 and 60 μm above the quartz surface) during separate RSPF experiments. The position of the focal plane was controlled with a 3-dimensional automated microscope translation stage (Model: MS-2000XYZ, Applied Scientific Instrumentation). Each video was recorded for 30 seconds at 31 Hz

frame rate. Three sequential videos were collected at each distance, and the whole set of videos (3 distances in triplicate for 4 strains/conditions) was conducted within 5 minutes.

The recognition of cell trajectories was conducted using Particle Tracking Analysis. Four sets of twenty random trajectories with more than 6 moving steps from DJ or FCCP-treated DJ at a distance of 20 or 60 μm above the surface were selected to analyze linearity and direction. The slopes and the coefficient of determination r^2 of these trajectories were calculated using general linear regressions.[30] Cell movement at the RSPF collector surface was highlighted in superimposed images from the videos.

Particle Tracking Analysis. To investigate patterns of cell movement, particle tracking was applied to video microscope images from the motility characterization and the RSPF experiments. Cells were first identified by setting up a threshold for all 1000 images in a video. The images were then transformed to binary images with only the cells and the background. The thresholds were chosen to include most of the bacterial cells in focus according to randomly selected original and transformed image comparisons. A Matlab algorithm was used to extract the location of cells in each image. A C++ code was developed to infer the trajectories of each cell by considering their location in consecutive images using a maximum likelihood approach. The code was verified extensively through visual comparison of the extracted trajectories with the videos. The image processing and trajectory analysis code is available upon request.

The mean squared displacement is calculated as:[31]

$$\mathrm{MSD(t)} = \frac{1}{m}\sum_{i=1}^{m}\left[\left(x_{t,i} - x_{0,i}\right)^2 + \left(y_{t,i} - y_{0,i}\right)^2\right]$$

where m is the number of trajectories identified, and $x_{t,i}$ and $y_{t,i}$ are the location of cell i (i.e. trajectory i) at time t. The MSD functions of time are fitted by a power function in the form of $\mathrm{MSD(t)} \approx \alpha t^{\beta}$. The values of α and β indicate the motion behavior of the cells. A value of $\beta = 1$ indicates purely Brownian diffusion while $\beta < 1$ shows sub-diffusion and $\beta > 1$ shows super diffusion. A $\beta = 2$ indicates ballistic motion with almost straight trajectories with little or no change in cell velocity during the trajectory.[23] In the analysis, some of the cells showed no significant movement, possibly due to attachment to the surface. These cells were excluded from the analysis. Global velocity magnitude distributions and deviation angles were also calculated from all the trajectories from the same strain using C++ code. The instantaneous velocity

magnitude was obtained using cell displacements over consecutive intervals. The deviation angle for each trajectory at each time step was calculated using the position of the bacteria at that time and the position at the previous and the following time-steps.

Cluster Analysis. From the trajectory analysis of the motile bacteria DJ and DJ77, at any given time, some of the cells showed a passive Brownian motion behavior while other cells were actively swimming. To extract the statistical parameters of actively moving bacteria, a cluster analysis was used to separate the trajectories of actively and passively moving cells, based on the overall deviation-angle standard deviation and mean velocity magnitude obtained from each trajectory. K-means method[32] was further applied to group different motility behaviors for the DJ wild-type and DJ77 strains, which is described as:

$$\underset{S}{\operatorname{argmin}} \sum_{i=1}^{k} \sum_{x_i \epsilon S_i} \|x_j - \mu_i\|^2$$

Where k is the number of cluster centroids, x is a two dimensional real vector containing the variance of turn angles and the mean velocity for the trajectory of each cell. S indicates the subset of swimming, non-swimming and mixed-behavior clusters, and μ is centroid for each cluster. The goal is to find the optimal clusters in a way that the sum of squared distances of all points (each point representing one trajectory) from its corresponding cluster's centroid is minimized and thereby identify the members in each cluster group. A Matlab 2-phase K-means algorithm was used to perform the clustering. Using the corresponding cluster centroids, the clusters were separated and velocity magnitude distributions and deviation angles from cluster groups of both DJ and DJ77 were computed.

Two-dimensional Micromodel Fabrication and Experiments. Silicon micromodels of porous media were used to visualize bacterial deposition in two dimensions under flow conditions. Fabrication and operation of the micromodels was as described previously.[16] A regular pattern of 1440 cylindrical collectors (180 μm diameter, 114 μm in pore-body size, 28 μm in pore throat size, porosity 0.4) was etched to 22 μm depth in a Si wafer. Influent was injected at an approaching velocity of 0.0002 m/s. Images were collected using a Leica microscope connected to a charge-coupled device (CCD) camera (Qimaging Retiga 2000R Fast 1394) and Image Pro 7.0 plus software. Grey-scale images of the entire micromodel collector field were collected at 2 μm resolution. The deposited bacterial cells on collectors were enumerated manually.

One set of micromodel experiments with DJ77 and JZ52 was previously used to quantify deposition dynamics, as indicated by the changes on overall η from 5 min to 15 min.[16] In the current work, additional analyses of data from those experiments are presented, along with the results from a second replicate of those experiments and duplicate micromodel experiments with strain DJ. The overall collection efficiency (η) was calculated as the ratio of the average rate of attachment per single collector divided by the rate of cells approaching one collector.[16] To quantify the distribution of bacterial deposition along the flowpath, η was compared for single collectors at 18 distances along the flowpath from the inlet (longitudinal η). The location of deposition was also examined here; individual values of η for the front (closer to the inlet) and back (further from the inlet) of the collectors were determined, using a line that bisected each collector perpendicular to the flow direction. The datasets for longitudinal η of 72 datapoints were compared among the strains using t-test (p=0.05). T-test (p=0.05) was also used to compare the η values of up to 72 datapoints obtained for the front and the back of the collectors among the strains.

4.4 Results and Discussion

Motility characterization under no-flow conditions. Based on our previous characterization, DJ77 is impaired in motility despite the presence of flagella, while strain JZ52 does not have flagella and is non-motile.[16] However, in this previous work the camera speed (5 Hz) limited our ability to perform detailed analyses of the trajectories for faster moving cells. The motility of the studied strains was therefore analyzed in more detail in the current work, as facilitated by use of a faster camera (31 Hz) and a newly developed algorithm with the ability to differentiate among groups with varied motility within a single strain, i.e. cluster analysis. Similar to the previous analyses,[16] the global analysis of trajectories revealed two types of movement: active swimming, as indicated by relatively smooth paths, and random Brownian motion, which exhibits more erratic movement with a smaller overall velocity. Representative trajectories of all four strains/conditions are shown in **Figure 15**A to provide a visual comparison of their motility. Both DJ and DJ77 trajectories exhibited both an active swimming motion and Brownian motion characteristics, while the trajectories of DJ had more pronounced instantaneous swimming speed. All trajectories of JZ52 and FCCP-treated DJ cells showed Brownian motion. The distributions of the velocity magnitude for individual DJ and DJ77 cells had longer tails due to the higher velocity

indicative of swimming motion (**Figure 16**A). DJ had an average instantaneous swimming speed of 13.1 μm/s. Flagellated DJ77 displayed a lower average speed of 8.7 μm/s, providing a quantitative measure of its restricted swimming ability. JZ52 and FCCP-treated DJ showed a narrower velocity range centering around 0-5 μm/s.

The mean square displacement (MSD) calculated from trajectories is a common metric for quantifying particle movement and is defined as the average of the squared displacements of a number of bacteria as a function of time [31] The MSD is plotted versus time in **Figure 15**B for all four strains/conditions which were DJ, DJ77, JZ52 and FCCP-treated DJ. The slopes of these fitted lines can be used to distinguish between random diffusive motion with slope of 1.0 and ballistic motion with slope of 2.0.[23] The slopes for all strains are larger than one, indicating movement that deviates from true Brownian motion. However, for DJ and DJ77, the movement was relatively ballistic, with slopes of 1.5 and 1.6, respectively. The movement of JZ52 and FCCP-treated DJ was closer to Brownian motion, with slopes of 1.2 and 1.3, respectively. The similar and low values for JZ52 and FCCP-treated DJ confirm that both types of cells are not actively motile. The MSDs for these three strains showed the same trend as was previously reported,[16] although the values obtained here were slightly higher. Displacement alone does not provide a clear description of the differences between strains DJ and DJ77.

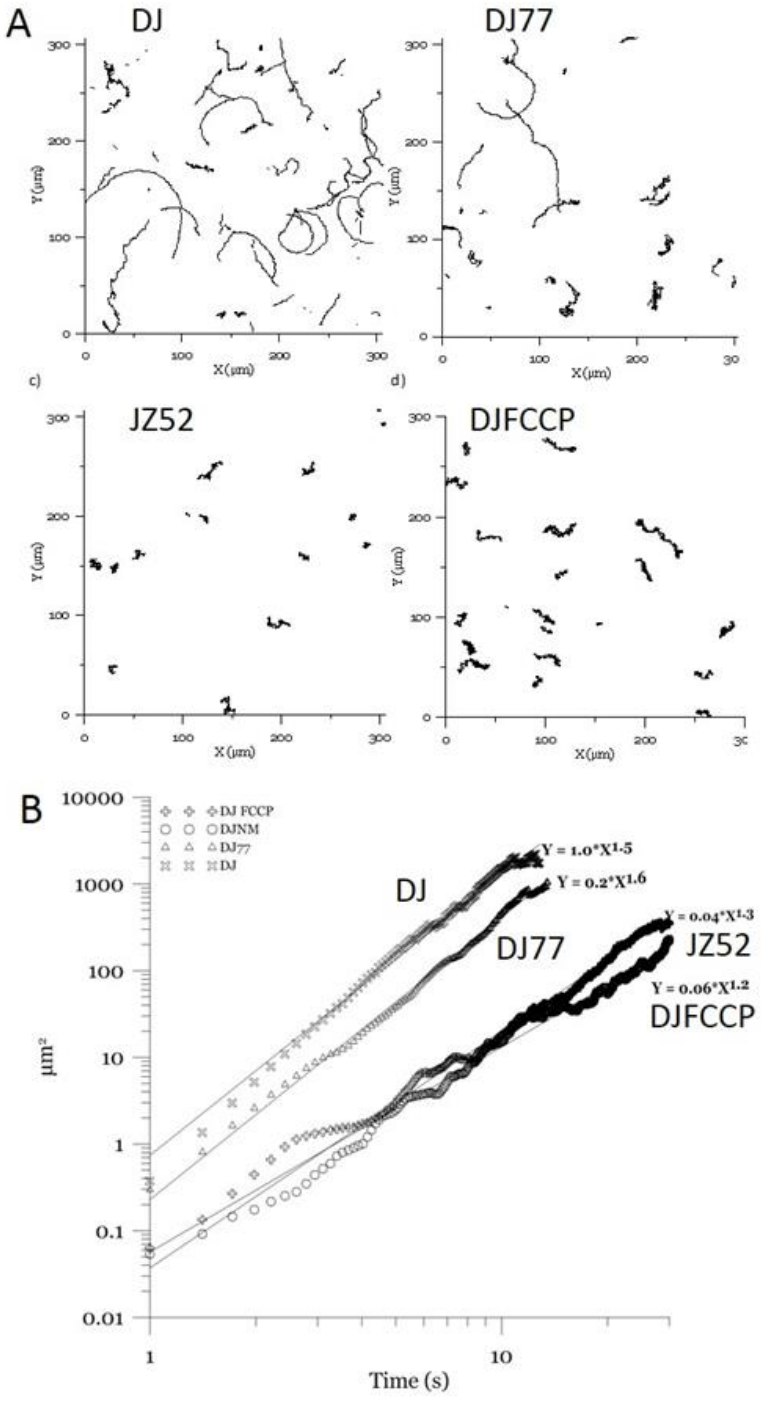

Figure 15 Motility of A. vinelandii strains. A) trajectories of individual cells from each strain/condition and B) mean square displacements versus time for each strain/condition. DJ is a wild-type strain, while DJ77 has restricted motility. JZ52 lacks motility and flagella. FCCP treatment de-energizes cells, rendering them non-motile. The motility tests were done in MOPS buffer with 100 mM KCl, pH 7.2. Video was taken at a frequency of 30 Hz.

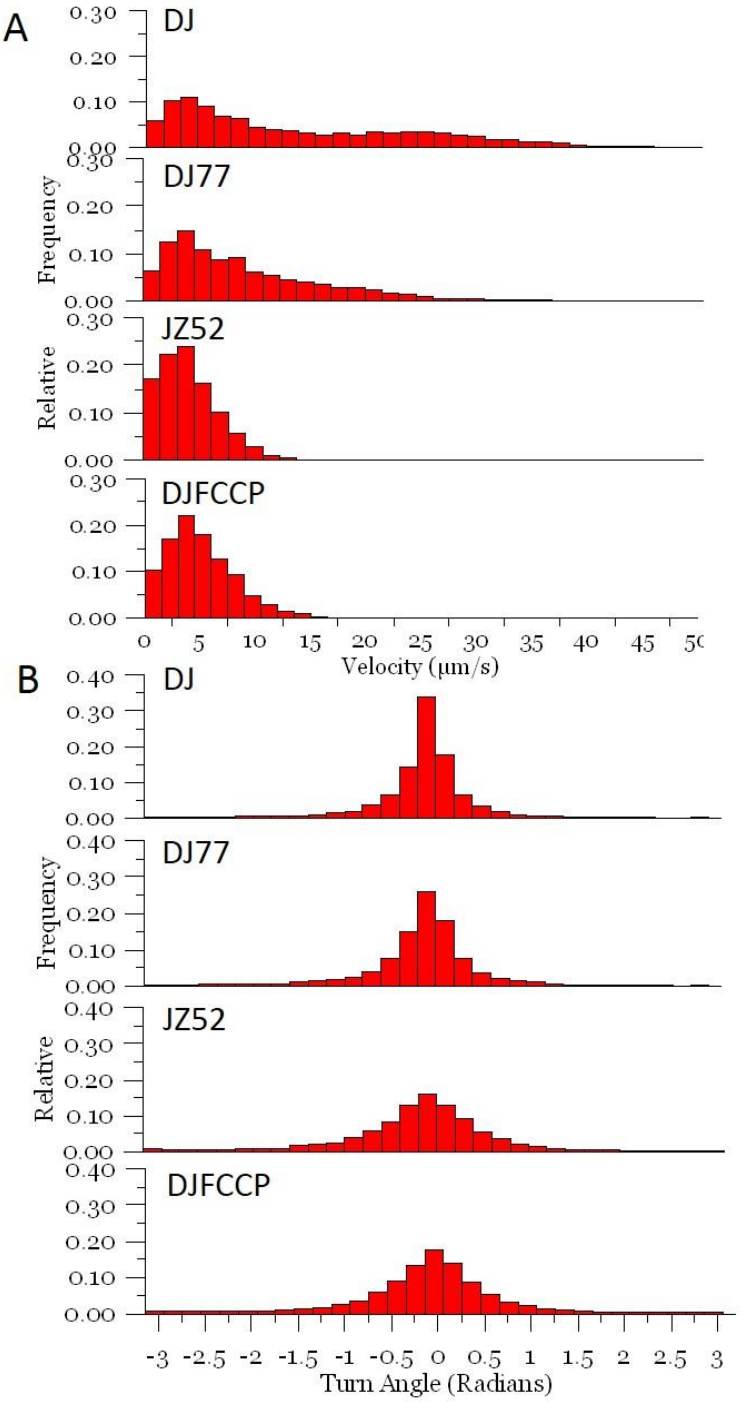

Figure 16 Distribution of motility parameters for A. vinelandii strains. Motility parameters include the relative frequency distributions of A) instantaneous speeds and B) turn angles. DJ is a wild-type strain, while DJ77 has restricted motility. JZ52 lacks motility and flagella. FCCP treatment de-energizes cells, rendering them non-motile. The motility tests were done in the same buffer solution as transport experiments, MOPS buffer with 100 mM KCl, pH 7.2. Video was taken at a frequency of 30 Hz.

Cluster analysis was applied to separate swimming and non-swimming cell trajectories for analysis of strains DJ and DJ77 (**Figure 17**). The turn angle was defined as the change in the direction of the bacterial cells in each image. Based on the turn angle variance and the mean velocity magnitude of each cell, the trajectories for both strains were classified into three clusters: swimming, non-swimming and mixed-behavior groups (**Figure 17**). In the swimming clusters, the velocity distribution was skewed toward higher values for DJ compared to DJ77, with average values of 25.6 and 17.4 μm/s, respectively. The discrete velocity distribution of the DJ77 swimming cluster and similar relative frequency of the swimming cluster as compared to that of DJ suggest that DJ77's restricted motility is due to a lower swimming speed. The velocity distributions for non-swimming clusters (**Figure 17**A) were very similar to the overall velocity distributions for non-motile strains/conditions (**Figure 16**A, JZ52 and FCCP-treated DJ); these small velocities are likely to represent Brownian motion.

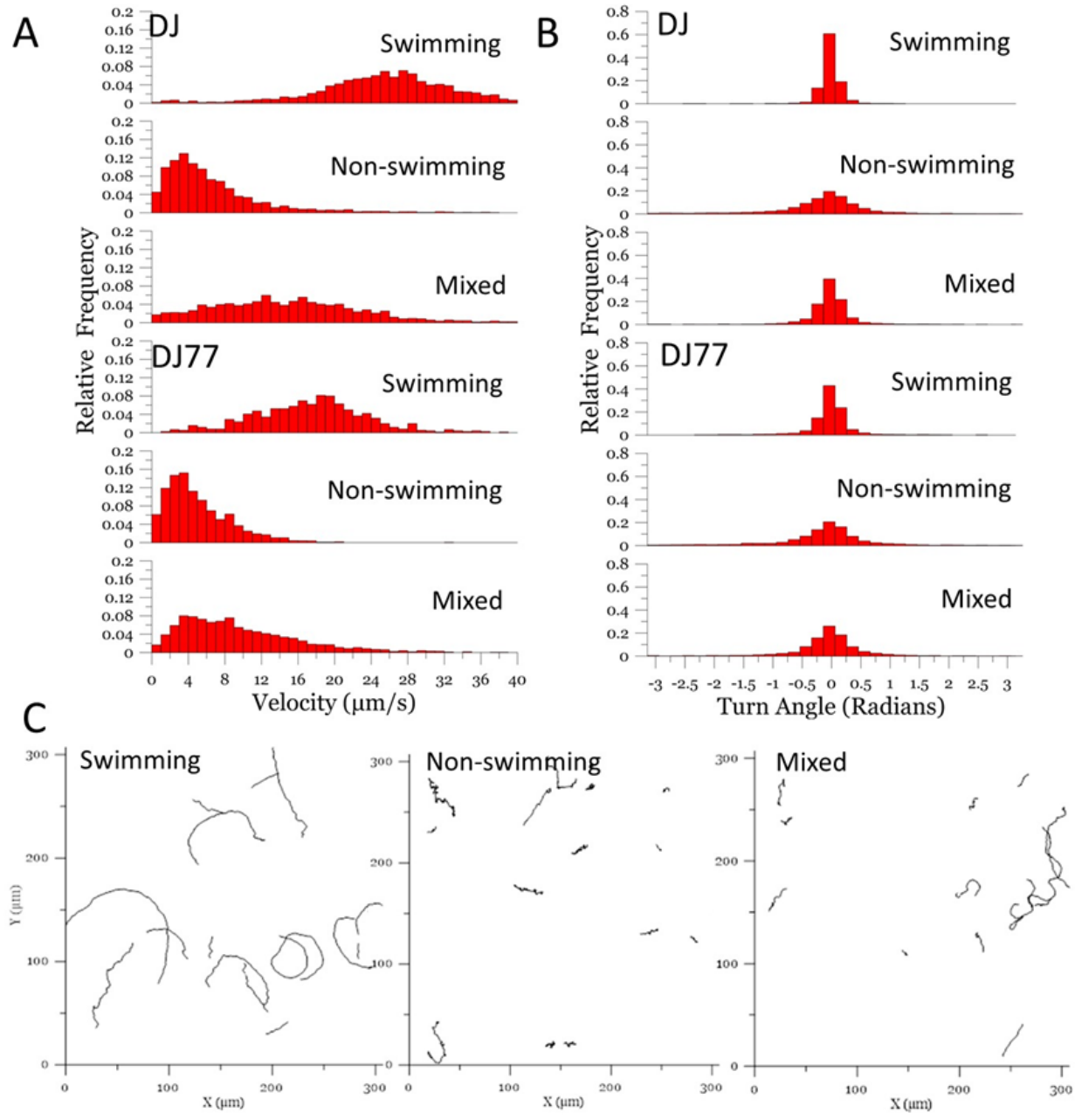

Figure 17 Cluster analysis-derived motility parameters for cells exhibiting a specific type of movement. Cluster analysis was used to divide DJ and DJ77 cell trajectories into three clusters: swimming, non-swimming, and mixed behavior. Motility parameters were calculated separately for each group, with the relative frequency distributions of A) instantaneous speeds and B) turn angles shown here. To provide a visual representation of the effectiveness of the clustering, representative trajectories from each cluster are also shown for C) strain DJ.

The analyses confirmed that DJ77 has impaired motility and provided new insight into the type of defect it exhibits. DJ77 cells shower slower movement than wild-type (DJ) cells, as observed visually in **Figure 15**A and quantified by the cluster analysis. The turn angle distribution for swimming DJ was also the narrowest (i.e. had the smallest variance) compared to the JZ52 and FCCP-treated DJ cells undergoing solely random Brownian motion (**Figure 16**B). Taken together, the three strains provide a motility gradient from strongly motile DJ, to impaired motility in DJ77 and concluding with the non-motile strain JZ52.

Bacterial deposition in the RSPF setup. To investigate the effects of motility on bacterial deposition, these three strains were studied in an RSPF setup, quantifying bacterial cell deposition onto the forward stagnation point of a collector surface in real-time and under well-controlled hydrodynamic conditions. Deposition was quantified using the slope of the deposited cell number normalized by the initial cell concentration and the viewing area over time (deposition rate coefficient). The deposition rate coefficients from duplicate experiments were the smallest for DJ (3.0×10^{-8} and 4.0×10^{-8} m/s), followed by DJ77 (5.0×10^{-8} and 8.0×10^{-8} m/s) and JZ52 (8.0×10^{-8} and 13×10^{-8} m/s). Multiple regression analysis revealed statistically significant differences between deposition of DJ as compared to DJ77 and JZ52 ($p<0.05$) and between DJ77 and JZ52 ($p<0.05$). In the current study, the non-motile strain JZ52 had a higher range of deposition rate coefficients than DJ77. This trend differs from our previous study with these two strains,[16] where the deposition rate coefficient for JZ52 was about four-fold lower than DJ77. This discrepancy is likely due to both flow rate reduction from 1 mL/min to 0.093 mL/min in this study and biological variability, for example in the percentage of swimming cells in different DJ77 cultures. However, we cannot conclusively prove this because the previous study used a lower speed camera and therefore the data are not suitable for cluster analysis as described above. Overall, less deposition was observed for the motile strain DJ. This is consistent with previous studies showing less deposition with motile bacterial cells under low flow conditions,[11, 17] but contradicts two previous RSPF studies.[9, 10] In one case,[9] the discrepancy is likely due to the use of different surfaces (silica dioxide in the current study versus positively charged poly-L-lysine coated surface) and different bacteria (*A.vinelandii* here versus *Pseudomonas aeruginosa*). Comparing to Haznedaroglu et al,[10] the discrepancy could be attributed to their slightly higher flow rate (1.5 mL/min v.s. 0.093 mL/min in this study) or differences among bacteria, as *Salmonella* strains were used in that work.

To identify behaviors that could affect deposition of motile bacterial cells, we analyzed the movement of individual cells at different distances above the RSPF collector surface. For swimming DJ and non-swimming, FCCP-treated DJ cells at 20 and 60 μm above the surface, twenty trajectories each were randomly selected to examine the significance of swimming under flow conditions. FCCP-treated DJ was selected for comparison with the swimming DJ strain because both types of cells have flagella. The trajectories of cells from both strains were all spreading out from the center of the images in radial directions as illustrated by representative trajectories at 20 μm above the surface in **Figure 18**. The slopes and coefficients of determination r^2 for the general linear regressions of these trajectories were compared to analyze their linearity and direction (**Figure 19**). The slope values for both strains at both focal planes ranged from – 5.5 to + 5.9 and centered at 0. A positive slope means that the cells traveled away from the center at angles between 0º-90º or between 180º-270º (**Figure 18**). A negative slope means that the cells traveled away from the center at angles between 90º-180º or between 270º-360º (**Figure 18**). The equal extension of slope values into both negative and positive regions in **Figure 19**A indicated that the trajectories spread out evenly in radial directions (arrows marked in **Figure 18**). The distributions of the slope values obtained for trajectories at the 20 and 60 μm focal planes were not statistically different between DJ and FCCP-treated DJ cells. This observation suggested that the flow overcame swimming motility and controlled the direction of movement at these locations. The values of r^2 in the general linear regression were close to 1 for all cases (**Figure 19**B) indicating that from 20 μm and above, bacterial cells followed the straight radial streamlines of the RSPF as shown in **Figure 18**.

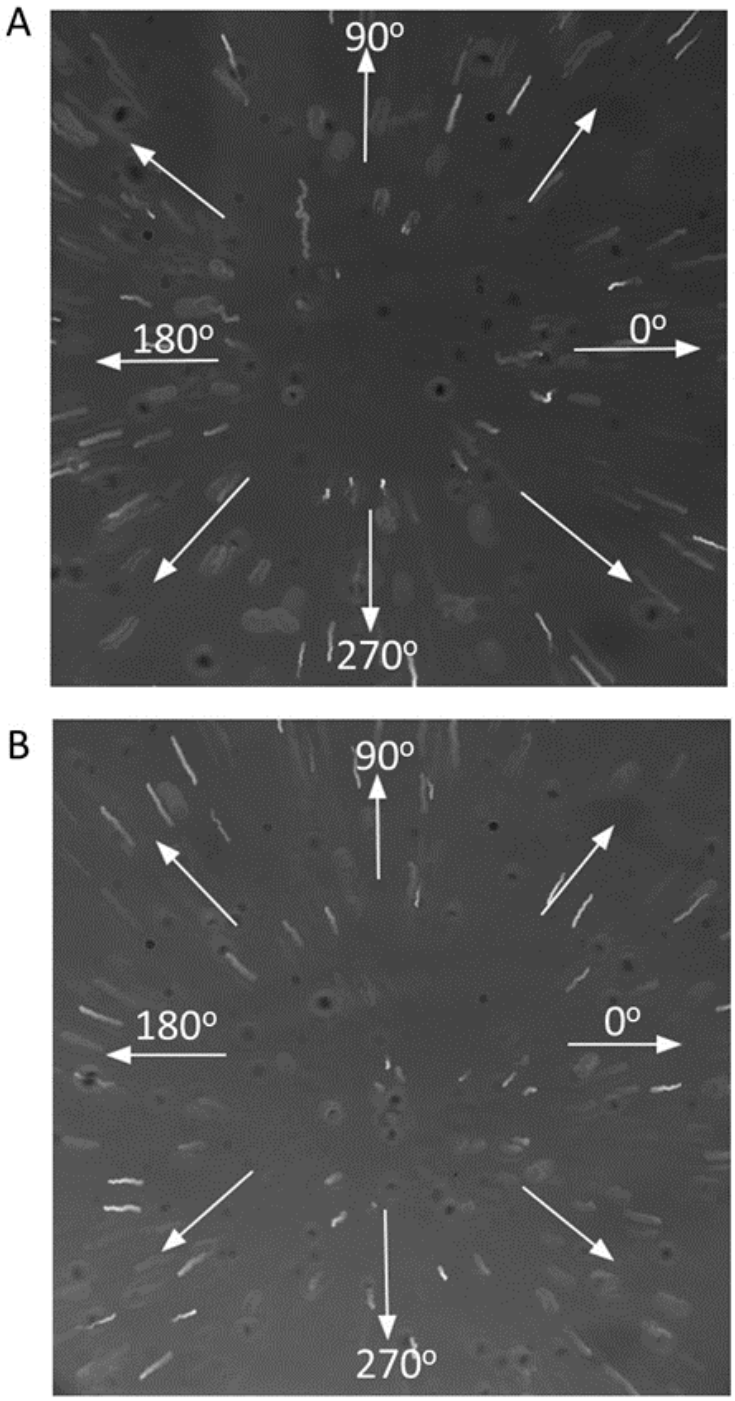

Figure 18 Representative cell trajectories from A) motile strain DJ and B) non-motile FCCP-treated DJ in RSPF experiments, depicting the cells 20 µm above the RSPF quartz surface moving along with the flow stream. The white arrows indicate the flow direction within RSPF flow chambers.

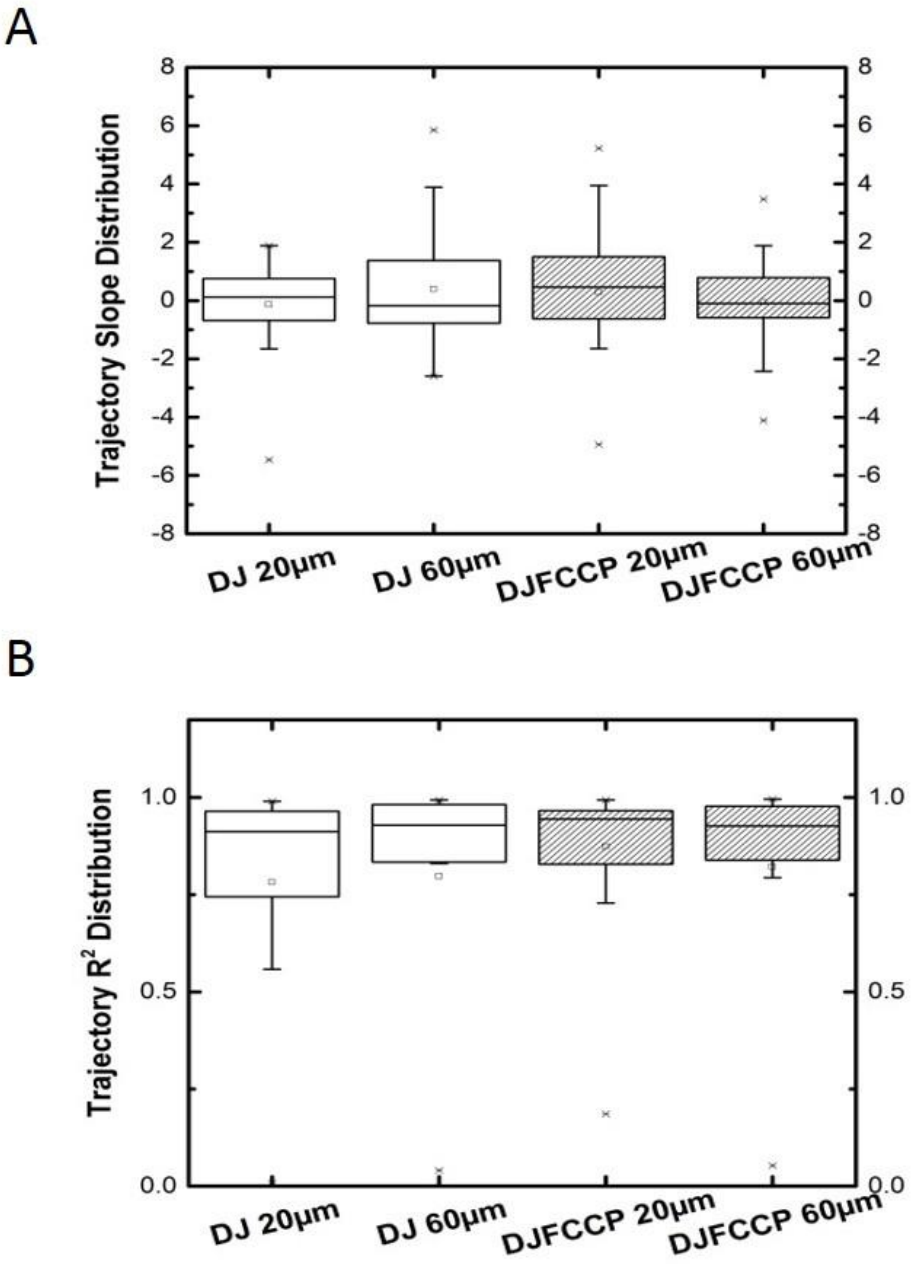

Figure 19 Characterization of cell trajectories from RSPF experiments. DJ is motile; FCCP-treated DJ cells are non-motile. 20 trajectories for each type of cell were selected randomly from RSPF videos and analyzed for A) slope and B) linearity distribution. This analysis was conducted at distances of 20 and 60 μm above the surface. The average slopes of all conditions centered around 0, with approximately equal expansion into negative and positive regions, indicating movement in the radial direction. The R^2 of the trajectories averaged close to 1, also suggesting that the cells were moving with the flow field.

When focusing on the surface, however, there were distinct differences between DJ and DJ77. The movement of DJ cells on the surface (**Figure 20**A&B, numbered arrows) were distinctive from the flow directions (**Figure 20**, plain arrows in radial directions) and included both horizontal and vertical movement, as illustrated in panels A and B, respectively. Cells 1 and 3 swam in straight lines deviating from the flow current at average speeds of 8.8 and 18.5 μm/s, respectively. Cell 2 swam at an average speed of 16.3 μm/s first in a straight line following the flow current and then turned, deviating from the flow path. Cell 4 displayed another type of movement with congregated trajectories. Vertical movement is indicated in these images by the light intensity of the trajectories; since the camera is underneath the surface, brighter cells are closer to the surface and camera, while weaker intensity shows cells that are farther away from the surface. Both Cells 1 and 2 came in and out of focus but remained at a close proximity to the surface. Comparing to swimming DJ, the FCCP-treated DJ cells consistently moved radially from the center following the flow stream and did not display vertical motion, as illustrated in **Figure 20**C. Thus, we suggest that these movements against the flow and vertically could be responsible for reducing swimming DJ cell attachment to the collector surface. Although not directly examined here, these patterns are likely to require tumbling, which is also thought to contribute to *E. coli* cells leaving the horizontal plane after circling near a surface.[21]

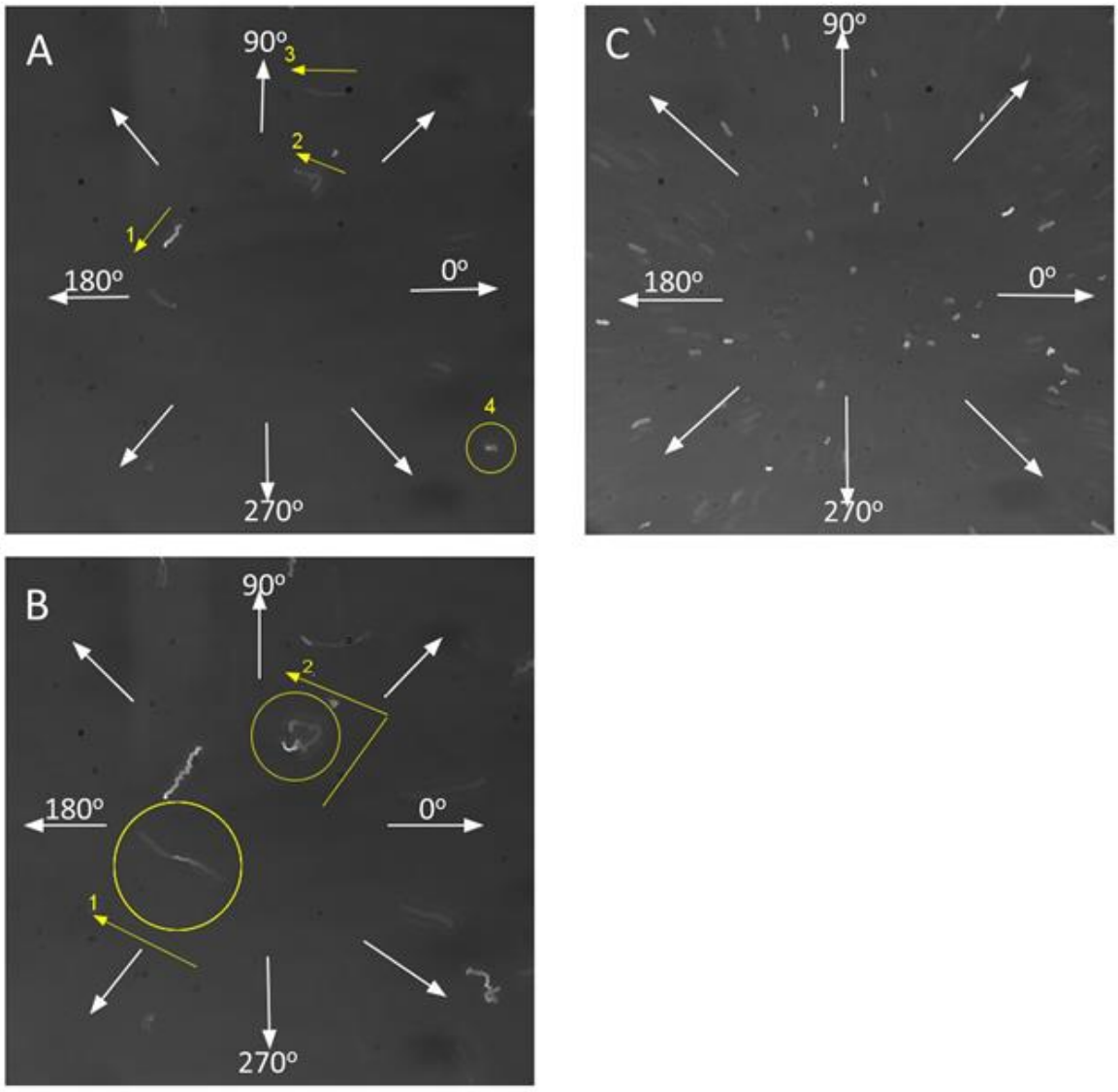

Figure 20 Representative cell trajectories on the collector surfaces from strain DJ in RSPF experiments, depicting A) horizontal and B) vertical movement of swimming DJ cells compared to C) the movement of FCCP-treated DJ cells above the RSPF quartz surface. The white arrows indicate the flow direction within RSPF flow chambers and the yellow arrows mark the direction of movement for individual cells.

In the above RSPF experiments, we found that swimming cells deposited less and showed different patterns of movement than non-motile cells. This finding encouraged us to pursue the investigation of swimming motility as it affects bacterial deposition and transport in porous media.

Bacterial deposition in the micromodel setup. A two-dimensional micromodel setup was used to observe the impact of swimming motility on deposition in porous media under flow

conditions. In the duplicate experiments analyzed here, the motile and flagellated DJ again showed the lowest deposition, with overall η of 1.7×10^{-5} and 1.1×10^{-4} over 5 minutes. The overall η for DJ77 (3.5×10^{-4} and 3.6×10^{-4}) and JZ52 (3.7×10^{-4} and 1.0×10^{-3}) were both slightly higher. This difference in η was also observed along the longitudinal direction for all three strains (**Figure 21**A); the longitudinal η for DJ were significantly smaller than those of DJ77 and JZ52 ($p<0.05$, t-test). For all strains, more deposition occurred on the collectors near the inlets and outlets compared to those in the middle of micromodel (**Figure 21**A), in agreement with previous studies.[33]

The deposition was also quantified separately for the front and back of the collectors, relative to the flow in the micromodel experiments (**Figure 21**B). The longitudinal η values determined for the back of the collectors were overlapping in the range from 1.4×10^{-5} to 2.7×10^{-4} for the motile strain DJ, the impaired motility starin DJ77 and non-swimming JZ52 cells. In contrast, on the front of the collectors, the η for DJ was significantly smaller than those for DJ77 and JZ52 ($p<0.05$). Duplicate experiments of JZ52 gave $\eta_{forward}$ of 5.4×10^{-4} and 1.1×10^{-3}, at least 5 times larger than those for DJ. This micromodel trend of lower $\eta_{forward}$ for the motile strain is consistent with the trend in RSPF deposition rate coefficients, where the motile strain also showed the lowest deposition of these three strains. The micromodel experiments further indicate that the difference in overall deposition is due to differences in front-side deposition.

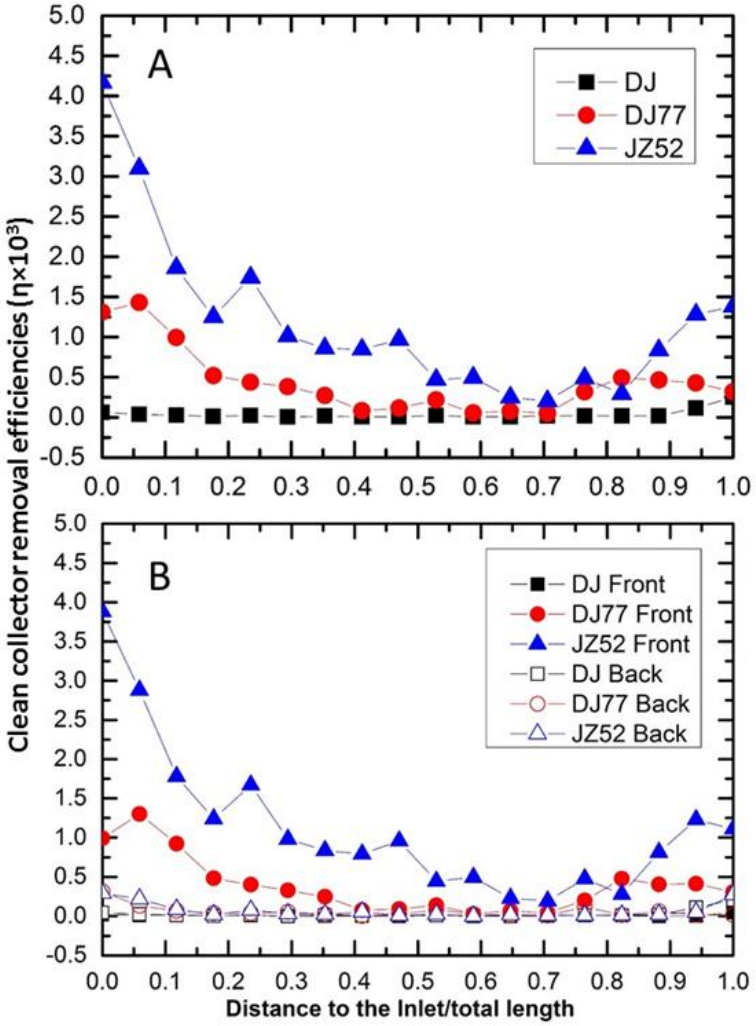

Figure 21 Effects of motility on deposition in porous media micromodel experiments. Clean collector removal efficiency (η) is shown in panel A for the three bacterial strains, DJ, DJ77, and JZ52 as averaged across each column (perpendicular to flow direction) along the flowpath of the micromodel (referred to as longitudinal η). Panel B shows the distribution of deposition between the front (solid symbols) and back (open symbols) of the collectors, relative to the direction of flow. The results from one micromodel experiment with each strain are presented here for clarity.

Since all three strains shared similar electrophoretic motilities at ionic strengths ranging from 1-200 mM KCl (**Figure 22**), electrostatic interactions alone cannot explain the unfavorable attachment of DJ. Several previous studies have suggested that motile cells are mainly involved in reversible surface association rather than irreversible attachment.[34-37] Attachment at secondary minimum was suggested to be the cause of backward deposition by colloids and bacterial cells,

reversibly or weakly attaching to the front of a collector surface and rolling along the surface to deposit on the back of the collector.[38-40] The secondary minima for all three *A. vinelandii* strains at the experimental ionic strength of 100 mM KCl were calculated using Derjaguin-Landau-Verwey-Overbeek (DLVO) theory developed and applied for bacterial adhesion.[41] For all strains, the secondary minima had a depth of 24.9 kT with a corresponding separation distance of 4.5 nm. However, we did not observe strong backward deposition with DJ77 and JZ52 in micromodel experiments. In our case, it is likely that all three strains overcome secondary minima due to the short distance between secondary minima (4.5 nm) and energy barriers (1 nm). Furthermore, given the different length scales of the flagellated cells vs. the secondary and thus primary minima, it may be expected that permanent primary attachment occurs less frequently for flagellated, motile, cells. Therefore, we propose that swimming motility controlled the surface attachment of the motile cells of *A. vinelandii*, instead of hydrodynamics or secondary minimum, based on direct microscopic evidence that swimming motility reduced attachment.

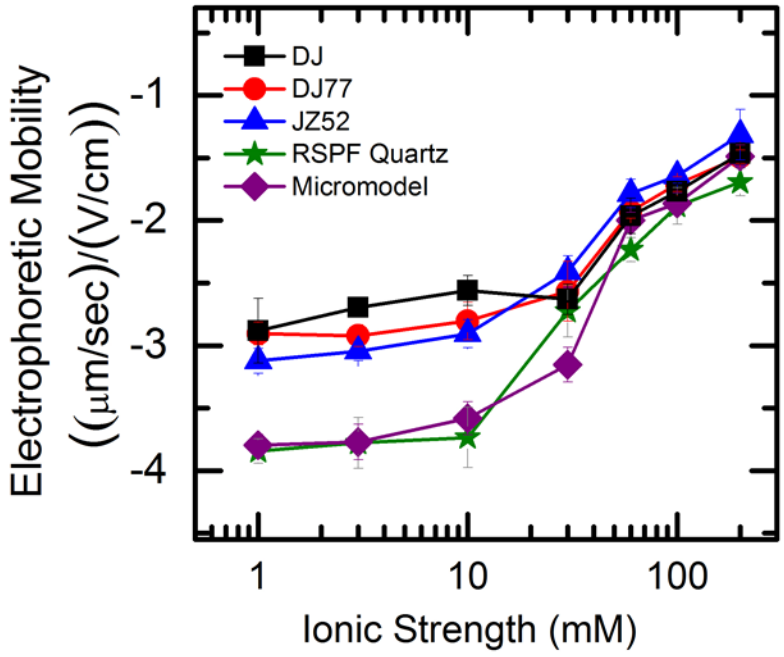

Figure 22 Surface Characterization of all bacterial strains and surfaces. The electrophoretic mobility of strain DJ was measured with a Zetasizer Nano ZS90 (Malvern Instruments, Southborough, MA) in MOPS buffer solutions with 1-100 mM KCl at pH 7.2. The cell concentration was diluted to 3.0×10^6 cells/mL. Electrophoretic mobility for the other strains and materials used in this work were reported previously and are included for comparison.[16]

4.5 Environmental Implications

This work used microscopically resolved, population-level quantification of individual cell movement to study bacterial transport and deposition in porous media, with *A. vinelandii* as a model organism. This approach provided insight linking microscopic observations of individual bacterial motility to bacterial transport and fate in the environment and could be applied to study other bacterial behaviors such as chemotaxis and gene transfer. Swimming motility, rather than hydrodynamics or secondary minimum, reduced surface attachment of *A. vinelandii* under the experimental conditions in this study. This swimming motility-surface attachment relationship, also suggested by other studies,[11, 18, 23] may help these bacterial cells travel farther and spread more broadly. Bioremediation processes could benefit from broader transport of bacterial cells to reach a larger area for contaminant treatment. On the other hand, the complexity of pathogen monitoring and control increases with broader transport in soil and groundwater environments.

4.6 Acknowledgements

This work was supported by NSF Grants No. 1066152, 121756, and 1114257 and part of the research was conducted in the William R. Wiley Environmental Molecular Sciences Laboratory, a scientific user facility of the United States Department of Energy's Office of Biological and Environmental Research and operated by the Pacific Northwest National Laboratory.

4.7 References

1. Hunter, K. S.; Wang, Y.; Van Cappellen, P., Kinetic Modeling of Microbially-Driven Redox Chemistry of Subsurface Environments: Coupling Transport, Microbial Metabolism and Geochemistry. *Journal of Hydrology* **1998,** *209*, (1–4), 53-80.

2. Murphy, E. M.; Ginn, T. R., Modeling Microbial Processes in Porous Media. *Hydrogeology Journal* **2000,** *8*, (1), 142-158.

3. Trevors, J.; Barkay, T.; Bourquin, A., Gene Transfer among Bacteria in Soil and Aquatic Environments: A Review. *Canadian Journal of Microbiology* **1987,** *33*, (3), 191-198.

4. Ginn, T. R.; Wood, B. D.; Nelson, K. E.; Scheibe, T. D.; Murphy, E. M.; Clement, T. P., Processes in Microbial Transport in the Natural Subsurface. *Advances in Water Resources 25*, (8-12), 1017-1042.

5. Tufenkji, N., Modeling Microbial Transport in Porous Media: Traditional Approaches and Recent Developments. *Advances in Water Resources* **2007,** *30*, (6-7), 1455-1469.

6. Sen, T. K.; Das, D.; Khilar, K. C.; Suraishkumar, G. K., Bacterial Transport in Porous Media: New Aspects of the Mathematical Model. *Colloids and Surfaces A: Physicochemical and Engineering Aspects* **2005,** *260*, (1-3), 53-62.

7. Walker, S. L.; Redman, J. A.; Elimelech, M., Influence of Growth Phase on Bacterial Deposition: Interaction Mechanisms in Packed-Bed Column and Radial Stagnation Point Flow Systems. *Environmental Science & Technology* **2005,** *39*, (17), 6405-6411.

8. Castro, F. D.; Tufenkji, N., Role of Oxygen Tension on the Transport and Retention of Two Pathogenic Bacteria in Saturated Porous Media. *Environmental Science & Technology* **2008,** *42*, (24), 9178-9183.

9. de Kerchove, A. J.; Elimelech, M., Bacterial Swimming Motility Enhances Cell Deposition and Surface Coverage. *Environmental Science & Technology* **2008,** *42*, (12), 4371-4377.

10. Haznedaroglu, B. Z.; Zorlu, O.; Hill, J. E.; Walker, S. L., Identifying the Role of Flagella in the Transport of Motile and Nonmotile *Salmonella enterica* Serovars *Environmental Science & Technology* **2010,** *44*, (11), 4184-4190.

11. McClaine, J. W.; Ford, R. M., Characterizing the Adhesion of Motile and Nonmotile *Escherichia coli* to a Glass Surface Using a Parallel-Plate Flow Chamber. *Biotechnology and Bioengineering* **2002,** *78*, (2), 179-189.

12. de Kerchove, A. J.; Elimelech, M., Calcium and Magnesium Cations Enhance the Adhesion of Motile and Nonmotile *Pseudomonas aeruginosa* on Alginate Films. *Langmuir* **2008,** *24*, (7), 3392-3399.

13. de Kerchove, A. J.; Elimelech, M., Impact of Alginate Conditioning Film on Deposition Kinetics of Motile and Nonmotile *Pseudomonas aeruginosa* Strains. *Applied and Environmental Microbiology* **2007,** *73*, (16), 5227-5234.

14. Reynolds, P. J.; Sharma, P.; Jenneman, G. E.; McInerney, M. J., Mechanisms of Microbial Movement in Subsurface Materials. *Applied and Environmental Microbiology* **1989,** *55*, (9), 2280-2286.

15. McCaulou, D. R.; Bales, R. C.; Arnold, R. G., Effect of Temperature-Controlled Motility on Transport of Bacteria and Microspheres through Saturated Sediment. *Water Resources Research* **1995,** *31*, (2), 271-280.

16. Lu, N.; Bevard, T.; Massoudieh, A.; Zhang, C.; Dohnalkova, A. C.; Zilles, J. L.; Nguyen, T. H., Flagella-Mediated Differences in Deposition Dynamics for *Azotobacter vinelandii* in Porous Media. *Environmental Science & Technology* **2013,** *47*, (10), 5162-5170.

17. Camesano, T. A.; Logan, B. E., Influence of Fluid Velocity and Cell Concentration on the Transport of Motile and Nonmotile Bacteria in Porous Media. *Environmental Science & Technology* **1998,** *32*, (11), 1699-1708.

18. McClaine, J. W.; Ford, R. M., Reversal of Flagellar Rotation Is Important in Initial Attachment of *Escherichia coli* to Glass in a Dynamic System with High- and Low-Ionic-Strength Buffers. *Applied and Environmental Microbiology* **2002,** *68*, (3), 1280-1289.

19. Frymier, P. D.; Ford, R. M., Analysis of Bacterial Swimming Speed Approaching a Solid–Liquid Interface. *Aiche Journal* **1997,** *43*, (5), 1341-1347.

20. Vigeant, M.; Ford, R., Interactions between Motile *Escherichia coli* and Glass in Media with Various Ionic Strengths, as Observed with a Three-Dimensional-Tracking Microscope. *Applied and Environmental Microbiology* **1997,** *63*, (9), 3474-3479.

21. Frymier, P. D.; Ford, R. M.; Berg, H. C.; Cummings, P. T., Three-Dimensional Tracking of Motile Bacteria near a Solid Planar Surface. *Proceedings of the National Academy of Sciences of the United States of America* **1995,** *92*, (13), 6195-6199.

22. Wu, M.; Roberts, J. W.; Kim, S.; Koch, D. L.; DeLisa, M. P., Collective Bacterial Dynamics Revealed Using a Three-Dimensional Population-Scale Defocused Particle Tracking Technique. *Applied and Environmental Microbiology* **2006,** *72*, (7), 4987-4994.

23. Conrad, J. C.; Gibiansky, M. L.; Jin, F.; Gordon, V. D.; Motto, D. A.; Mathewson, M. A.; Stopka, W. G.; Zelasko, D. C.; Shrout, J. D.; Wong, G. C. L., Flagella and Pili-Mediated near-Surface Single-Cell Motility Mechanisms. *Biophysical Journal* **2011,** *100*, 1608-1616.

24. Page, W. J.; von Tigerstrom, M., Optimal Conditions for Transformation of *Azotobacter vinelandii Journal of Bacteriology* **1979,** *139*, (3), 1058-1061.

25. Lorenz, M. G.; Wackernagel, W., Bacterial Gene Transfer by Natural Genetic Transformation in the Environment. *Microbiological Reviews* **1994,** *58*, (3), 563-602.

26. Jacobson, M. R.; Brigle, K. E.; Bennett, L. T.; Setterquist, R. A.; Wilson, M. S.; Cash, V. L.; Beynon, J.; Newton, W. E.; Dean, D. R., Physical and Genetic Map of the Major Nif Gene Cluster from *Azotobacter vinelandii*. *Journal of Bacteriology* **1989,** *171*, (2), 1017-1027.

27. Strandberg, G.; Wilson, P., Formation of the Nitrogen-Fixing Enzyme System in *Azotobacter vinelandii*. *Canadian Journal of Microbiology* **1968,** *14*, (1), 25-31.

28. Turner, L.; Ryu, W. S.; Berg, H. C., Real-Time Imaging of Fluorescent Flagellar Filaments. *Journal of Bacteriology* **2000,** *182*, (10), 2793-2801.

29. Neter, J.; Wasserman, W.; Kutner, M., Applied Linear Statistical Models: Regression, Analysis of Variance, and Experimental Designs. **1990**.

30. Nelder, J. A.; Baker, R., *Generalized Linear Models*. Wiley Online Library: 1972.

31. Qian, H.; Sheetz, M. P.; Elson, E. L., Single Particle Tracking. Analysis of Diffusion and Flow in Two-Dimensional Systems. *Biophysical Journal* **1991,** *60*, (4), 910-921.

32. MacQueen, J. In *Some Methods for Classification and Analysis of Multivariate Observations*, Proceedings of the fifth Berkeley symposium on mathematical statistics and probability, 1967; California, USA: 1967; p 14.

33. Liu, Y.; Zhang, C.; Hilpert, M.; Kuhlenschmidt, M. S.; Kuhlenschmidt, T. B.; Nguyen, T. H., Transport of *Cryptosporidium parvum* Oocysts in a Silicon Micromodel. *Environmental Science & Technology* **2012,** *46*, (3), 1471-1479.

34. Kusy, K.; Ford, R. M., Surface Association of Motile Bacteria at Granular Porous Media Interfaces. *Environmental Science & Technology* **2009,** *43*, (10), 3712-3719.

35. Narayanaswamy, K.; Ford, R. M.; Smith, J. A.; Fernandez, E. J., Surface Association of Motile Bacteria and Apparent Tortuosity Values in Packed Column Experiments. *Water Resources Research* **2009,** *45*, (7), W07411.

36. Liu, J.; Ford, R. M., Idling Time of Swimming Bacteria near Particulate Surfaces Contributes to Apparent Adsorption Coefficients at the Macroscopic Scale under Static Conditions. *Environmental Science & Technology* **2009,** *43*, (23), 8874-8880.

37. Liu, J.; Ford, R. M.; Smith, J. A., Idling Time of Motile Bacteria Contributes to Retardation and Dispersion in Sand Porous Medium. *Environmental Science & Technology* **2011,** *45*, (9), 3945-3951.

38. Elimelech, M.; O'Melia, C. R., Kinetics of Deposition of Colloidal Particles in Porous Media. *Environmental Science & Technology* **1990,** *24*, (10), 1528-1536.
39. Kuznar, Z. A.; Elimelech, M., Direct Microscopic Observation of Particle Deposition in Porous Media: Role of the Secondary Energy Minimum. *Colloids and Surfaces A: Physicochemical and Engineering Aspects* **2007,** *294*, (1), 156-162.
40. Hermansson, M., The DLVO Theory in Microbial Adhesion. *Colloids and Surfaces B: Biointerfaces* **1999,** *14*, (1-4), 105-119.
41. Redman, J. A.; Walker, S. L.; Elimelech, M., Bacterial Adhesion and Transport in Porous Media: Role of the Secondary Energy Minimum. *Environmental Science & Technology* **2004,** *38*, (6), 1777-1785.

CHAPTER 5

A KINETIC MODEL OF GENE TRANSFER VIA NATURAL TRANSFORMATION FOR SOIL BACTERIUM *AZOTOBACTER VINELANDII*

In preparation:

Lu, N.; Massoudieh, A.; Liang, X.; Kamai, T.; Zilles, J. L.; Nguyen, T. H.; Ginn, T. R., A Kinetic Model of Gene Transfer via Natural Transformation for Soil Bacterium *Azotobacter vinelandii*.

Contribution: I conducted and analyzed all the experiments included in this chapter.

5.1 Abstract

The rates of horizontal gene transfer of a tetracycline resistance gene through natural transformation were studied for motile and non-motile strains of *Azotobacter vinelandii* using a series of experiments and modeling. A rapid initial increase in transformation was observed that decreased in the first 30 minutes of the experiment and eventually diminished at a given cell and DNA concentration. One-time point transformation experiments were also conducted with varied cell or DNA concentrations to explore the relationship between transformation frequency and varied DNA or cell concentrations. Based on these data a kinetic model was developed that considers both DNA and cell concentrations (included in Appendix at the end of the thesis). The modeling results support the hypothesis that under the given experimental conditions, the transformation rate was limited by the abundance of tetracycline resistance gene and by cellular activities associated with cell-DNA interactions. The differences between the rates of horizontal gene transfer for motile and non-motile strains in these experiments were not statistically significant.

5.2 Introduction

Horizontal gene transfer (HGT) is an important mechanism of bacterial adaptation (e.g., [1-3]) and facilitates the spread of metabolic traits throughout a microbial community. Key examples include the development of antibiotic resistance among pathogenic bacteria[4-6] and the spread of biodegradation capabilities for phytoremediation of toluene;[7] for chlorocatechol degradation in activated sludge,[8] and for dehalogenation of chlorinated compounds.[9] While substantial effort has been devoted to modeling conjugation and transduction, to our knowledge, mathematical models for the third mechanism of HGT, natural transformation, are not available, leaving a critical gap in our ability to understand the occurrence of HGT in the environment.

Natural transformation requires extracellular DNA and competent cells, both of which are present in the soil.[10-13] Extracellular DNA is released either actively by live cells or as a result of cell lysis. In soil it can persist from hours to years, because adsorption to soil surfaces protects it from nuclease activity.[11, 12, 14] Despite being adsorbed, this extracellular DNA is still accessible to microorganisms, as has been documented for *Pseudomonas stutzeri*,[15] *Bacillus subtilis*,[16] and

Azotobacter vinelandii.[17, 18] The development of competence is typically regulated by bacteria, and hence the availability of competent cells depends on the growth conditions.[10] In the current work, *A. vinelandii* was used as the model organism because it is native to soil, naturally competent/transformable, indiscriminant in its uptake of DNA,[19] and motile through peritrichous flagella.[20] For *A. vinelandii*, one condition that induces competence is iron limitation.[21] Natural transformation rates also typically depend on the concentration of DNA, with the transformation frequency for *A. vinelandii* leveling off at around 0.1 μg of DNA per 10^7 cells.[22]

Because transformation requires contact between the extracellular DNA and the cell, bacterial motility might also be expected to influence transformation rates, especially in porous media. A connection between natural transformation and twitching motility, which is mediated by type IV pili and occurs on a surface, has been documented in multiple microorganisms. However, this connection appears to be due to an involvement of some of the components of the pilus in DNA uptake, rather than an effect of movement.[23] Although flagellar motility affects bacterial transport and deposition,[24-27] to our knowledge the effect of flagellar motility on natural transformation frequencies or rates has not been examined previously.

Several models have been developed to describe rate-limited conjugation.[28-31] Most of these models are based on the mass-action relationship proposed by Levin et al.,[28] where it is assumed that the gene transfer rate is proportional to the product of local donor and recipient cell number densities. Freter et al.[32] modified the model to include plasmid transfer from newly formed transconjugants to additional recipients, and Knudsen et al.[31] added growth and decay of donors, recipients and transconjugants and also the transfer of genes from newly formed transconjugates to the recipients. Andrup et al.[33] and Andrup and Andersen[34] explained the lag and sudden non-linear increase in transconjugation rate they observed in their data by assuming a mating-pair formation time, a donor recovery time, and a transconjugant maturation time. In more recent modeling studies, the impacts of attachment to surfaces, biofilm formation, and heterogeneity on conjugation have been incorporated into models based on Levin's mass-action transfer. Lagido et al.[35] developed a model of conjugative transfer on surfaces where they considered the spatial heterogeneity of donors and recipients. Imran et al.[36] constructed a continuously stirred tank reactor (CSTR) model where conjugation can occur in attached and planktonic phases and considered cases where a plasmid can enhance the bacteria's ability to form biofilms. Massoudieh et al.[30] developed a model of conjugative gene transfer for porous

media, where one-dimensional transport and attachment and detachment of bacteria to solid surfaces as well as the lags associated with transconjugant maturation time and donor recover time were also considered. Ponciano et al.[37] incorporated environmental stochasticity into their model by representing the transfer, growth, and selection of plasmid-free and plasmid containing bacteria using a hidden Markov model, while Philipsen et al.[38] represented conjugative transfer via a stochastic ordinary differential equation based on Levin's mass-action model.

However, conjugation does not always follow Levin's mass-action model (e.g. [39]); instead a brief period of rapid conjugation may be observed followed by no further increase in the number of transconjugants. Turner[40] showed that the conjugation rate for plasmid pB15 in *E. coli* in poorly mixed environments was not linearly proportional to the recipient cell density. Ponciano et al.[37] considered the conjugation rate to be dependent on recipients not linearly but via a Monod type relationship, while Zhong et al.[41] considered mating pair formation as an intermediate step and rate limiting process in conjugative transfer. Kinetic models for transduction have also been developed. Bajaj et al.[42] described the temporal changes in retroviral transduction on a surface using a one-dimensional diffusive transport model. Tayi et al.[43] developed a model for retrovirus-mediated gene transfer when a homogeneous layer of cells were immobile at the bottom of a culture dish with an overlying suspension of retroviruses being transported through diffusion and settling.

The kinetics of horizontal gene transfer through natural transformation have not been modeled quantitatively. Also, although the impact of bacterial motility on the rate of conjugation has been recognized,[39] to our knowledge no studies have compared the natural transformation rates of motile vs. non-motile bacteria. In this study we developed a new kinetic model of transformation, building from models of conjugation but including dynamically changing available DNA to address the case of natural transformation, and applied the new model to transformation data collected under controlled laboratory conditions. This new model was used to test the hypothesis that the availability of DNA is the controlling factor in the rate. Our experiments used different strains of *A. vinelandii* to specifically investigate the effects of flagellar motility.

5.3 Materials and Methods

Strains and growth conditions. Three strains of *A. vinelandii* were used in this work. These bacterial strains were chosen to test the influence of swimming motility on natural transformation. DJ is a wild type, motile strain. DJ77 contains a 128 bp deletion in *nifH*, resulting in a defect in nitrogen fixation in the presence of molybdenum.[44] DJ77 exhibits reduced motility as compared to DJ. Looking at their mean squared displacement, which is a metric quantifying movement,[45] DJ77 has approximately an order of magnitude smaller mean squared displacement than DJ.[43] Both of these strains were obtained from Dr. Dennis Dean and were used as recipients in the transformation experiments. The third strain was JZ52, which contains the *tetA*(C) tetracycline resistance gene inserted in the *flhC* gene.[20] The *A. vinelandii* strains were routinely cultivated on Burke's medium.[47] Chromosomal DNA was extracted from JZ52 for use in the transformation experiments via standard phenol-chloroform extraction methods.[46] The concentration of donor DNA was measured with both Nanodrop® ND-1000 (Thermo Scientific) and Qubit® 2.0 Fluorometer (Life Technologies, Thermo Fisher Scientific Inc.). Competent cells were prepared by growing on no molybdenum Burke's medium plates with addition of 13mM ammonium acetate at 30°C for 2 days and then inoculating in Burke's liquid medium without molybdenum or iron, shaking at 170 rpm for 18 to 20 h. These conditions are known to induce competence.[48, 49] To quantify the starting cell concentration, a hemocytometer was used for direct counting of suspended cells under light microscope in a controlled volume. The starting cell concentration was then adjusted as desired through dilution.

Transformation assays. Transformations were conducted by mixing 200 µL of competent cells (with varying target concentrations), 200 µL of MOPS buffer with 1 mM Mg^{2+}, and 10µL of donor chromosomal DNA (with varying concentrations) sequentially. After incubating at room temperature for 30 min (standard condition) or varying amounts of time (kinetic experiments), the transformation reaction was terminated by adding 2 enzyme units of DNase I and incubating for 10 min. The resulting mixture was diluted 10 times in Burke's medium with 13mM ammonium acetate and incubated at 30°C for 24 h before being plated. Transformants were quantified by duplicate plating on selective medium (Burke's medium with 12.5µg/mL tetracycline and 13mM ammonium acetate). Viable cells were quantified by duplicate plating on non-selective medium (Burke's medium with 13mM ammonium acetate).

Plates were grown at 30°C for 3-5 days. Transformation frequency was determined by dividing the number of transformants by that of viable cells. Parallel transformations were conducted within a batch of competent cells for each condition (duplicate transformations), and each experiment was repeated twice with independent preparations of competent cells (biological replicates). Due to known variation between batches of competent cells,[18] a representative biological replicate is presented rather than an average. Results from both biological replicates were used for modeling. Spontaneous mutations and selectivity of the plates were tested with no-DNA controls in each set of experiments. Control experiments comparing the transformation frequency for DJ77 and JZ52 with wild type chromosomal DNA and selection for nitrogen fixation demonstrated that the *flhC* mutation does not impair transformation.

There were three sets of natural transformation experiments with dissolved DNA to investigate the influence of cell concentration, DNA concentration, and transformation time. In the first set, the cell concentration was varied from 3.7×10^7 to 9.8×10^8 and from 6.0×10^7 to 8.7×10^8 cells/mL for DJ and DJ77, respectively. The cell concentration range between 5.0×10^7 to 1.0×10^9 cells/mL allows transformant detection. The DNA concentration was held constant at 0.25µg/mL and the transformation time was 30 min. The second set was with varying DNA concentration: from 0.00025 to 2.5µg/mL for both recipient strains. For these experiments the cell concentration averaged $1.0\times10^8 \pm 8.2\times10^7$ (standard deviation) cells/mL for DJ and $7.8\times10^7 \pm 3.1\times10^7$ (standard deviation) cells/mL for DJ77. The biological replicates differed in their transformation time, 15 min and 30 min. The final set was conducted with transformation times ranging from 0 to 90 min, with $5.0\times10^7 \pm 3.9\times10^7$ (standard deviation) for DJ and $4.6\times10^7 \pm 8.6\times10^6$ (standard deviation) cells/mL for DJ77 and 0.25µg DNA/mL.

5.4 Results and Discussion

Transformation experiments. The transformation frequencies dropped as the concentrations of cells increased from around 10^7 to 10^9 (**Figure 23**). Because the transformation frequency was defined as transformants normalized by viable cells, this decrease reflects the fact that increasing the number of viable cells in the experiment did not generate a corresponding increase in transformants; there was a nonlinear relationship between the rate of increase in the number of transformations and the increasing cell concentration. The decreased transformation

frequencies with more viable cells can be explained by postulating that the access of each competent cell to a transforming gene on the DNA molecule decreased as competent cell number increases. Alternatively, with higher cell concentrations, one individual cell could experience less contact with DNA because of the competition or impedance from the surrounding cells. In contrast, for DNA concentrations ranging from 0.00025 to 2.5µg/mL the transformation frequencies for both strains showed an almost linear relationship in standard 30 min transformation assays (**Figure 24**). The relationship between transformation frequency and DNA concentration was consistent with Levin's original mass-action and indicated that transformation kinetics were limited by DNA under our experimental conditions.

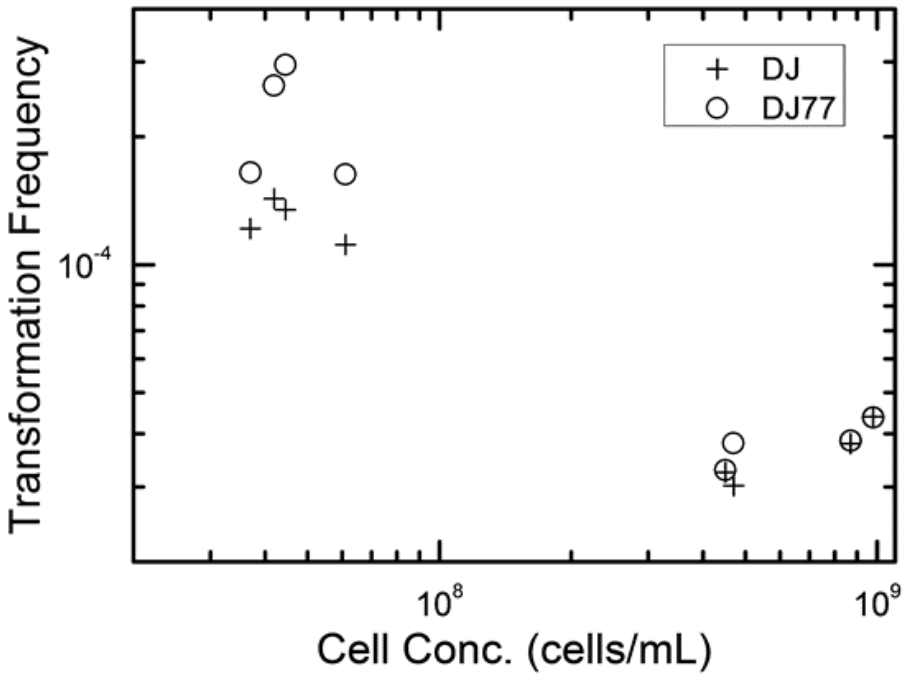

Figure 23 Transformation frequency of A. vinelandii DJ (wild type) and DJ77 with varying cell concentration in the transformation mixture. The DNA concentration was 0.25 µg/mL and the transformation time was 30 min. Transformation frequency was normalized to viable cell concentration for each reaction. Data points are the average of duplicate plates. Duplicate transformations from the same batch of competent cells are shown separately.

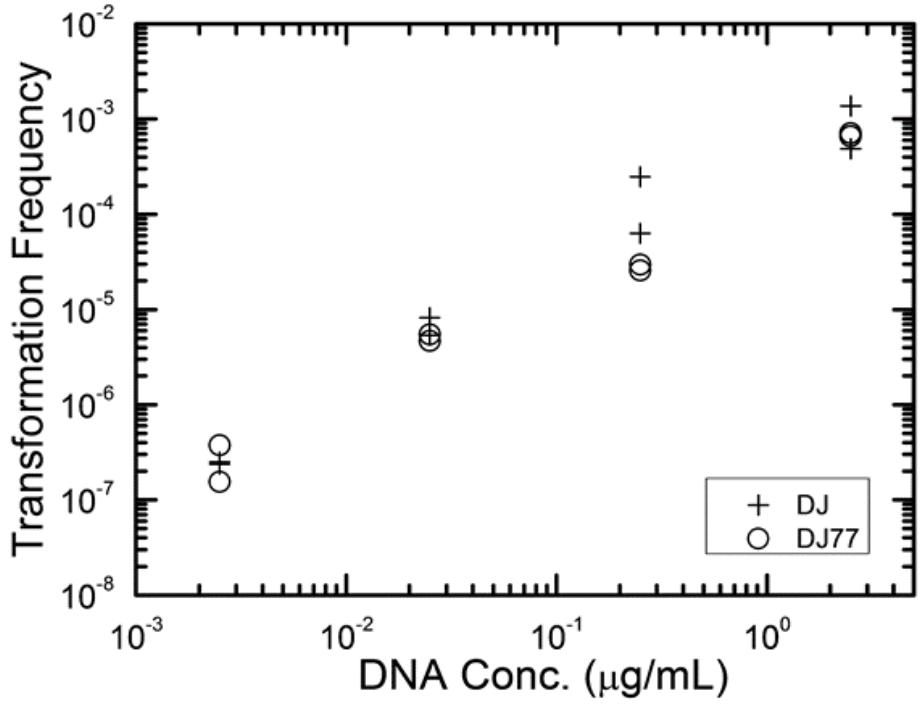

Figure 24 Transformation frequency of *A.vinelandii* DJ and DJ77 at different DNA concentrations. The cell concentration averaged $1.0\times10^8 \pm 8.2\times10^7$ (standard deviation) cells/mL for DJ and $7.8\times10^7 \pm 3.1\times10^7$ (standard deviation) cells/mL for DJ77. The Transformation time was 30 minutes. Transformation frequency was normalized to viable cell concentration for each reaction. Data points are the average of duplicate plates. Duplicate transformations from the same batch of competent cells are shown separately.

The transformation frequency versus time plot (**Figure 25**) shows that the transformation frequencies increased rapidly at the beginning, then slowed down, stabilizing after about 30 minutes. This was not due to loss of competence. When competent cells were incubated under the reaction conditions but without DNA for varying times before being used in a transformation experiment, the cells maintained both viability and competence for 48 h, well beyond the duration of the experiments described here. The transformation reactions were only mixed once, at the beginning of the transformation period. To test the possibility that mixing limitations were affecting the transformation kinetics, an additional transformation experiment was conducted where a second round of mixing and 30 minute incubation was done after the initial mixing and incubation. The transformation rate for this case was compared with a case where the second set had 30 minutes of incubation without mixing. No statistically significant difference was

observed. This rejects the mixing limitation hypothesis. We hypothesize that the temporal decrease in the transformation rate was a result of depletion of the transforming gene pool. Secretion of nucleases was not directly tested here, but previous reports suggest that *A. vinelandii* does not produce extracellular nucleases during natural transformation.[50] The concave relationship between transformation frequency and time suggested that the transforming genes were consumed given enough time; this result was consistent with the results of experiments varying either DNA or cell concentrations.

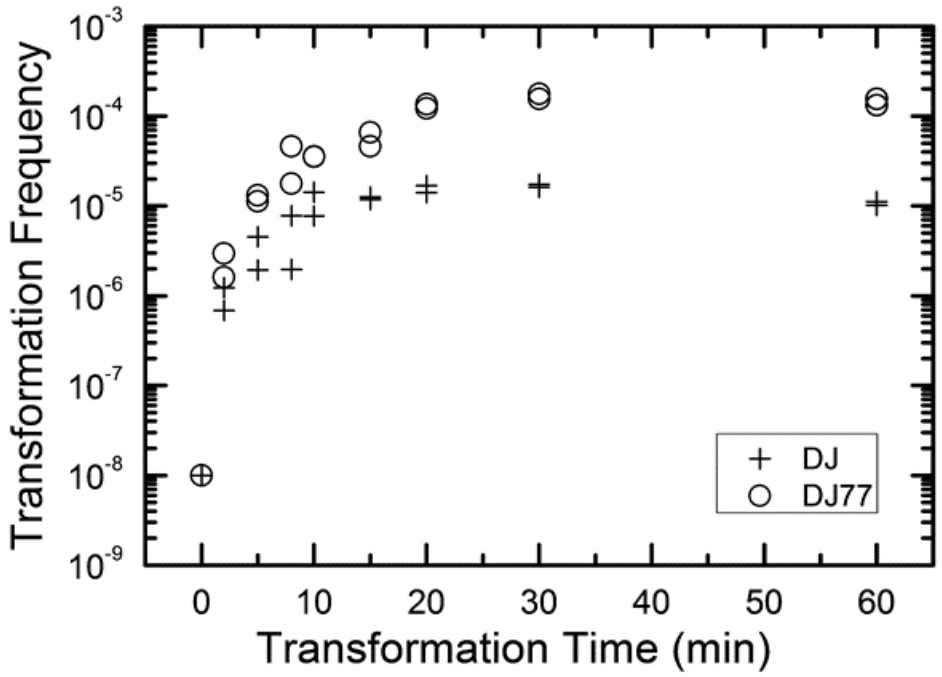

Figure 25 Transformation frequency as a function of time. These experiments were conducted with $5.0\times10^7 \pm 3.9\times10^7$ (standard deviation) for DJ and $4.6\times10^7 \pm 8.6\times10^6$ (standard deviation) cells/mL for DJ77 and with 0.25 µg DNA/mL. Transformation frequency was normalized to viable cell concentration for each reaction. Data points are the average of duplicate plates. Duplicate transformations from the same batch of competent cells are shown separately.

Modeling. Based on this experimental data, a kinetic model was developed that considers both DNA and cell concentrations. The modified Levin's mass action model developed and tested by our collaborators fit this experimental data well. The modeling methods and results are documented in the Appendix. The kinetic model describes the limits of natural transformation

quantitatively. The model showed lower transformation of motile strain DJ quantified by the modeling (compared to the motility-impaired strain DJ77), which could be explained by longer interactions between the motility-impaired cells and DNA. In addition to this effect on transformation, swimming motility could affect transformation rates through its effects on cell transport. The estimated values of DNA involved in transformation were lower than the theoretical fraction of DNA containing the gene being selected for. This could reflect variation in cellular and DNA properties related to the cell-DNA interaction, such as DNA contact with cells, transport into cells, incorporation into the genome, and/or gene expression. Identification of the molecular mechanism(s) underlying this limit on transformation that relates to the DNA concentration requires further study.

5.5 Environmental Implications

It was hypothesized that the transformation rates depend on cell and DNA concentrations as well as the swimming motility of bacterial cells. For the range of cell concentrations used in this work, transformation rates did not increase linearly with increasing cell concentrations. The dependence on DNA concentration was linear. Considering the observed data, the most parsimonious conclusion is that transformation frequencies are limited primarily by the abundance of the transforming gene. In the environment, however, a broader range of cell concentrations could lead to cell concentration also being a limiting parameter. The fundamental understanding of biological processes controlling transformation is essential for developing robust and rigorous mathematical modeling of horizontal gene transfer.

5.6 Acknowledgements

This project research was supported by the NSF (Project Award Number 1114274, "Collaborative Research: Horizontal Gene Transfer in Porous Media: Experiments and Modeling;" and Project Award Number 1215756, "Collaborative Research: Near-Surface Repulsion and Mixing-Limitations: Upscaling of Colloid Transport in Non-Uniform Media under Unfavorable Conditions").

5.7 References

1. Marri, P.; Hao, W.; Golding, G. B., The Role of Laterally Transferred Genes in Adaptive Evolution. *BMC Evolutionary Biology* **2007,** *7*, (Suppl 1), S8.
2. Skippington, E.; Ragan, M. A., Lateral Genetic Transfer and the Construction of Genetic Exchange Communities. *FEMS Microbiology Reviews* **2011,** *35*, (5), 707-735.
3. Aminov, R. I., The Extent and Regulation of Lateral Gene Transfer in Natural Microbial Ecosystems. In *Horizontal Gene Transfer in Microorganisms*, Francino, M. P., Ed. Caister Academic Press: 2012.
4. Andam, C. P.; Fournier, G. P.; Gogarten, J. P., Multilevel Populations and the Evolution of Antibiotic Resistance through Horizontal Gene Transfer. *FEMS Microbiology Reviews* **2011,** *35*, (5), 756-767.
5. Heuer, H.; Schmitt, H.; Smalla, K., Antibiotic Resistance Gene Spread Due to Manure Application on Agricultural Fields. *Current Opinion in Microbiology* **2011,** *14*, (3), 236-243.
6. McDermott, M. T.; Haugen, B. R.; Black, J. N.; Wood, W. M.; Gordon, D. F.; Ridgway, E. C., Congenital Isolated Central Hypothyroidism Caused by a "Hot Spot" Mutation in the Thyrotropin-Beta Gene. *Thyroid* **2002,** *12*, (12), 1141-1146.
7. Taghavi, S.; Barac, T.; Greenberg, B.; Borremans, B.; Vangronsveld, J.; van der Lelie, D., Horizontal Gene Transfer to Endogenous Endophytic Bacteria from Poplar Improves Phytoremediation of Toluene. *Applied and Environmental Microbiology* **2005,** *71*, (12), 8500-8505.
8. Ravatn, R.; Zehnder, A. J. B.; van der Meer, J. R., Low-Frequency Horizontal Transfer of an Element Containing the Chlorocatechol Degradation Genes from *Pseudomonas* sp. Strain B13 to *Pseudomonas putida* F1 and to Indigenous Bacteria in Laboratory-Scale Activated-Sludge Microcosms. *Applied and Environmental Microbiology* **1998,** *64*, (6), 2126-2132.
9. Liang, B.; Jiang, J. D.; Zhang, J.; Zhao, Y. F.; Li, S. P., Horizontal Transfer of Dehalogenase Genes Involved in the Catalysis of Chlorinated Compounds: Evidence and Ecological Role. *Critical Reviews in Microbiology* **2012,** *38*, (2), 95-110.
10. Lorenz, M. G.; Wackernagel, W., Bacterial Gene Transfer by Natural Genetic Transformation in the Environment. *Microbiological Reviews* **1994,** *58*, (3), 563-602.

11. Paget, E.; Simonet, P., On the Track of Natural Transformation in Soil. *FEMS Microbiology Ecology* **1994,** *15*, (1-2), 109-117.

12. Levy-Booth, D. J.; Campbell, R. G.; Gulden, R. H.; Hart, M. M.; Powell, J. R.; Klironomos, J. N.; Pauls, K. P.; Swanton, C. J.; Trevors, J. T.; Dunfield, K. E., Cycling of Extracellular DNA in the Soil Environment. *Soil Biology & Biochemistry* **2007,** *39*, (12), 2977-2991.

13. Pietramellara, G.; Ascher, J.; Borgogni, F.; Ceccherini, M. T.; Guerri, G.; Nannipieri, P., Extracellular DNA in Soil and Sediment: Fate and Ecological Relevance. *Biology and Fertility of Soils* **2009,** *45*, (3), 219-235.

14. Yu, W. H.; Li, N.; Tong, D. S.; Zhou, C. H.; Lin, C. X.; Xu, C. Y., Adsorption of Proteins and Nucleic Acids on Clay Minerals and Their Interactions: A Review. *Applied Clay Science* **2013,** *80–81*, (0), 443-452.

15. Lorenz, M. G.; Wackernagel, W., Natual Genetic Transformation of *Pseudomonas stutzeri* by Sand Bound DNA. *Archives of Microbiology* **1990,** *154*, (4), 380-385.

16. Khanna, M.; Stotzky, G., Transformation of *Bacillus subtilis* by DNA Bound on Montmorillonite and Effect of Dnase on the Transforming Ability of Bound DNA. *Applied and Environmental Microbiology* **1992,** *58*, (6), 1930-1939.

17. Lu, N.; Mylon, S. E.; Kong, R.; Bhargava, R.; Zilles, J. L.; Nguyen, T. H., Interactions between Dissolved Natural Organic Matter and Adsorbed DNA and Their Effect on Natural Transformation of *Azotobacter vinelandii*. *Science of The Total Environment* **2012,** *426*, (0), 430-435.

18. Lu, N.; Zilles, J. L.; Nguyen, T. H., Adsorption of Extracellular Chromosomal DNA and Its Effects on Natural Transformation of *Azotobacter vinelandii*. *Applied and Environmental Microbiology* **2010,** *76*, (13), 4179-4184.

19. Renaud, C. S.; Pasternak, J.; Glick, B. R., Integration of Exogenous DNA into the Genome of *Azotobacter vinelandii*. *Archives of Microbiology* **1989,** *152*, (5), 437-440.

20. Lu, N.; Bevard, T.; Massoudieh, A.; Zhang, C.; Dohnalkova, A. C.; Zilles, J. L.; Nguyen, T. H., Flagella-Mediated Differences in Deposition Dynamics for *Azotobacter vinelandii* in Porous Media. *Environmental Science & Technology* **2013,** *47*, (10), 5162-5170.

21. Page, W. J.; Vontigerstrom, M., Induction of Transformation Competence in *Azotobacter vinelandii* Iron-Limited Cultures. *Canadian Journal of Microbiology* **1978,** *24*, (12), 1590-1594.

22. Doran, J. L.; Bingle, W. H.; Roy, K. L.; Hiratsuka, K.; Page, W. J., Plasmid Transfermation of *Azotobacter vinelandii*. *Journal of General Microbiology* **1987,** *133*, 2059-2072.

23. Chen, I.; Dubnau, D., DNA Uptake During Bacterial Transformation. *Nature Reviews Microbiology* **2004,** *2*, (3), 241-249.

24. Camesano, T. A.; Logan, B. E., Influence of Fluid Velocity and Cell Concentration on the Transport of Motile and Nonmotile Bacteria in Porous Media. *Environmental Science & Technology* **1998,** *32*, (11), 1699-1708.

25. Haznedaroglu, B. Z.; Zorlu, O.; Hill, J. E.; Walker, S. L., Identifying the Role of Flagella in the Transport of Motile and Nonmotile *Salmonella enterica* Serovars *Environmental Science & Technology* **2010,** *44*, (11), 4184-4190.

26. Massoudieh, A.; Lu, N.; Liang, X.; Nguyen, T. H.; Ginn, T. R., Bayesian Process-Identification in Bacteria Transport in Porous Media. *Journal of Contaminant Hydrology* **2013**, (In press).

27. McClaine, J. W.; Ford, R. M., Characterizing the Adhesion of Motile and Nonmotile *Escherichia coli* to a Glass Surface Using a Parallel-Plate Flow Chamber. *Biotechnology and Bioengineering* **2002,** *78*, (2), 179-189.

28. Levin, B. R.; Stewart, F. M.; Rice, V. A., Kinetics of Conjungative Plasmid Transmission - Fit of a Simple Mass Action Model. *Plasmid* **1979,** *2*, (2), 247-260.

29. Massoudieh, A.; Crain, C.; Lambertini, E.; Nelson, K. E.; Barkouki, T.; L'Amoreaux, P.; Loge, F. J.; Ginn, T. R., Kinetics of Conjugative Gene Transfer on Surfaces in Granular Porous Media. *Journal of Contaminant Hydrology* **2010,** *112*, (1-4), 91-102.

30. Massoudieh, A.; Mathew, A.; Lambertini, E.; Nelson, K. E.; Ginn, T. R., Horizontal Gene Transfer on Surfaces in Natural Porous Media: Conjugation and Kinetics. *Vadose Zone Journal* **2007,** *6*, (2), 306-315.

31. Knudsen, G. R.; Walter, M. V.; Porteous, L. A.; Prince, V. J.; Armstrong, J. L.; Seidler, R. J., Predictive Model of Conjungative Plasmid Transfer in the Rhizosphere and Phyllosphere. *Applied and Environmental Microbiology* **1988,** *54*, (2), 343-347.

32. Freter, R.; Freter, R. R.; Brickner, H., Experimental and Mathematical Models of *Escherichia coli* Plasmid Transfer in Vitro and in Vivo. *Infection and Immunity* **1983,** *39*, (1), 60-84.

33. Andrup, L.; Smidt, L.; Andersen, K.; Boe, L., Kinetics of Conjugative Transfer: A Study of the Plasmid Pxo16 from *Bacillus thuringiensis* Subsp. Israelensis. *Plasmid* **1998,** *40*, (1), 30-43.

34. Andrup, L.; Andersen, K., A Comparison of the Kinetics of Plasmid Transfer in the Conjugation Systems Encoded by the F Plasmid from *Escherichia coli* and Plasmid Pcf10 from *Enterococcus faecalis*. *Microbiology-Uk* **1999,** *145*, 2001-2009.

35. Lagido, C.; Wilson, I. J.; Glover, L. A.; Prosser, J. I., A Model for Bacterial Conjugal Gene Transfer on Solid Surfaces. *FEMS Microbiology Ecology* **2003,** *44*, (1), 67-78.

36. Imran, M.; Jones, D.; Smith, H., Biofilms and the Plasmid Maintenance Question. *Mathematical Biosciences* **2005,** *193*, (2), 183-204.

37. Ponciano, J. M.; Gelder, L.; Top, E. M.; Joyce, P., The Population Biology of Bacterial Plasmids: A Hidden Markov Model Approach. *Genetics* **2007,** *176*, (2), 957-968.

38. Philipsen, K. R.; Christiansen, L. E.; Hasman, H.; Madsen, H., Modelling Conjugation with Stochastic Differential Equations. *Journal of Theoretical Biology* **2010,** *263*, (1), 134-142.

39. Licht, T. R.; Christensen, B. B.; Krogfelt, K. A.; Molin, S., Plasmid Transfer in the Animal Intestine and Other Dynamic Bacterial Populations: The Role of Community Structure and Environment. *Microbiology-UK* **1999,** *145*, 2615-2622.

40. Turner, P. E., Phenotypic Plasticity in Bacterial Plasmids. *Genetics* **2004,** *167*, (1), 9-20.

41. Zhong, X.; Krol, J. E.; Top, E. M.; Krone, S. M., Accounting for Mating Pair Formation in Plasmid Population Dynamics. *Journal of Theoretical Biology* **2010,** *262*, (4), 711-719.

42. Bajaj, B.; Lei, P.; Andreadis, S. T., High Efficiencies of Gene Transfer with Immobilized Recombinant Retrovirus: Kinetics and Optimization. *Biotechnology Progress* **2001,** *17*, (4), 587-596.

43. Tayi, V. S.; Bowen, B. D.; Piret, J. M., Mathematical Model of the Rate-Limiting Steps for Retrovirus-Mediated Gene Transfer into Mammalian Cells. *Biotechnology and Bioengineering* **2010,** *105*, (1), 195-209.

44. Jacobson, M. R.; Brigle, K. E.; Bennett, L. T.; Setterquist, R. A.; Wilson, M. S.; Cash, V. L.; Beynon, J.; Newton, W. E.; Dean, D. R., Physical and Genetic Map of the Major Nif Gene Cluster from *Azotobacter vinelandii*. *Journal of Bacteriology* **1989,** *171*, (2), 1017-1027.

45. Qian, H.; Sheetz, M. P.; Elson, E. L., Single Particle Tracking. Analysis of Diffusion and Flow in Two-Dimensional Systems. *Biophysical Journal* **1991,** *60*, (4), 910-921.

46. Contreras, A.; Casadesus, J., Tn10 Mutagenesis in *Azotobacter vinelandii*. *Molecular & General Genetics* **1987,** *209*, (2), 276-282.

47. Strandberg, G. W.; Wilson, P. W., Formation of the Nitrogen-Fixing Enzyme System in *Azotobacter vinelandii*. *Canadian Journal of Microbiology* **1968,** *14*, (1), 25-31.

48. Page, W. J., Optimal Conditions for Induction of Competence in Nitrogen-Fixing *Azotobacter vinelandii*. *Canadian Journal of Microbiology* **1982,** *28*, (4), 389-397.

49. Jacobson, M. R.; Brigle, K. E.; Bennett, L. T.; Setterquist, R. A.; Wilson, M. S.; Cash, V. L.; Beynon, J.; Newton, W. E.; Dean, D. R., Physical and Genetic Map Pf the Major Nif Gene Cluster from *Azotobacter vinelandii*. *Journal of Bacteriology* **1989,** *171*, (2), 1017-1027.

50. Doran, J. L.; Page, W. J., Heat Sensitivity of *Azotobacter vinelandii* Genetic Transformation. *Journal of Bacteriology* **1983,** *155*, (1), 159-168.

CHAPTER 6

CONCLUSIONS

6.1 Conclusions

Our findings of this thesis are summarized in this section.

A positive correlation between the rates of NOM attachment onto DNA layer on the NOM-coated silica surfaces and the carboxylate group density for dissolved NOM in solutions was found by measuring the attachment rates of NOM by quartz crystal microbalance with dissipation (QCM-D). The attachment rates were also positively correlated with the total dissolved organic carbon (DOC) concentrations of the NOM solution, likely due to divalent cation complexation with NOM carboxylate groups and the phosphate backbone of the DNA. It was indicated by the results of the Fourier transform infrared spectroscopy (FTIR) for dissolved DNA and DNA adsorbed on silica beads that adsorption may result from divalent cation complexation with the DNA's backbone and phosphate groups. The interactions, between DNA and NOM, however, did not significantly affect natural transformation of *Azotobacter vinelandii* by DNA. DNA adsorbed to NOM-coated silica or otherwise complexed with NOM remains transformable by *A.vinelandii* in this study. The results suggest that it is likely the NOM will not affect adsorbed DNA transformability in the environment and adsorbed DNA provides an genetic reservoir for soil microorganisms.

The effects of flagella on deposition dynamics of *Azotobacter vinelandii* in porous media, independent of motility, were confirmed a key factor to the deposition kinetics. Fla^- strain deposition was more than that of DJ77 in the two-dimensional silicon microfluidic models (micromodels) and in the columns packed with glass beads. In a radial stagnation point flow cell (RSPF), the deposition rate of a flagellated strain with limited motility, DJ77, was higher than that of a non-flagellated (Fla-) strain on quartz. The trend of the RSPF deposition of DJ77 versus Fla- was reversal to those of micromodel and column setups. In both micromodel and column experiments, we observed decreasing deposition over time, suggesting that approaching cells were blocked from deposition since the surface was occupied by previously deposited cells. Modeling results indicated that blocking started to become effective for DJ77 strain at lower

ionic strengths (1mM and 10mM), while Fla$^-$ strain showed similar blocking effects at all ionic strengths. Ripening came to effect at the late stage of micromodel experiments, and appeared earlier for the Fla$^-$ strain. In RSPF and column experiments, deposition of the flagellated strain was influenced by ionic strength, while ionic strength dependence was not observed for the Fla$^-$ strain. In contrast, the observations in all three setups suggested flagella affect deposition dynamics, and in particular result in greater sensitivity to ionic strength. The deposition dynamics changed at different stages of bacteria transport and at the presence of flagella in this study suggest that it is important to conduct experiments at multiple scales and that modeling efforts should be based on observations across scales in order to fully capture bacterial fate and transport.

Microoscopic evidence showed that strong swimming motility reduced attachment of *Azotobacter vinelandii* bacterium to silica surfaces. The instantaneous speed and turn angles of four strain/conditions of *A. vinelandii* under non-flow condition analyzed using global and cluster analyses confirmed strong swimming for flagellated DJ wild-type, impaired swimming for flagellated DJ77, and non-swimming for non-flagellated JZ52 and chemically treated DJ. Real-time images taken at different distances from the collector surface of a radial stagnation point flow cell (RSPF) were used to quantitatively analyze the trajectories and revealed that swimming DJ and non-swimming chemically treated DJ moved with the flow at a distance of at least 20 μm from the collector surface. A combination of horizontal and vertical movement with the near-surface strong swimming strain of DJ, deviating from the flow streamline, suggested that strong swimming reduced DJ cell attachment to the collector surface. The deposition rates obtained by both the RSPF and the two-dimensional multiple-collector micromodels were lowest for the DJ and similar for DJ77 and JZ52. The results concluded that strong swimming instead of hydrodynamics or secondary minimum reduced surface attachment of *A. vinelandii* under the experimental conditions in this study.

Finally, a rapid increase for swimming and swimming-impaired strains of *Azotobacter vinelandii* in transformation was observed in the first 30 minutes of the experiment and the rate increase eventually diminished at a given cell and DNA concentration. Both the experimental observation and the modeling results supported the hypothesis that under the given experimental conditions, the transformation rate was limited by the abundance of tetracycline resistance gene and by cellular activities associated with cell-DNA interactions. Statistical analysis results

suggested that the difference between swimming and swimming-impaired strains in transformation rates were not significantly different. The transformation rate model took different parameter values for swimming and swimming-impaired strains but did not result in a change of model structure to reproduce the experimental observation.

6.2 Contributions

This research developed an experimental approach to systematically investigate the environmental factors controlling natural transformation in the subsurface. The investigation on each of the two components, extracellular DNA and bacterial cells, provided fundamental understanding of the environmental influence on each component and consequently on the natural transformation. Three main contributions are listed here.

First, the work concluded that the presence of dissolved or surface-adsorbed NOM did not affect natural transformation. The significance of natural transformation in the subsurface was traditionally underestimated because of the assumptions that extracellular DNA cannot persist in the environment and once exposed to the subsurface environment, complex constituents such as NOM will disrupt the natural transformation processes. However, this work provided evidence that the adsorbed DNA maintained available for natural transformation in the absence or in the presence of NOM. The finding in this work suggested that natural transformation is likely to have a contribution to genetic flow in the subsurface.

Second, this work developed a multiple scale approach to investigate the role of biological characteristics, i.e. flagella and swimming motility, on bacterial fate and transport. Flagella and swimming motility affected different aspects of bacterial transport and fate. The separation of flagella and swimming resolved in better examination of the transport mechanisms. Flagella did not change the process of blocking but instead delayed the process of ripening in bacterial attachment. The presence of flagella resulted in a dependence of attachment on ionic strength. Swimming motility overcame hydrodynamics and caused bacterial cells to attach less.

Third, natural transformation rate experiments were conducted. The rate experiments were based on both swimming and swimming-impaired bacterial strains with different surface attaching ability. Different transformation rates were expected since different surface attachment potentials may result in different cell-DNA interaction or contact time. However, no significant

transformation rate difference was observed potentially because of the insignificance of different surface attaching potentials. A natural transformation rate model (Appendix) was constructed based on the experimental data presented in this thesis. This rate model was the first model providing quantitative measures of the natural transformation and the parameter analysis concluded the strong dependence on the availability of transforming DNA.

6.3 Future Prospects

This research provided experimental evidence that natural transformation has its niche in the subsurface environment. Adsorbed DNA was found available for natural transformation in the subsurface condition. In my opinion, the future research can take two directions forward, namely, fundamental understanding and practical application. On one hand, since natural transformation is the only pathway for extracellular genetic materials to return to the biosphere from the environment, better understanding on the mechanism is needed to assess the consequences of natural transformation. The physicochemical and biological factors affecting natural transformation should be identified to improve fundamental understanding. For example, one new fundamental question that was raised from this work is how do bacterial cells pull adsorbed DNA from surface, overcome attaching forces and take up adsorbed DNA in similar frequencies as freely dissolved DNA in the solution.

On the other hand, the specific processes of natural transformation should be pinpointed and targeted in future research studies to develop monitoring and controlling measures, especially with those organisms or gene having public health risks.

The multiple scale approach to investigate bacterial fate and transport in the porous media developed in this work is applicable to other physicochemical and biological factors. Collector surface heterogeneity, bacterial active detachment, and bacterial growth and decay and so on are all relevant to the bacterial fate and transport and other biological processes in the subsurface. The microscopic monitoring with the RSPF cell and the micromodel can provide real-time observation of individual bacterial behaviors. These individual bacterial behaviors then can be linked with large-scale bacterial processes quantitatively.

APPENDIX

MODELING METHOD AND RESULT FOR CHAPTER 5: A KINETIC MODEL OF GENE TRANSFER VIA NATURAL TRANSFORMATION FOR SOIL BACTERIUM *AZOTOBACTER VINELANDII*

In preparation:

Lu, N.; Massoudieh, A.; Liang, X.; Kamai, T.; Zilles, J. L.; Nguyen, T. H.; Ginn, T. R., A Kinetic Model of Gene Transfer via Natural Transformation for Soil Bacterium *Azotobacter vinelandii*.

Contribution: Massoudieh, A.; Liang, X.; Kamai, T. and Ginn, T. R. conducted and analyzed all the modeling in this chapter.

Mathematical model. From these kinetic data a few observations can be made: 1) the transformation frequency's increase is time-dependent, with a higher slope at the beginning that decreases with time and eventually approaches zero as the incubation time approaches 30 minutes. 2) There is a strong concave non-linear relationship between the cell concentration and transformation frequency. This means that transformation per unit cell concentration decreases as the cell concentration increases. 3) The maximum observed transformation constitutes only a small fraction of the total number of viable cells. 4) Different batches of cells have different transformation frequencies with dissolved DNA under similar conditions as reported previously.[1]

Considering that only a fraction of genomic DNA fragments hold the tetracycline resistance gene required for detection of a transformation event in our assay, Levin's mass action model can be applied to express the temporal change in the concentration of transformants as:

$$\frac{dT}{dt} = \lambda C' D' \qquad (1)$$

where T is the concentration of transformed bacteria, t is time, λ is the transformation rate constant, D' is the number concentration of transforming DNA (molecules of DNA/mL) and C' is the concentration of viable and competent cells. The DNA number concentration was calculated based on the mass of DNA added, the average molecular weight of double-stranded DNA, and an approximate DNA fragment size of 30kb (as estimated from agarose gels). Accounting for the facts that some fraction of the total number of DNA molecules contain the tetracycline resistance gene, that the eventual expression of the tetracycline resistance gene also depends on cellular activities, D (i.e. $D' = \alpha D$), and that the concentration of competent cells is a fraction β of the total viable cell concentration, C (i.e. $C' = \beta C$), Levin's mass action relationship can be written as:

$$\frac{dT}{dt} = \lambda \alpha \beta C D \qquad (2)$$

The value of α is the fraction of the tetracycline resistance gene over the total DNA that was eventually expressed in the cells, and the value of β is the ratio of bacterial cells involved in transformation to the number of viable cells. The balance equations for D and C can be written as:

$$\alpha D = \alpha D_0 - T \qquad (3a)$$

$$\beta C = \beta C_0 - T \qquad (3b)$$

where D_0 and C_0 are respectively the initial concentrations of DNA and cells. Substituting Eqs. (3a and b) into Eq. (2) yields:

$$\frac{dT}{dt} = \lambda\left(\beta C_0 - T\right)\left(\alpha D_0 - T\right) \qquad (4)$$

The analytical solution to Eq. (4) with initial condition of $T(t=0)=0$ can be found as:

$$T = \alpha\beta C_0 D_0 \frac{1-e^{\lambda t\left(\alpha D_0 - \beta C_0\right)}}{\beta C_0 - \alpha D_0 e^{\lambda t\left(\alpha D_0 - \beta C_0\right)}} \qquad (5)$$

If dimensionless quantities including dimensionless initial DNA, effective transformation frequency, and dimensionless time are defined respectively as $D_0^* = \alpha D_0 / \beta C_0$, $T^* = T/\beta C_0$, $t^* = \lambda t \beta C_0$ the dimensionless form of Eq. (5) expressing the effective transformation frequency (transformation per unit competent and viable cell concentration) can be written as:

$$T^* = D_0^* \frac{1-e^{t^*\left(D_0^*-1\right)}}{1-D_0^* e^{t^*\left(D_0^*-1\right)}} \qquad (6)$$

Based on Eq. (5) or (6) when $\beta C_0 \gg \alpha D_0$ the ultimate concentration of transformed cells will be equal to αD_0 and when $\beta C_0 \ll \alpha D_0$ the ultimate number concentration will be equal to βC_0. **Figure 26** provides a graphical depiction of the variation of effective transformation frequency as a function of D_0^* and t^*. When $D^* < 1$ the limiting transformed cell concentration at $t^* \gg 1$ approaches to D_0^* which indicates DNA limitation and it approaches to 1 (i.e. $T = \beta C_0$) when $D^* > 1$ that represents a cell limiting condition.

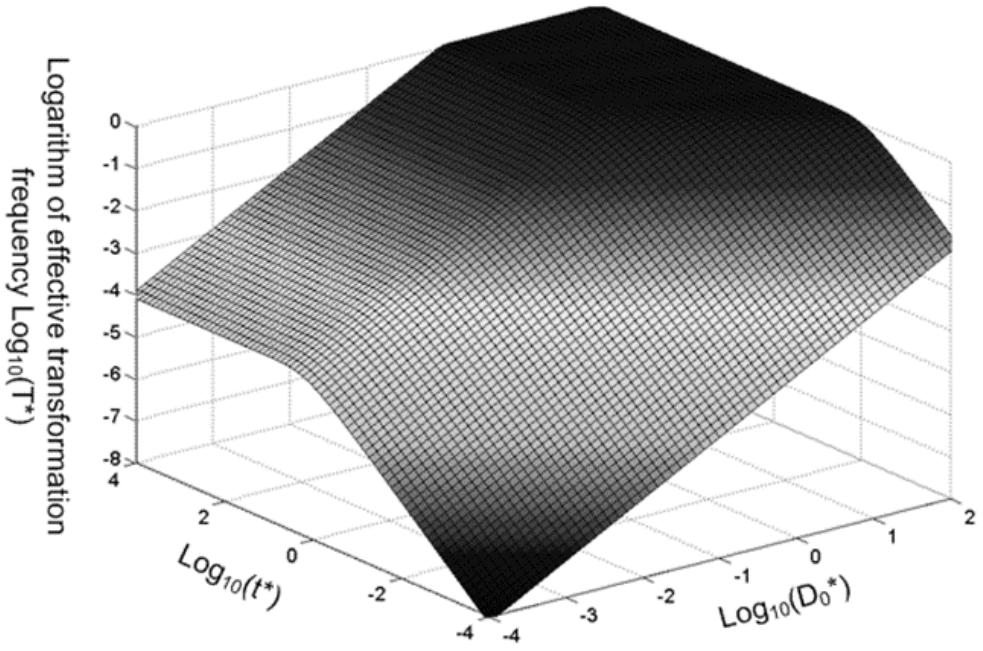

Figure 26 Typical variation of transformation frequency as a function of dimensionless transferable DNA and dimensionless time.

Parameter Estimation. To estimate the model parameters (i.e. α, β and λ), maximum likelihood via an optimization algorithm was used, minimizing the sum of squared differences between the measured and modeled log-transformed transformant number densities. The combined data from all transformation experiments was used as measured values. The log-transformation was performed because the distributions of the observed transformants were closer to a log-normal distribution than a normal distribution, and with proportional errors, log-transformation is expected to render errors more approximately normal. Initially a single set of parameters was considered for the two strains, but the agreement between modeled and measured transformant concentration (not shown here) was not acceptable. Since the parameters quantified the changes in transformation frequency in response to DNA and cell concentrations, this indicates that DJ and DJ77 responded differently to DNA and cell concentrations, despite showing no significant difference in their overall transformation frequency. Different parameters were therefore considered for the two strains.

Due to the uncertainties associated with measured viable cell and transformed cell concentrations, there are also uncertainties associated with the maximum likelihood estimates of the model parameters. To assess these uncertainties a Bayesian inference using Markov Chain Monte Carlo (MCMC) approach was performed to find the joint probability distributions of the model parameters. Assuming conditional independence of observed transformant concentrations, non-informative priors for the parameters, and log-normal and multiplicative error structure, the posterior distribution of the model parameters can be written as:[2]

$$\ln\left[\pi(\boldsymbol{\alpha},\lambda,\sigma)\right] = -\frac{n}{2}\ln\sigma - \frac{1}{2\sigma^2}\sum_{i=1}^{n}\left(T_i - \tilde{T}_i\right)^2 + A \qquad (7)$$

where n is the number of observations (total data points), $\boldsymbol{\alpha} = \left[\alpha_1 \ldots \alpha_n\right]$ is a vector of the parameters α per observation (per batch), σ is the standard deviation of log-transformed observation error, T_i and $\tilde{T}$ are respectively the modeled and observed transformant concentration in sample i, and A is a constant that only depends on observed data and is irrelevant when using MCMC to draw samples from the posterior distribution.

The Metropolis-Hasting MCMC algorithm[3] was used to sample from the posterior distribution. The algorithm draws a large number of samples from the posterior distribution (Eq. 5).

Modeling results. Parameters α, β, and λ were estimated from the combined data in **Figure 23**, **Figure 24** and **Figure 25** using maximum likelihood with an optimization algorithm as detailed in the methods. The coefficient α varied substantially depending on the batches of cells prepared. This was surprising, since the coefficient α acts on the number of transforming DNA molecules and not on the cell concentration or abundance of competent cells. Two potential causes for this are: variation in the fraction of DNA containing the tetracycline resistance gene from experiment to experiment, and/or variation in cellular activity from batch to batch. The fraction of tetracycline resistance genes was well-controlled, since DNA from multiple extractions was pooled and then aliquoted for the transformation experiments. We therefore conclude that the variation of α likely reflects variation in a cellular activity associated with DNA-cell interactions.

Figure 27 shows 95% credible intervals (C.I.) and medians for the parameters obtained from the posterior distributions of the model parameters α and λ. The range in values of α was consistent for experiments with the motile and non-motile strains. This observation agrees with

our definition of α as reflecting the fraction of DNA produced detectable transformation events in our assay, which should not be dependent on motility. The highest value of α was around 10^{-6}. Since *A. vinelandii*'s chromosome size is 5365 kb and the tetracycline resistance gene is 1.2 kb, 2×10^{-4} of the genomic DNA would be expected to contain the tetracycline resistance gene. The fact that α was even lower than 2×10^{-4} suggests that either not all copies of the genome contain the tetracycline resistance gene or other characteristics of the cells are limiting the ultimate expression of tetracycline resistance gene. These characteristics could affect DNA uptake or its subsequent incorporation into the recipient cell genome and the expression for the assay detection. The 95% intervals for λ and β are wide indicating equifinality (i.e., the non-unique combination of the two parameters can result in equally good agreement between modeled and measured values). For the experimental results shown here, a model without β could explain the data, but considering the broader range of cell concentrations in the environment a cell concentration parameter was included for versatility. As shown in **Figure 27**c, the 95% interval value of β varied between almost zero to 0.93 for DJ77 and zero to 0.8 for DJ strains, with expected average values of ~0.2 and ~0.1, respectively.

In the posterior distributions, β and λ were correlated, meaning a decrease in β and a proportional increase in λ resulted in the same numbers of transformation events. This correlation is due to the fact that the concentration of competent cells did not control the ultimate transformed concentrations in these experiments. Figure 6a shows the 95% confidence interval for the quantity βλ (referred to as the effective transformation rate constant).

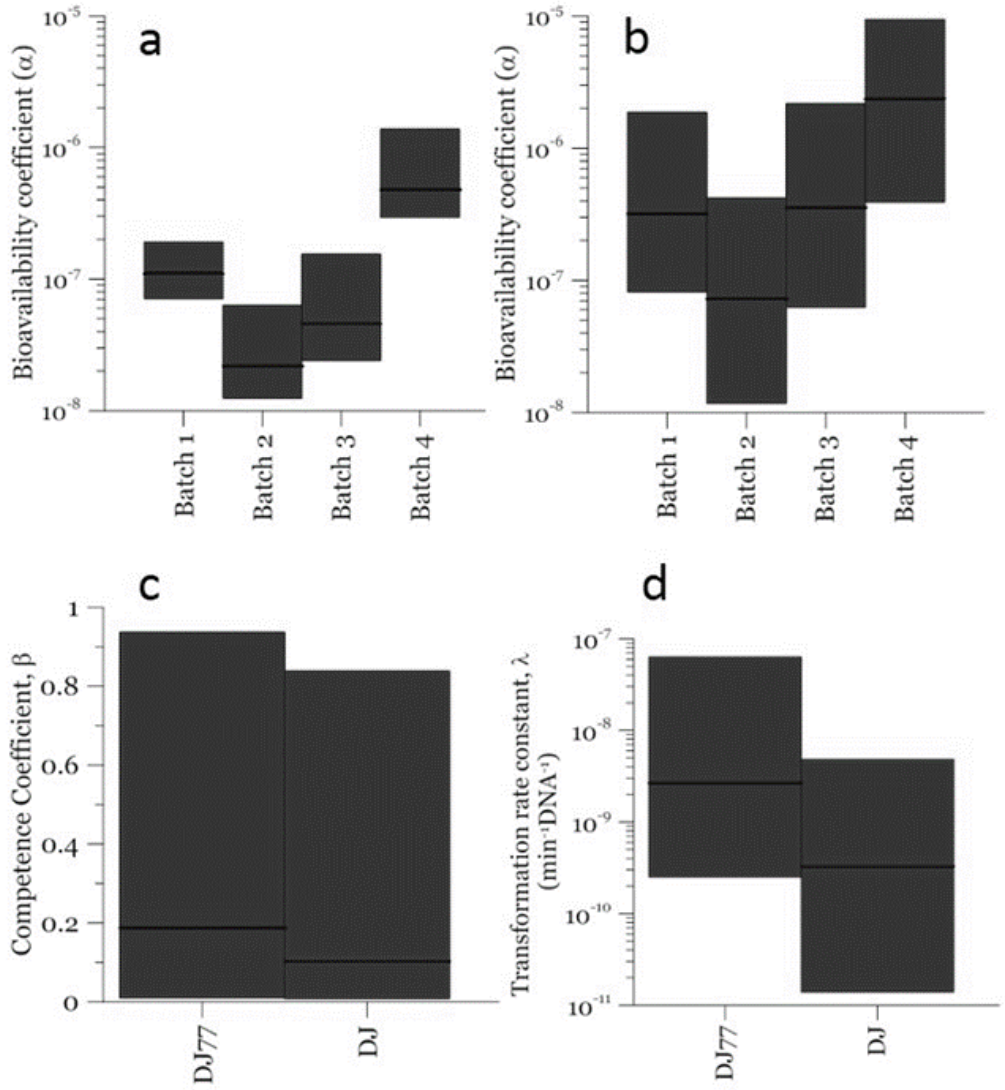

Figure 27 95% Credible intervals for the model parameters including DNA coefficient *α* for four batches of competence cells used in the study for a) DJ77 and b) DJ, c) transformation rate constant λ for both strains and d) cell coefficient β.

Figure 28b shows the possibility space of β and λ obtained using the outcome of the MCMC analysis and the strong correlation between the posterior distributions of the logarithms of the two parameters are evident. The 95% brackets for the product of the two parameters is much narrower than λ indicating its better identifiability. Theoretically a better confidence could be obtained regarding β by conducting the experiments either with a much larger DNA

concentration or a much smaller cell concentration, so that viable and competent cells become the limiting factor of the ultimate transformation frequency. However, this solution was not feasible due to the amount of DNA required and the detection limits in the transformation assay. The βλ value for the two strains overlapped, with the expected average value of βλ for DJ77 roughly one order of magnitude larger. The p-value for the hypothesis that the βλ for DJ77 is larger than DJ strain (i.e. the probability that the βλ for DJ is larger) was found to be 0.00751. We attribute this difference to the difference in motility between the two strains, rather than to DJ77's Nif$^-$ phenotype, because fixed nitrogen was provided throughout the experiment. A motility defect could affect transformation by allowing longer contact time between the cells and extracellular DNA. However, this difference was not substantial enough to lead to a distinctive model structure.

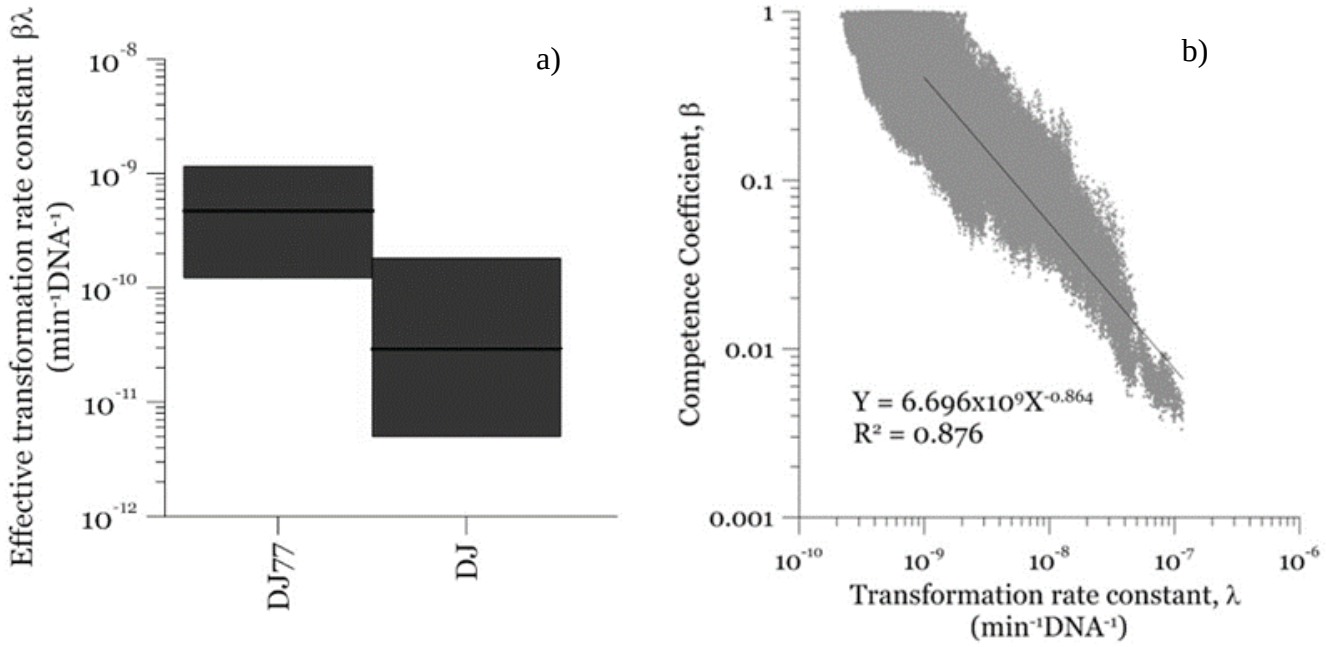

Figure 28 a) 95% Credible interval for the effective transformation rate constant βλ and b) the scatter plot of posterior MCMC samples of competence coefficient β and transformation rate constant λ showing the posterior correlation between the two parameters.

The modeled transformation frequencies were compared to the experimental results using all measured data (**Figure 29**), as well as data from transformation experiments featuring only transformation kinetics (**Figure 30**), cell concentrations (**Figure 31**), or DNA concentrations (**Figure 32**). The R^2 values reported in Figure 7 were calculated based on the log-transformed

transformed concentrations. Using all of the measured data (**Figure 29**), the predicted values are the likeliest parameter sets obtained through minimization of squared error between measured and modeled data. R^2 values of 0.92 (DJ) and 0.96 (DJ77) were obtained using the log-transformed modeled and measured transformed concentrations. In addition to the proposed model, we tested alternative models including Levin's mass action without considering the reduction of DNA as well as a few other models where the relationship between transformation rate and D and C were considered non-linear through power law relationships. The proposed model was able to reproduce the observed data significantly better as evaluated using R^2 and the Bayesian Information Criteria.

Figure 30 shows modeled and observed transformation kinetics. Since the cell concentration cannot be maintained at a pre-specified value, each of the points in **Figure 30** is a different cell concentration. Therefore we present two modeled transformation frequency curves, one based on the minimum experimental viable cell concentration (the solid curve) and the other one based on the maximum experimental viable cell concentration (the dash curve). The values of α, β, and λ used to generate these plots are the likeliest values obtained through deterministic maximization of the likelihood function. Considering the effect of cell concentration, in one set of experiments for each strain DJ and DJ77 the cell concentration was varied by less than one order of magnitude (**Figure 31**, panels a and c), while in the second set of experiments (**Figure 31**, panels b and d) the cell concentration was varied by about two orders of magnitude, from $3x10^7$ to 10^9 cells/mL. For both strains the model describes the decreasing trend in transformation frequency as a result of increase in the cell concentration well. **Figure 31** shows modeled vs. measured transformation frequencies in the experiment where DNA concentrations were varied by four orders of magnitude.

Similar to **Figure 29**, the model predictions based on the largest and smallest cell concentrations in each experiment are presented. The sensitivity towards the cell concentration is small compared to DNA concentration, indicating DNA limitation. The almost linear (slightly convex) relationship between the transformation frequency and DNA concentration is captured by the model.

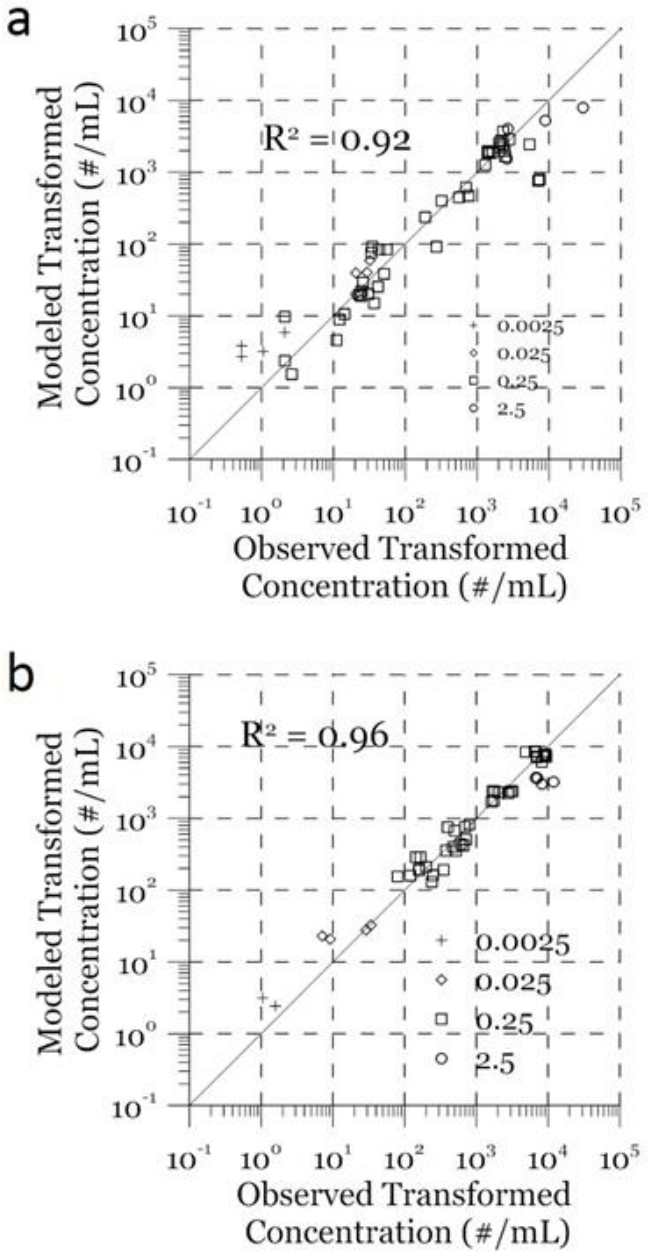

Figure 29 Agreement between modeled and measured transformed cell concentrations for a) DJ and b) DJ77. The symbols indicate DNA mass concentrations. The numbers in the legend correspond to the DNA concentration in µg/mL.

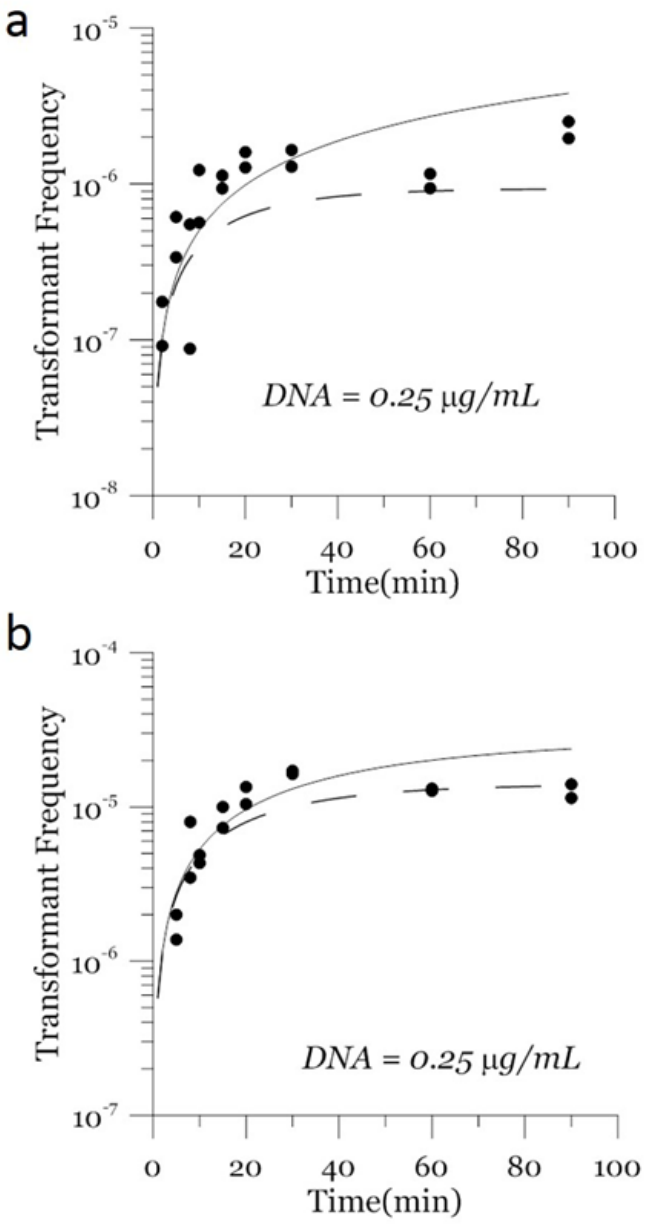

Figure 30 Modeled and measured transformation kinetics for a) DJ and b) DJ77. The two curves in each figure represent the modeled concentrations based on the lowest and highest cell concentrations in each experiment.

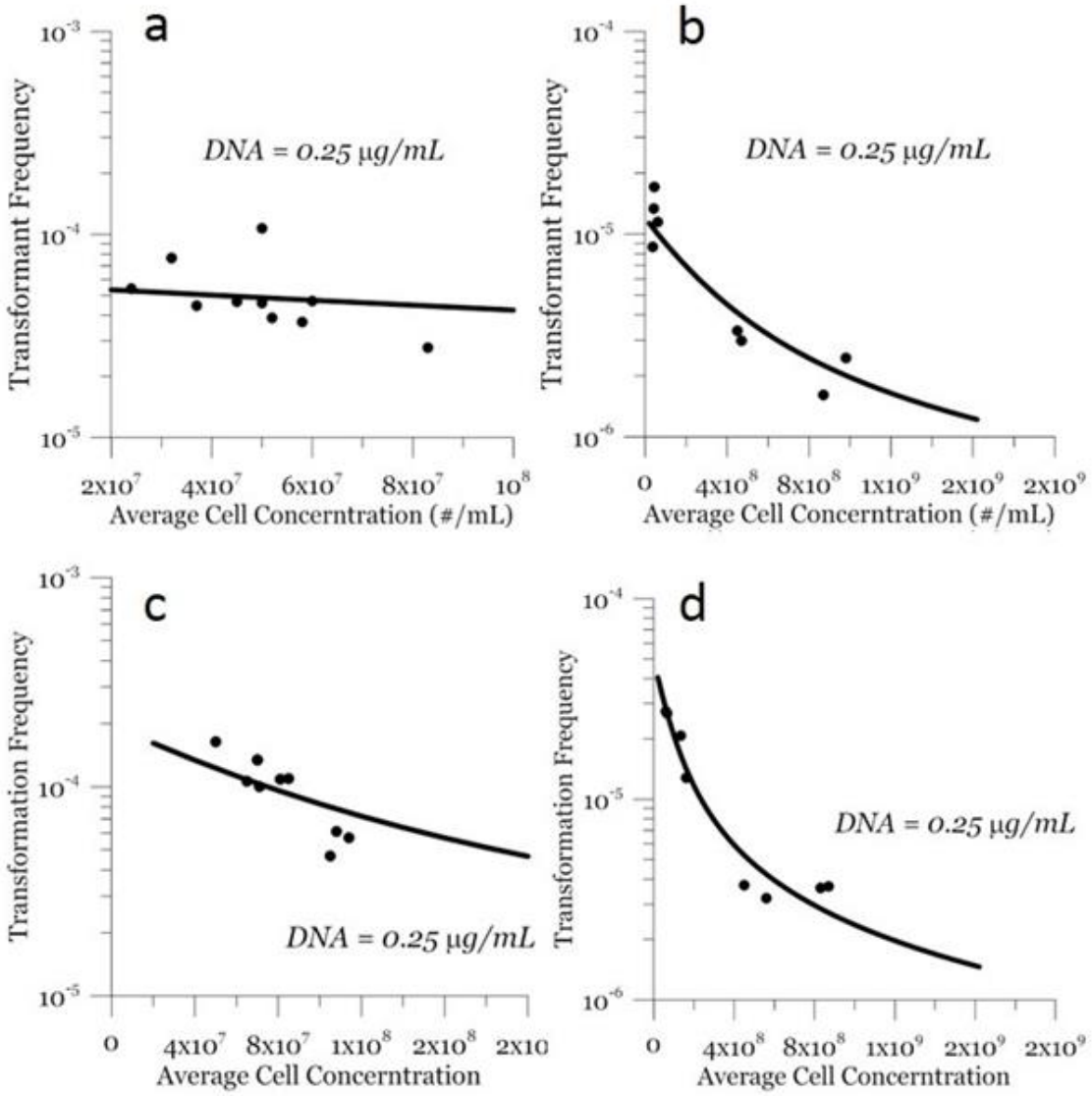

Figure 31 Modeled and measured transformation frequencies as a function of cell concentrations for a) First batch of DJ b) second batch of DJ c) First batch of DJ77 b) second batch of DJ77. The incubation time for all the data is 30 minutes.

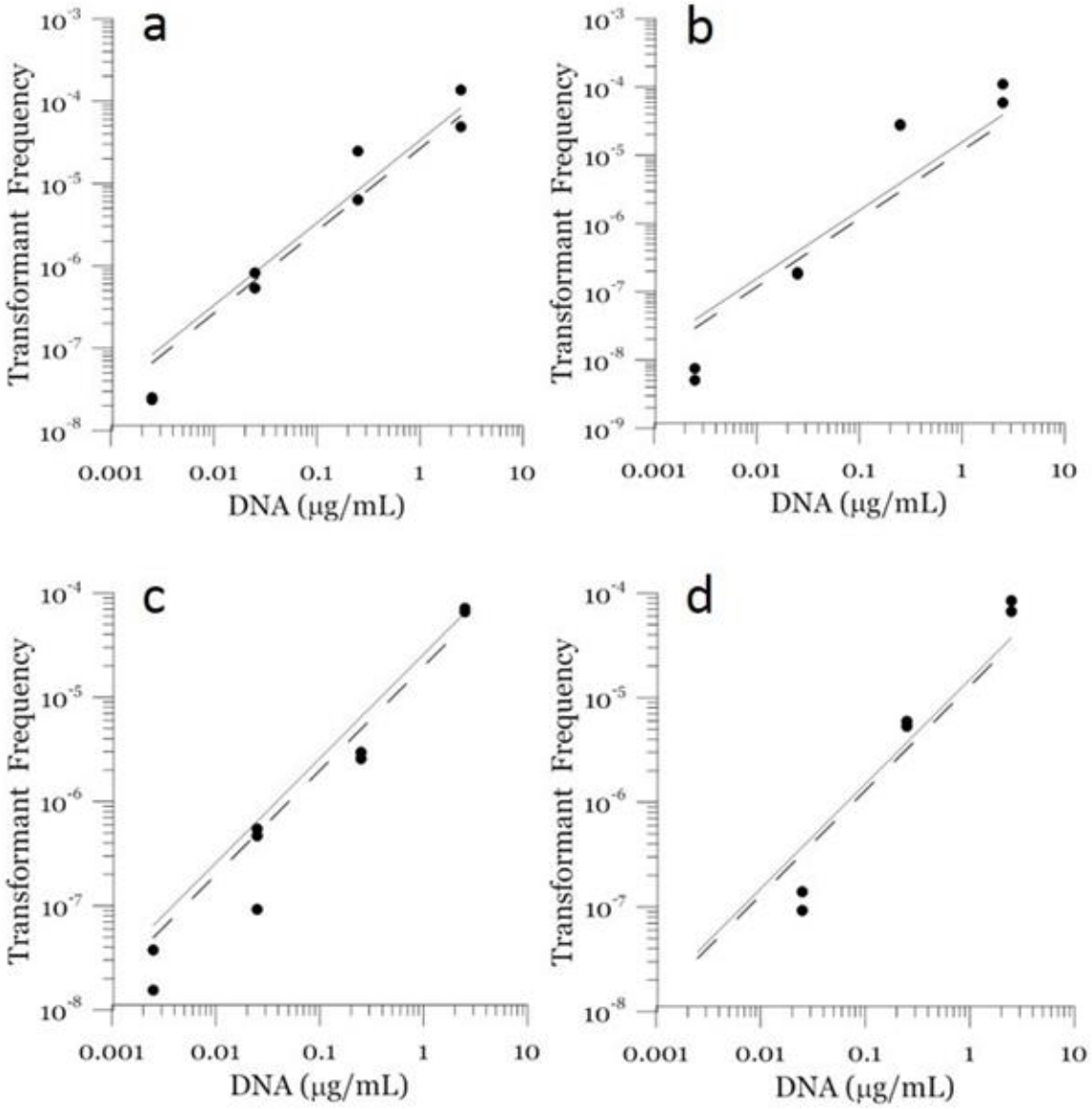

Figure 32 Modeled and measured transformation frequencies as a function of cell concentrations for a) First batch of DJ b) second batch of DJ c) First batch of DJ77 b) second batch of DJ77. The incubation time for all the data is 30 minutes.

References:

1. Lu, N.; Mylon, S. E.; Kong, R.; Bhargava, R.; Zilles, J. L.; Nguyen, T. H., Interactions between Dissolved Natural Organic Matter and Adsorbed DNA and Their Effect on Natural

Transformation of *Azotobacter vinelandii*. *Science of The Total Environment* **2012,** *426*, (0), 430-435.

2. Kaipio, J.; E., S., *Statistical and Computational Inverse Problems (Applied Mathematical Sciences)*. Springer: 2005; p 344.

3. Metropolis, N.; Rosenbluth, A. W.; Rosenbluth, M. N.; Teller, A. H.; Teller, E., Equations of State Calculations by Fast Computing Machines. *Journal of Chemical Physics* **1953,** *21*, (6), 1087-1092.